STUDY OF RESONANT BRILLOUIN SCATTERING BY AMPLIFIED ACOUSTIC PHONONS IN CdS AND ZnSe

A Thesis
Submitted to the Faculty
of
Osaka University
by

Koushi Ando

In Partial Fulfillment of the
Requirements for the Degree
of
Doctor of Philosophy

March 1977

Acknowledgement

The author would like to express his appreciation to Professor C. Hamaguchi for stimulating and helpful advice, criticism and continual encouragement throughout the course of this work. He wishes to acknowledge Professor J. Nakai for his helpful advice, guidance and critical reading. He also thanks to Professors A. Mitsuishi, T. Hanawa, S. Nakamura, and Y. Matsuo for their critical reading of this thesis. He appreciates Dr. M. Yamada for his helpful suggestions and K. Yamabe for his collaboration on the work reported in Chapters VI and VII. He is indebted to Drs. T. Shirakawa, A. Moritani and Y. Sasaki for helpful advice and discussions. He is grateful to Dr. M. Fukai, Central Research Laboratory, Matsushita Electronic Industrial Co.,Ltd.,for supplying single crystals used in the present work and to Drs. G. Kano and S. Ichikawa, Matsushita Electronic Corporation for orientating the samples by X-ray diffraction. He wishes to thank colleagues of the Semiconductor Research Group in Department of Electronics, Faculty of Engineering, Osaka University for their many forms of assistance and illuminating discussions in the course of the experiment, in particular; M. San'ya, M. Yokogawa, S. Adachi and S. Hamada. Special thanks are also due to Professor R. Bray of Purdue University for the invaluable suggestions. The finantial support of the Japan Scholarship Foundation is gratefully acknowledged. The author also recognized his parents who have continually encouraged him in his educational endeavors.

TABLE CONTENTS

Page

LIST OF TABLES v

LIST OF FIGURES vi

ABSTRACT xi

I. INTRODUCTION 1

II. THEORETICAL BACKGROUND 8

2.1. Introduction 8

2.2.1. Basic Theory of Brillouin Scattering (Macroscopic-Treatment) 9

2.2.2. Brillouin Scattering Cross Sections for each Acoustic Mode 18

2.3. Basic Theory of Resonant Brillouin Scattering (Microscopic-Treatment) 21

2.4. Excitonic Resonant Brillouin Scattering 30

2.5. Matrix Elements of Deformation Potential Scattering by Long Wavelength Acoustic Phonons . . 32

2.6. Construction of 2- and 3-Band Models in Resonant Brillouin Scattering 36

2.7. Advanced Theory of Resonant Brillouin Scattering. 39

2.8. Summary 44

III. EXPERIMENTAL PROCEDURE 46

3.1. Introduction 46

3.2. Experimental Procedure and Sample Construction . . 47

3.3. Resolution of Acoustic Frequency 51

3.4. Summary 54

IV. RESONANT BRILLOUIN SCATTERING IN CdS and ZnSe 55

4.1. Introduction 55

4.2.1. Resonant Brillouin Scattering by Piezoelectrically-Active Mode Phonons in CdS 56

4.2.2. Resonant Brillouin Scattering by Mode-Converted Phonons in CdS 65

4.3.1. Resonant Brillouin Scattering by Injected Acoustic Phonons in ZnSe 71

Page

4.3.2. Derivation of Relevant Photoelastic Constants from Static Birefringence Theory . . 77
4.4. Summary 83

V. OPTICAL MODULATION AND RESONANT BRILLOUIN SCATTERING IN CdS 84

5.1. Introduction 84
5.2. Experimental Results and Discussions 86
5.3. Summary 94

VI. BREAK DOWN OF SELECTION RULE IN RESONANT BRILLOUIN SCATTERING IN CdS 96

6.1. Introduction 96
6.2. Experimental Results and Discussions 97
6.3. Summary 112

VII. APPLICATION OF ACOUSTIC PULSE-INJECTION INTO SEMICONDUCTORS 113

7.1. Introduction 113
7.2. Acoustic Field Equations and Transmission Efficiency 114
7.3 Application of Acoustic Injection of Elastic Properties 123
7.3.1. Determination of Elastic Stiffness Constants in ZnSe and ZnTe 124
7.3.2. Frequency Dependence of Attenuation Coefficients of Injected Sound Waves in ZnSe and ZnTe . . . 126
7.4. Summary 128

VIII. CONCLUSIONS 129

APPENDIX I. General Formulation of Resonant Brillouin Scattering in Higher Energy Region 132

APPENDIX II. Correction of Strong Absorption and Depletion of Incident and Scattered Lights in Anisotropic Crystals 134

APPENDIX III. Representation of Elastic Constant Tensor for Arbitrary Coordinate System in Cubic Crystals . 136

LIST OF REFERENCES 139

LIST OF TABLES

Table		Page
2. I.	Experimental configuration for each acoustic mode in CdS and ZnSe.	18
2. II.	Relevant Photoelastic constants and polarization relations in the Brillouin scattering.	21
2.III.	Nonzero strain components for the three different acoustic modes in CdS.	32
2. IV.	Matrix elements of deformation potential scattering in CdS and ZnSe.	35
3. I.	Characteristics of CdS and ZnSe samples used in the present work.	50
4. I.	Parameters used in the calculation of resonant enhancement of the Brilliuin scattering cross sections for the mode-converted phonons in CdS.	68
4. II.	Values of parameters used in the calculation of total scattering cross section for T1 and T2-mode phonons. Superscripts(1) and (2) correspond to the strong and weak contribution to the scattering cross section,respectively.	75
4.III.	Values of parameters used in the calculation of dispersions of photoelastic constant from static piezobirefringence theory.	81
6. I.	Parameters used in the estimation of forbidden-resonant Brillouin scattering in CdS.	108
7. I.	The particle displacement velocity[v], the phase velocity V_p, the stress components[T] and the complex acoustic Poynting vector[P_{ac}] of incident, reflected and transmitted acoustic waves.	121
7. II.	Values of the elastic stiffness constants obtained by the best fitting.	126

LIST OF FIGURES

Figure		Page
2-1.	Schematic explanation of direct, indirect and rotational Brillouin scattering	11
2-2.	Momentum conservation between the incident and scattered photons and phonons for aniso- and isotropic crystals	12
2-3.	Calculated dispersions of resonant Brillouin tensor $R_{is}(\omega_i,\omega_q,\omega_s)$ for acoustic frequency 1.0 GHz. In the calculation three kinds of broadening parameters(Γ/ω_g=0, Γ/ω_g=0.01 and Γ/ω_g= 0.02) are used	28
2-4.	Schematic diagram of selection rule in optical transition at Γ-point	36
2-5.	Schematic diagram of dominant transition process for each acoustic mode in CdS	38
3-1.	Schematic diagram of the experimental apparatus. The specimen is mounted on the rotatable table and incident angle θ_i and scattered angle θ_d are set to detect light scattered by phonons with a specific frequency	48
3-2.	Block diagram of trigger-system in experimental apparatus	48
3-3.	Current waveform and typical optical signals .	48
3-4.	Schematic arrangement of the acoustic packet introduced from semiconductive CdS into insulating ZnSe	50
3-5.	Schematic diagram of focussed light beam and detector cone used in the present work	53
3-6.	The estimated values of $\Delta\delta$ and $\Delta\omega_q/\omega_q$ versus incident light wavelength	53
4-1.	Brillouin scattering signals for T2-mode phonons in CdS. The ratios of Brillouin scattered light intensity I_s to the incident light intensity I_o are plotted as a function of incident light wavelength	57
4-2.	Brillouin scattering cross section plotted as a function of incident light wavelength in CdS .	59

Figure		Page
4-3.	Dispersion curves of Brillouin scattering cross section for 0.5 and 1.0 GHz phonons. Solid curves are calculated by taking into account the exciton effects with optical band gap: E_{gi}=2.494 eV for the incident light and optical band gap; E_{gs}=2.480 eV for the scattered light. Dotted and dashed curved are estimated by Loudon's theory with band gaps: E_{gi}=2.40 eV and E_{gs}=2.38 eV, and with E_{gi}=2.494 eV, E_{gs}=2.480 eV, respectively	63
4-4.	Brillouin scattering signals for T1-mode phonons in CdS. Data points (O) and (●) are obtained by phonon beams reflected at the end of the specimen and the solid lines are obtained by the phonon beams injected into the end-bonded specimen.	66
4-5.	Dispersion curve of Brillouin scattering cross section for PL-mode phonons in CdS. For comparison the dispersion curve observed by Tell et al. is also plotted	66
4-6.	Comparison of experimental data with theoretical dispersion curves of resonant Brillouin scattering by T1-mode phonons in CdS	69
4-7.	Comparison of experimental data with theoretical dispersion curve of resonant Brillouin scattering by PL-mode phonon in CdS	69
4-8.	Schematic arrangement for studying resonant Brillouin scattering in ZnSe	71
4-9.	Brillouin scattering dispersion curves for 0.2 and 0.3 GHz T1-mode phonons in ZnSe. Experimental points are normalized by transmitted light intensity I_t	73
4-10.	Brillouin scattering dispersion curves for 0.2 and 0.8 GHz T2-mode phonons in ZnSe. Experimental points are normalized by transmitted light intensity I_t	73
4-11.	The plots of $\sqrt{\sigma_B}$ versus incident light wavelength for T1- and T2-mode phonons	74
4-12.	Comparison of experimental with theoretical dispersion curves are obtained by using the Loudon's theory and dashed lines are obtained by taking into account the exciton	76

Figure		Page
4-13.	Same as Fig. 4-12. but for the T2-mode phonons	76
4-14.	Experimental points and fitted curves of $(P_{11}-P_{12})^2$ and $(P_{11}-P_{12})$ calculated from the P.B.-theory in ZnSe	82
4-15.	Same as Fig. 4-14. but for the T2-mode and P_{44} and $(P_{44})^2$	82
5-1.	Field dependence of O.M. in CdS. O.M. signals are obtained by using the light with wavelength: 5200, 5250 and 5300 Å	85
5-2.	Schematic diagram of polarization conditions and optical signals in the measurement of O.M in CdS. Optical signal (a) originates from the active domain and (b) originates from the inactive (reflected) domain	86
5-3.	Dispersion spectra of O.M observed under the two polarization condition: (a) $I_E//I_{TA}//$c-axis and (b) $(I_E//I_{TA})\perp$c-axis near the fundamental absorption edge of CdS. The data points of (●) and (■) are obtained by using the active domains and (⊙) and (⊡) are obtained by using the inactive (reflected) domain	87
5-4.	Dispersion spectra of O.M. in the wavelength region from 5200 to 6500 A in CdS observed under the two polarization conditions (a) (O) and (b) (●). For comparison the resonant dispersions of Brillouin scattering by 1.0 GHz phonons are plotted	89
5-5.	Comparison of experimental dispersions of O.M. induced by the active acoustic domain with estimated dispersions from resonant light scattering	92
5-6.	Same as Fig. 5-5. but for the inactive acoustic domain	92
6-1	Brillouin scattering signals versus polarization angle θ for each incident light wavelength. The angle $\theta=0^\circ$ refers to the polarization condition $I_E//I_A$ and $\theta=90^\circ$ to that of $I_E\perp I_A$	99
6-2.	Brillouin scattering signals for forbidden polarization condition; $I_E//I_A$ by 0.5 GHz piezoelectrically active TA phonons. For comparison disper-	

Figure Page

sion spectrum of normal Brillouin scattering cross section observed under the allowed polarization condition is plotted 101

6-3. Dispersion curves of Brillouin scattering cross sections for normal ($I_E \perp I_A$) condition and forbidden ($I_E // I_A$) conditions by 0.5 and 0.8 GHz piezoelectrically active TA phonons 101

6-4. Dispersion curves of Brillouin scattering cross section observed under the forbidden condition at 300 K and 77 K in CdS 103

6-5. Dispersion curves of Brillouin scattering cross section by piezoelectrically inactive TA phonons observed under the forbidden polarization condition 103

6-6. Schematic diagram of optical and acoustic transitions of intermediate virtual excitations in CdS 106

6-7. Schematic diagram of dominant transition process of virtual states in the case of forbidden resonant light scattering by piezoelectrically active and inactive TA phonons in CdS 106

6-8. Comparison of experimental dispersion of forbidden Brillouin scattering by piezoelectrically active TA phonons with the theoretical dispersion at 300 K. Solid line is estimated by taking into account of B and C virtual excitons 110

6-9. Comparison of experimental dispersion of forbidden Brillouin scattering by active TA phonons with the theoretical dispersion at 77 K. Broken line is estimated by taking into account of the B- and C-virtual excitons 111

6-10. Comparison of experimental dispersion of forbidden Brillouin scattering by inactive TA phonons with the theoretical dispersion at 300 K. Solid line is calculated by taking into account of the A- and B-virtual excitons 111

7-1. Schematic arrangement of acoustic wave injection for CdS-ZnSe and CdS-ZnTe systems where θ is the angle between the propagation vector of injected sound wave and [001] crystal direction in the $(1\bar{1}0)$ plane 115

7-2. Polarization angle $\phi_{\_}$ of injected QT phonons

Figure		Page
	into ZnSe and ZnTe as a function of propagation angle θ	119
7-3.	Calculated transmission and reflection coefficients of the complex Poynting vectors in CdS-ZnSe and CdS-ZnTe bonded systems . . .	122
7-4.	Frequency dependence of transmission coefficients of acoustic Poynting vectors in CdS-ZnSe bonded system	122
7-5.	The phase velocity of QT-acoustic waves in ZnSe with frequency 1 GHz as a function of propagation direction in the ($1\bar{1}0$) plane. The solid line represents the best fitted theoretical variation of velocity using the values of elastic stiffness constants in Table 7.II	125
7-6.	Same as in Fig. 7-5. but for the ZnTe	125
7-7.	The attenuation coefficients of pure transverse sound waves propagating in the [001] direction with polarization vector parallel to the [110] direction as a function of the frequency in ZnSe	127
7-8.	Same as in Fig. 7-7. but for the ZnTe and T2-mode	127
A-I.	Joint density of states and real part of modulated dielectric constants and Brillouin efficiencies versus incident photon energy for 3-dimensional critical points.	134

ABSTRACT

Koushi, Ando. Ph.D., Osaka University, March 1977.
Study of Resonant Brillouin scattering by Amplified Acoustic-Phonons in CdS and ZnSe. : Major Professor: Chihiro, Hamaguchi.

Present work is concerned with study of resonant Brillouin scattering in semiconductive CdS and semi-insulating ZnSe. Acoustic injection method is also presented and theoretical treatment is given mainly in the case of CdS-ZnSe system where acoustoelectric domains amplified in CdS are transmitted into ZnSe. The method is shown to have a versatile to such study reported here. Most of the present work were carried out by making use of intense acoustic phonons amplified through the acoustoelectric effect instead of thermal phonons, which enabled us to investigate Brillouin scattering cross sections in the region near the band gap. The CdS crystal belonging to wurtzite type semiconductor has not only large piezoelectricity but also strong optical anisotropy and therefore it is very interesting to examine the resonance effect of Brillouin scattering cross section in the photon energy region close to the fundamental absorption edge. Acoustic pulse injection developed in the present work enabled us to study the resonant Brillouin scattering in semi-insulating ZnSe belonging to zinc-blende and thus we can discuss the physical mechanism of resonant light scattering in both types of crystals.

In Chapter I, historical background of resonant light scattering is reviewed and the significance of the present work is explained. In Chapter II. basic formulations of resonant and nonresonant light scattering are presented by using the microscopic and macroscopic treatments. Resonant behaviors of scattering efficiency near the

critical point are interpreted by the microscopic theory of light scattering, where electronic excitation plays an important role. From the selection rule of deformation potentital scattering of virtual states by acoustic phonons 2- ans 3-Band models of transition process of virtual states are proposed to explain the present observations. Advance theory of resonant light scattering is also introduced by making use of the treatment of non-linear susceptibility to examine the resonant behaviors arising from higher energy 3-dimensional critical points(M_1,M_2, and M_3).

In Chapter III, experimental procedure and detailed explanation of the sample construction used in the present work are presented. In order to estimate the dispersion of intrinsic scattering efficiency resolution of acoustic frequency is discussed mainly in connection with the present experimental conditions.

Chapter IV deals with the experimental results and discussions on the resonant Brillouin scattering in CdS and ZnSe. In the observed dispersion spectra one can find a sharp resonant enhancement and antiresonance structure in the dispersion curves of Brillouin scattering cross section by pure TA-mode phonons in CdS and ZnSe. Resonant feature of scattering efficiency by pure LA-mode phonon is found to be quite different from that of TA-mode, where only a sharp resonant increase(no resonant cancellation is observed). Those dispersions obtained in the present work are compared with the theory and it is found that the expression of resonant Brillouin scattering taking into account of the exciton contributions has well explained the experimental data.

In Chapter V, dispersion spectra of optical modulation induced by the acoustic domain in CdS are presented. Optical modulation signals are observed in the photon energy region not only close

to the fundamental absorption edge but also in the transparent region. A comparison of dispersion spectra of the optical modulation with resonant Brillouin scattering cross sections is carried out and one can find that the dispersion curves of optical modulation signals agree well with those of resonant Brillouin scattering in CdS.

In Chapter VI, the experimental results and discussions on Breakdown of selection rule in Brillouin scattering in CdS are presented. It is found that the Brillouin scattering efficiency observed under the forbidden-condition shows a resonant enhancement near the intrinsic band edge. By means of the analysis based upon tne deformation potential scattering of virtual electronic states by TA phonons the physical mechanism of break-down of selection rule is discussed and the 3-Band model of transition process for forbidden-resonant light scattering is found to explain the present observations.

In Chapter VII an application of acoustic pulse injection technique is presented with theoretical treatments of acoustic matching theory. By making use of the injected acoustic packets into ZnSe and ZnTe the sound velocities of quasi-transverse mode propagating in several directions are measured and important elastic parameters such as; elastic stiffness constants and propagation loss are determined.

In Chapter VIII, the conclusions obtained in the present study are summarized.

Chapter I. Introduction

Since the development of the transistors the investigation of solid state physics has made a remarkable progress. It never seems to be an exaggerated expression that the present prosperity of the electronic industries is largely attributed to the reseach of physical properties of semiconductors. The research-field so called 'Solid State Physics' has made a great advance especially in semiconductors with strong help of Quantum theory, which was extensively studied in those days. The study of light scattering (including Brillouin and Raman scatterings) was one of the important part of such investigation field and fundamental treatment of light scattering were established considerably long ago.

The first prediction of light scattering by long-wavelength elastic sound waves was presented by Brillouin[1] in 1922. Subsequently Smekal[2] developed in 1923 the theory of light scattering by a system with two quantized energy levels; this theory contained the essential characteristics of the phenomena discovered by Raman.[3]

In the initial stage the experiments of the light scattering were performed as an excellent tool to study the excitation of molecules and molecular-structures. In 1940's emphasis has been shifted to the systematic investigation of single crystals to obtain the informations of the lattice dynamics. However, the experiments seemed to be difficult because of poor light source and small scattering intensity. The appearance of laser in 1960 was to change this situation rather drastically. The monochromaticity, coherence and power were also to change the character of light scattering. Ever since the discovery of the laser one could easily obtain the detailed experimental data enough to be compared with detailed theory.

In the early days of light scattering experimental work was only possible with materials transparent to the scattering radiation . This is due to the fact that the scattering volume,limitted by the absorption length, was too small in opaque samples to make observation possible. In order to make the study of light scattering in the opaque photon energy region possible the measurements were performed in the back-scattering configuration which has become later the standard technique for the investigation of resonance effect. As the progress of the experimental technique one became to be able to obtain the high qualitative data from the light scattering even in the case where the incident photons create the electronic excitations in the crystals. This is also applied to some of the features (critical points) in the second-order spectra and made the resonant Raman scattering an ideal technique to study the effect of perturbations on the phonon spectra.

Generally, in the opaque photon energy region the scattering by phonons occurs mainly through the intermediate virtual electronic excitations. Thus, for incident and scattered photons near the energy of interband transitions such band structures must be appeared in the dispersion spectra of Raman and Brillouin scattering. This structure can be used for studying the electronic transitions in a way similar to that used in modulation spectroscopy.[4)]

The first measurement of resonant Raman scattering in semiconductors was performed in CdS using the discrete lines of the A_r^+-laser.[5)] Later, measurement for CdS by Ralston et al.[6)] confirmed the resonant enhancement of Raman scattering cross section close to the critical point and established the existence of an antiresonance structure in the dispersion spectra. For recent years a lot of experiments of first- and second-order resonant Raman effect

in variable II-VI and III-V compound semiconductors[7-13] were performed.

On the other hand the resonant Brillouin scattering in CdS, which is main object of the present work was first performed by Pine[14] using the high-resolution confocal spherical Fabry-Perot. In the case of Brillouin scattering by acoustic phonons such a high resolution-interferometer is essential because of small Brillouin shift. In this measurement, however, one could find only the slight resonance feature of scattering cross section near the intrinsic absorption edge of CdS.

The new experimental technique of resonant Brillouin scattering by using the strongly amplified acoustic domain through the acousto-electric effect in piezoelectric semiconductors[32-37] was proposed by Garrod and Bray[15] and they actually demonstrated the possibility of measurement in resonant Brillouin scattering by using the acoustic domain generated in n-GaAs. In the dispersions of Brillouin scattering cross section observed by them one could clearly confirmed the existence of resonant enhancement near the edge and resonant cancellation at the photon energy just below the fundamental absoption edge of GaAs.[15] This measurement is the starting point of the investigation in resonant Brillouin scattering by using the high density acoustic flux. It should be noted that initial stage of Brillouin scattering experiments in opaque photon energy region has just corresponded to the age, where the study of acoustic instability[32-37] has been studied vigorously and the excellent technique of acoustic-amplification was constructed. After the experiments by Garrod and Bray[15] the observations of resonant Brillouin scattering by using the acoustic domains were performed in semiconductive CdS by the present author[16,18;19] independently by Gelbart and

Many[17] in which the resonant enhancement and cancellation were well explained by using the Loudon's theory[20] taking into account of the exciton contributions[21]. In those measurements the continuous light source dispersed by conventional monochromator instead of laser is used because the intense acoustic phonon beams provide the strong scattering signals.

Subsequently the several kinds of piezoelectric-semiconductors such as CdS[22,23] CdSe[24] and ZnO[23] were used in the experiments of resonant Brillouin scattering and similar features of resonant enhancement and cancellation structures were confirmed.

In those days, however, experimental method of resonant Brillouin effect was restricted to only crystals having strong piezoelectricity, but such disadvantage was successfully overcome by the development of acoustic pulse injection[25-27] by the present author. It was found that the technique of acoustic injection made us possible to investigate the resonant Brillouin scattering even in the non-piezoelectric crystals where one cannot directly generate the acoustic domains.[29,30]

The present work is concerned with the study of resonant Brillouin scattering in semiconductive CdS and semi-insulating ZnSe. The characteristic feature of the present work is that a strongly amplified acoustic domains instead of thermal phonons are used in CdS and that injected acoustic waves are used in the case of ZnSe which means that one can perform the experiment without tunable dye-laser. The CdS crystal belonging to the wurtzite type semiconductors has a strong optical anisotropy and therefore it is interesting to study the resonant behavior of Brillouin scattering efficiency near the fundamental edge taking into account of such an optical anisotropy. The acoustic pulse injection developed in the

present work enabled us to investigate the resonant Brillouin effect also in semi-insulating semiconductor ZnSe belonging to the zincblende and we can discuss the physical mechanism of resonance effect for both types of crystals.

Chapter II of this paper is devoted to describe the basic-treatment of light scattering by using the phenomenological expression and quantum theory. Brillouin scattering cross section for each acoustic mode in CdS are presented and the detailed microscopic treatments of resonant Brillouin scattering near the fundamental edge are reviewed. From the analyses of deformation potential scattering of intermediate virtual states by acoustic phonons it is found that the 3-Band model has an important role to understand the essential resonance effect.[18,19] The expressions of excitonic-resonant Brillouin scattering are also reviewed.[21] In this section general expression of theoretical treatment in resonant Brillouin effect by using the Green function method is derived, which is very useful to discuss the light scattering in the higher photon energy region. By using this theory the correspondence of resonant Brillouin scattering with the modulation spectroscopy is obtained.

In Chapter III, the experimental procedure of the present work and sample construction are reviewed. In order to estimate the correct scattering efficiency in the experiment the resolution of acoustic frequency is discussed.

Chapter IV deals with the experimental results of resonant Brillouin scattering in CdS and ZnSe.[18,19,29] It is foundin comparison with the theory that Brillouin scattering cross section due to the piezo-active acoustic phonons are well explained by the

theory of excitonic resonant scattering taking into account of 3-Band model. The resonant cancellation (anti-resonance) is also found in the dispersion curve of piezo-active phonons. The resonant enhancement of Brillouin scattering cross section for mode-converted phonons in CdS[19] are presented and discussed by using the modified Loudon's theory. In this Chapter the experimental results and discussions of resonant Brillouin scattering for two kinds of transverse acoustic mode in ZnSe are given[29]. By taking into account of the band structure at Γ-point of the specimen 3-Band model is constructed.

In Chapter V, dispersion spectra of the optical modulation due to the propagating domain of CdS are presented.[96-102] It is known that the acoustoelectric domains can significantly modulate the intensity of light transmitted through the region of such domains. Several models have been proposed to explain the physical mechanism of this effect.[92-97] We have performed the comparison between the optical modulation and resonant Brillouin scattering. It is found that the dispersion curves of modulation signals are found to well agree with the dispersions of resonant Brillouin scattering. It can be concluded that the acoustic domain induced-Optical modulation of CdS is mainly caused by the light scattering from high density-acoustic phonons inside the domain.[100,102]

In Chapter VI, the experimental results and discussions of the Break-down of symmetry induced selection rule in Brillouin scattering in CdS are reviewed. As it is well known the Brillouin tensor is determined by the tensor representation of photoelastic constant. The polarization relations of incident and radiated photons have been decided based upon the such tensor expressions. In the present work it is observed that the Brillouin scattering

cross section for forbidden configuration shows a resonant enhacement near the fundamental edge of CdS. Such a resonant enhancement in forbidden scattering is also found for the mode converted phonons. The present experimental results suggest that the crystal symmetry induced Brillouin tensor must be reconsidered in the resonant region.

Application of acoustic pulse injection technique is presented in Chapter VII with the theoretical treatments of acoustic matching theory.[78] By using the injected acoustic waves into ZnSe and ZnTe the sound velocities for mixed acoustic modes propagating in several directions are measured and three independent elastic stiffness-constants C_{11},C_{12} and C_{44} of ZnSe and ZnTe are determined by best-fitting the data to the theoretical expressions.[26,78] Attenuation coefficients of propagating acoustic waves are also determined in the acoustic frequency range from 0.2 to 1.5 GHz.

In Chapter VIII the conclusions obtained in the present work are summarized.

In Appendix I the detailed discussion of 3-Band model is presented

In Appendix II the correction of strong absorption and depletion of incident and scattered lights for the case of anisotropic crystals is discussed.

In Appendix III the expressionsof tensor formulation of elastic constant [C"] for arbitrary coordinate system in cubic crystals are presented.

Chapter II. Theoretical Background

2.1. Introduction

Brillouin scattering has many advantages to study the properties of acoustic phonons in both iso- and anisotropic crystals. The macroscopic theory of Brillouin scattering was first derived by Benedek and Fritsch.[31] It is very useful to investigate the Brillouin scattering due to both the thermal phonons and amplified phonons in cubic crystals. Original formulation of Brillouin scattering cross section is, generally, obtained from the relation of momentum conservation between the incident and scattered photons and phonons in the crystals. It is not important in the construction of momentum-triangle to take into account the optical anisotropy in the case of cubic crystals such as ZnSe. However, one finds that the consideration of birefringence character in anisotropic crystals has an important role in the estimation of Brillouin scatterig cross sections.[40] It is well known that the Brillouin scattering technique is very available to observe the features of amplification in the propagating acoustic domains in piezoelectric semiconductors.[34-37] In the case of CdS the expression of Benedek and Fritsch cannot be applied to the analyses of scattering cross section because of strong optical anisotropy.

Hope,[38] Nelson et al.[39] and Hamaguchi[40] have calculated the Brillouin scattering cross section of anisotropic crystals by taking into account of the strong birefringence and internal reflection. At the present work the expressions of Brillouin scattering cross section derived by Benedk et al. is used in the case of ZnSe and that of Hamaguchi is applied to the case of CdS because their formulations are very advatageous to the present configurations.

Here it should be noted that the formulations mentioned above are useful only in the transparent optical frequency range, where the incident photons never excite the electronic excitations in the crystals. In the photon energy region close to the critical points of the band structure the macroscopic treatments of Brillouin scattering are not valid since such treatments never take into account the electronic contributions. The microscopic expression including the effect of electronic excitations was first derived by Loudon.[20] He predicted that the scattering efficiency should increase drastically when the excitation energy approaches to the band gap energy in semiconductors.[20] After his prediction many investigators were devoted to the study of resonance effect in semiconductors and a lot of theoretical formulations were presented.[4.21,41-49]

It is also found that the deformation potential scattering of intermediate virtual states (electronic-excitations) by phonons plays a very important role in the discussion of resonance-effect.[18] Based upon the selection rule of deformation potential scattering 2- and 3-Band models of transition process of virtual states are constructed. This Chapter is devoted to show the explanation of macroscopic treatment in the Brillouin scattering and scattering cross sections for each acoustic mode in iso- and anisotropic crystals are derived. In the latter part of this Chapter, microscopic treatments are discussed, based on the Loudon's original formulation where the exciton-contributions are taken into account.

2.2.1 Basic Theory of Brillouin Scattering(Macroscopic-Treatment)

Macroscopic treatments of Brillouin scattering from isotropic

crystals has been derived by Benedek and Fritsch,[31] in which the integral equations are solved. In the case of anisotropic crystals such as CdS it is essential for analyzing the scattering cross section to take into account the strong birefringence of the crystals. The following discussion is based upon the treatment of Hamaguchi[40] who extends the theory of Benedk and Fritsch to the case of anisotropic crystals. When field of light,

$$E = E_0 \exp[\, i\,(k_i \cdot r - \omega_i t)\,] \qquad (2.2\text{-}1)$$

is incident on a crystal, the scattered light field amplitude at an arbitrary position R is given by

$$E'(R,t) = -\left(\frac{\omega_i}{c}\right)^2 \frac{1}{4\pi R} \exp[\, i\,(k' \cdot R - \omega_i t)\,] \times I_k \times [I_k \times \int_v \delta\varepsilon(r,t) E_o \cdot \exp[i(K_i - k') \cdot r\,]\, dr \qquad (2.2\text{-}2)$$

where ω_i and c are the angular frequency and the velocity of the incident light in the free space, respectively. The wave vectors K_i and k' are defined by the following relations;

$$k_i = \frac{n_i}{c}\omega_i I_{ko}\,, \qquad k' = \frac{n_d \omega_i}{c} I_k \qquad (2.2\text{-}3)$$

where n_i and n_d are the refractive indices for the incident and scattered lights, and I_{ko} and I_k are the unit vectors in the directions of the incident and scattered lights wave vectors. The fluctuation in the dielectric constant can be originated from the existence of acoustic waves, in which there exist three possible process; (a) direct photoelastic effect (b) indirect photoelastic effect through the electro-optic effect and (c) body rotation of the atomic displacement. The effect of (a) is so called usual Brillouin scattering, (b) is indirect Brillouin scattering and (c) is the rotational contribution[39], which is shown schematically

in Fig. 2.1.

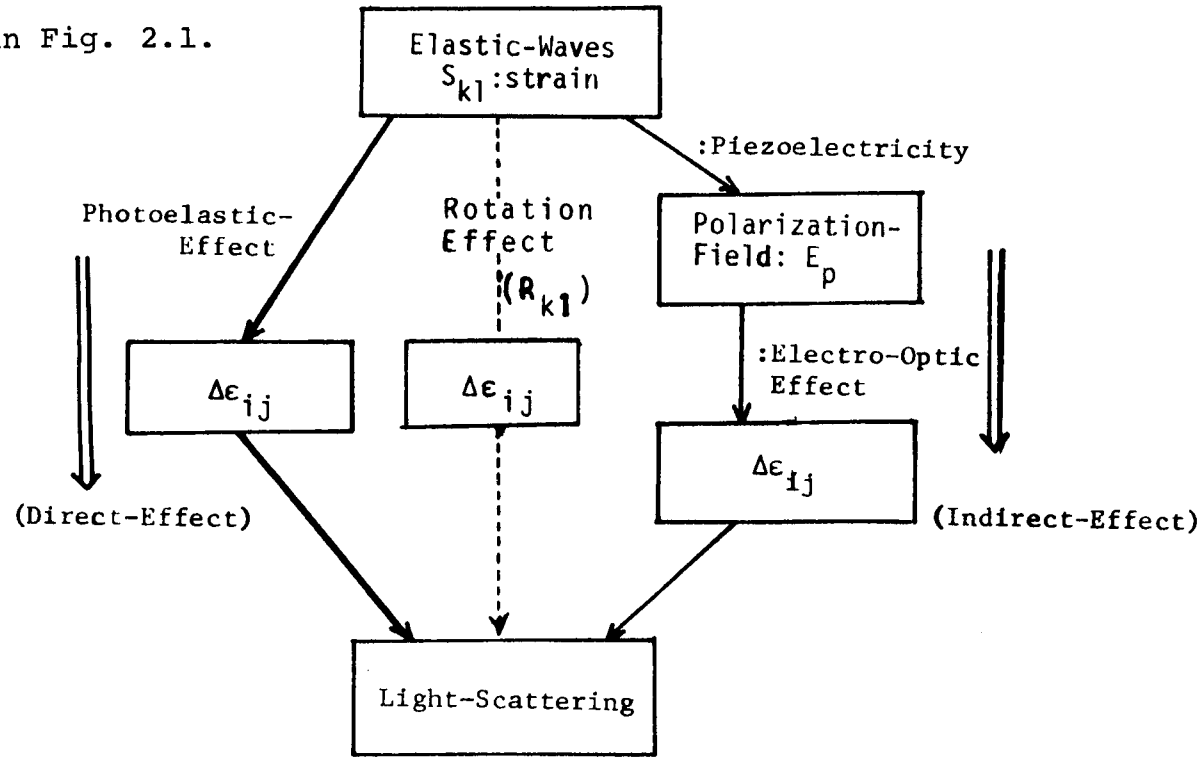

Fig. 2.1. Schematic explanation of direct, indirect and rotational Brillouin scattering.

As shown in Fig. 2.1 the indirect Brillouin scattering originates from the electro-optic effect, and thus this effect strongly dpends on the magnitudes of existing fluctuating field and electro-optic constant of the crystals. Indirect effect was pointed out by Nelson et al.[85] and by San'ya et al.[91] in CdS crystals, however, in the present experiment of resonant Brillouin scattering it is found to be unimportant event for the piezo-active acoustic phonons in CdS.[18,22] Rotational contribution is also found to be negligible effect.[18] Therefore we discuss only the direct photoelastic effect in this section. The fluctuation in the dielectrc constant $\delta\varepsilon$ due to the strain in the crystals can be expressed in terms of Fourier components;

$$\delta\varepsilon^{\mu}(r,t) = \left(\frac{1}{2\pi}\right)^{3/2}\sum_{\mu}\int |dq|\,\delta\varepsilon^{\mu}(q)\exp\left[i(q\cdot r \pm \omega_{\mu}(q)t'\right] \quad (2.2\text{-}4)$$

where $2\pi/|q|$ is the wavelength of the dielectric fluctuation.

The index μ denotes the possibility of a number of acoustic branches and $\omega_\mu(q)$ is the angular frequency of acoustic mode μ. By substituting eq.(2.2-4) into eq.(2.2-2) one obtains the magnitude of scattered light field $E'(R,t)$ at the point R,

$$E'(R,t) = -\left(\frac{\omega_i}{c}\right)^2 \frac{(2\pi)^{3/2}}{4\pi R} \cdot \sum_{\mu} \exp\left[i\{ k_s \cdot R - (\omega_i \pm \omega_\mu(q))t \}\right]$$
$$\times I_k \times [\, I_k \times (\delta\varepsilon^{\mu}(q) \cdot E_o)\,] \qquad (2.2\text{-}5)$$

where acoustic wave vector q is represented by the scattered light wave vector $k_s (= n_d[\omega_i \pm \omega_\mu(q)] I_k/c)$ as;

$$q = k_s - k_i \qquad (2.2\text{-}6)$$

Equation(2.2-6) means the momentum conservation between the incident and scattered photons and acoustic phonons. The term $\omega_i \pm \omega_\mu(q) = \omega_s$ refers to the angular frequency of scattered light, which corresponds to the energy conservation-law for stokes(+) and antistokes (-) scattering. First we estimate the incident and scattered light angles (θ_i and θ_d) in the Brillouin scattering of iso- and anisotropic crystals by considering the triangles of the momentum conservation(Fig.2.2).

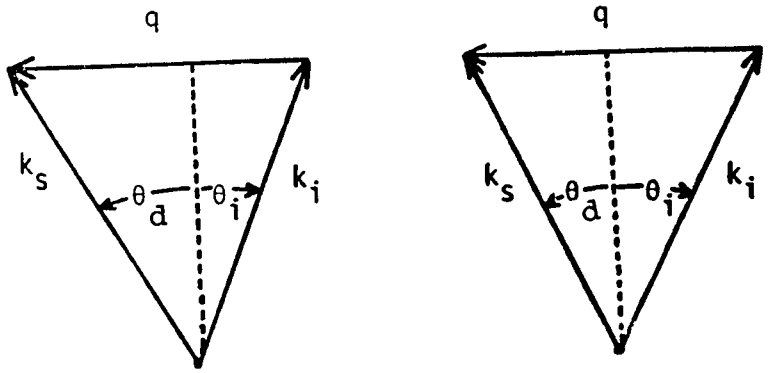

(a) anisotropic crystal

(b) isotropic crystal

Fig. 2.2. Momentum conservation between the incident and scattered photons and phonons for aniso- and isotropic crystals.

In Fig.2.2 the vectors k_i,k_s and q are waves vectors of incident and scattered lights and acoustic phonons, respectively. Generally the incident and scattered light angles(θ_i and θ_d) are not same in the anisotropic crystals, while θ_i is equal to θ_d in the case of isotropic crystals(Fig.2.2.(b)). From eq.(2.2-3) and Fig.2.2 one can obtain the following relations for the angles (θ_i and θ_d) to the case of anisotropic crystals;

$$\sin\theta_i = \frac{\lambda}{2n_i v_\mu}\left[f_q + \frac{v_\mu^2}{f_q\lambda^2}\left(n_i^2 - n_d^2 \right) \right] \qquad (2.2\text{-}7)$$

$$\sin\theta_d = \frac{\lambda}{2n_d v_\mu}\left[f_q - \frac{v_\mu^2}{f_q\lambda^2}\left(n_i^2 - n_d^2 \right) \right] \qquad (2.2\text{-}8)$$

where the subscripts'i' and 'd' denote'incident'and'scattered' respectively, λ is the incident light wavelength in the free space, v_μ the sound velocity of acoustic mode μ and f_q the frequency of the acoustic waves. On the other hand one can obtainthe following simple equation of θ_i and θ_d by using the relation; $n_i = n_d = n$ for the isotropic crystal;

$$\theta_i = \theta_d = \sin^{-1}\left(\frac{\lambda f_q}{2nv_\mu}\right) \qquad (2.2\text{-}9)$$

It should be noted here that the expressions of eqs.(2.2-7),(2.2-8) and (.2-9) are valid for the case, where the acoustic wave vector q is parallel to the surface of crystals(off axis angle $\delta = 0$).[40]

Now we evaluate the Brillouin scattering cross sectin for iso- and anisotropic crystals. The total power dI'(q,R) in all frequencies scattered into a solid angle $d\Omega'$at the field point R is proportional to the mean square field strength,

$$dI' = \frac{c}{8\pi}\left|\langle E'(q,t)\rangle\right|^2 R^2 d\Omega' \qquad (2.2\text{-}10)$$

The fluctuation $\delta\varepsilon^{\mu}(q,t)$ produces a corresponding flucuation in the electric displacement vector $\delta D(q,t)$ $(=\delta\varepsilon^{\mu}(q,t)\cdot E_o)$. As mentioned before in the direct Brillouin scattering mechanism the fluctuation of dielectric constant $\delta\varepsilon$ originates from that of the strain e_{kl}. Here the strain component e_{kl} is written in a convenient form by using the spacial Fourier-transformation as;

$$e_{kl}(q,t) = \frac{1}{(2\pi)^{3/2}} \int \frac{|dr|}{2} \left(\frac{\partial u_k}{\partial x_l} + \frac{\partial u_l}{\partial x_k}\right)$$

$$= \frac{i}{2} [u_k(q,t)q_l + u_l(q,t)q_k] \qquad (2.2\text{-}11)$$

where u_α refers to the α-component of displacement vector U and q_β to the β-componemnt of acoustic wave vector q. One can express the fluctuation in dielectric tensor component $\delta\varepsilon_{ij}(q,t)$ as a linear function of the elastic strain component $e_{kl}(q,t)$,

$$-\frac{\delta\varepsilon_{ij}(q,t)}{\varepsilon_{ii}\varepsilon_{jj}} = P_{ijkl}\cdot e_{kl}(q,t) \qquad (2.2\text{-}12)$$

where ε_{ii} is the diagonal component of the dielectric constant tensor in the absence of strains;

$$[\varepsilon_o] = \begin{bmatrix} \varepsilon_{11} & 0 & 0 \\ 0 & \varepsilon_{11} & 0 \\ 0 & 0 & \varepsilon_{33} \end{bmatrix} \quad \text{with} \quad \varepsilon_{11}=n_o^2 \text{ and } \varepsilon_{33}=n_e^2 \qquad (2.2\text{-}13)$$

and P_{ijkl} is the component of the photoelastic tensor [P]. The formulation of tensor [P] is very important to determine the complicated connection of $\delta\varepsilon_{ij}$ with existing strain components. One finds that the symmetry induced selection rule of Brillouin scattering is mainly determined by using the formulation of photoelastic constant tensor [P]. The tensor [P] is represented for the crystal with symmetry 6mm(CdS belongs to this symmetry) as,

$$\begin{bmatrix} P_{11} & P_{12} & P_{13} & 0 & 0 & 0 \\ P_{12} & P_{11} & P_{13} & 0 & 0 & 0 \\ P_{31} & P_{31} & P_{33} & 0 & 0 & 0 \\ 0 & 0 & 0 & P_{44} & 0 & 0 \\ 0 & 0 & 0 & 0 & P_{44} & 0 \\ 0 & 0 & 0 & 0 & 0 & P_{66} \end{bmatrix} \quad \text{with } P_{66}=(P_{11}-P_{12})/2 \qquad (2.2\text{-}14)$$

where the contracted notation is used in which pairs of indices are reduced to a single subscript running from 1 to 6. The one can write eq.(2.2-13) by using the above formulation of [P],

$$-\delta\varepsilon_{ij}(q,t) = 2P_{44}\cdot\varepsilon_{ii}\varepsilon_{jj}e_{ij}-2P_{44}\varepsilon_{ii}e_{ii}\delta_{ij}+\sum_{1'}P_{i1'}\varepsilon_{ii}e_{1'1'}\delta_{ij}$$

$$+2\left(\frac{P_{11}-P_{12}}{2}-P_{44}\right)\varepsilon_{11}^{2}e_{ij}(\delta_{i1}\delta_{j2}+\delta_{i2}\delta_{j1}) \qquad (2.2\text{-}15)$$

and thus the fluctuation in the electric displacement vector in the crystals δD is written,

$$\delta D(q,t) = \delta\varepsilon^{\mu}(q,t)\cdot E_o = \frac{\varepsilon_{11}^{2}}{i}E_o u^{\mu}(q,t)\zeta^{\mu} \qquad (2.2\text{-}16)$$

where, $\zeta^{\mu} = \frac{P_{44}}{\varepsilon_{11}^{2}}[\varepsilon_o\cdot\pi(\varepsilon_o I_q\cdot I_E)+(\varepsilon_o\pi\cdot I_E)\varepsilon_o I_q]-\frac{2P_{44}}{\varepsilon_{11}^{2}}\sum_{1'}\varepsilon_{1'1'}^{2}(\pi)_{1'}(I_q)_{1'}(I_E)_{1'}I_{1'}$

$$+\sum\left[\sum_{1'}P_{m1'}(\varepsilon_{mm}^{2}/\varepsilon_{11}^{2})(\pi)_{1'}\right](I_E)_m I_m+\left(\frac{P_{11}-P_{12}}{2}-P_{44}\right)\times$$

$$[\,(\pi)_1(I_q)_2(I_E)_2I_1+(\pi)_2(I_q)_1(I_E)_2I_1$$

$$+(\pi)_2(I_q)_1(I_E)_1I_2+(\pi)_1(I_q)_2(I_E)_1I_2\,] \qquad (2.2\text{-}17)$$

In eq.(2.2-17) the subscription $q=I_q|q|$, and $E_o=I_E|E_o|$ habe been introduced and π is the unit polarization vector in the direction of displacement vector U(q,t). The vector I_1(l=1,2 and 3) is unit vector along the cube axis OX_1,OX_2 and OX_3 defined in the text of Nye[50] where OX_3 is parallel to the c-axis of the crystals. It should be noted that one can observe not ζ^{μ}but the component of ζ^{μ} in the plan perpendicular to the scattered wave vector k_s, which

is given by

$$\xi^{\mu} = I_k \times (I_k \times \zeta^{\mu}) \qquad (2.2\text{-}18)$$

The vector ξ^{μ} therefore determine explicitly the polarization direction of the scattered light from each acoustic mode μ. From eqs.(2.2-5),(2.2-10) and (2.2-16) we obtain the power dI' of scattered light under the condition ; $h\omega^{\mu}(q) \ll k_B T$,

$$dI' = \frac{cE_o^2}{8\pi} \left(\frac{\omega_i}{c}\right)^4 \frac{V}{(4\pi)^2} \sum_{\mu} \frac{|\xi^{\mu}|^2}{2\rho v_{\mu}^2} h\omega_{\mu}(q) [<n_{\mu}(q)>+1+<n_{\mu}(q)>] d\Omega' \qquad (2.2\text{-}19)$$

where $n_{\mu}(q)$ is the occupation number of acoustic phonons for mode μ. Finally the intensity of light scattered into the solid angle $d\Omega'$ during the optical path length b is given by,

$$dI' = I_o \frac{\pi^2 n_o^8}{\lambda^4} \sum_{\mu} \frac{k_B T}{2} \frac{|\xi^{\mu}|^2}{\rho v_{\mu}^2} b d\Omega' \qquad (2.2\text{-}20)$$

where I_o is the intensity of incident light. It is found that the solid angle $d\Omega'$ is the internal solid angle in the specimen, therefore the internal solid angle $d\Omega'$ should be replaced by external solid angle $d\Omega_o$ using the following relation;[40] $d\Omega' = \cos\theta_d \cdot d\Omega_o / (n_d \times \sqrt{n_d^2 - \sin^2\theta_d})$.[40] The term of $d\Omega'$ is found to slightly depend upon the wavelength of the incident light. In the present study the amplified accustic phonons of the order of $10^6 \sim 10^8$ above the thermal phonons were mainly used and therefore the factor $k_B T$ is eq.(2.2-20) should be also replaced by the acoustic flux energy Φ_{ac}.
By considering those facts one can finally find the Brillouin scattering cross section σ_B as,

$$\sigma_B = \frac{\pi^2 n_o^8}{\lambda^4} \sum_{\mu} \frac{\Phi_{ac}}{2} \frac{|\xi^{\mu}|^2}{\rho v_{\mu}^2} d\Omega' \qquad (2.2\text{-}21)$$

The expression of eq.(2.2-21) is useful for both iso- and anisotropic crystals and is found just to correspond to that of Nelson et al..[39] Now as mentioned above, it should be kept in mined that

eq.(2.2-21) is valid only for the transparent photon energy region, where there exist no electronic excitations(no interband excitations of electrons), and scattering cross section σ_B is described by the form: $\sigma_B \propto \lambda^{-4}$. However, the expressions of σ_B derived in this section never predict the resonance-structure near the intrisic band edge of crystals. In the case of cubic crystals such as ZnSe, those discussion stated above are essentially valid. The photoelastic constant tensor of ZnSe belonging to the class $\bar{4}3m$ is represented as,

$$\begin{pmatrix} P_{11} & P_{12} & P_{12} & 0 & 0 & 0 \\ P_{12} & P_{11} & P_{12} & 0 & 0 & 0 \\ P_{12} & P_{12} & P_{11} & 0 & 0 & 0 \\ 0 & 0 & 0 & P_{44} & 0 & 0 \\ 0 & 0 & 0 & 0 & P_{44} & 0 \\ 0 & 0 & 0 & 0 & 0 & P_{44} \end{pmatrix} \qquad (2.2\text{-}22)$$

As shown from eq.(2.2-22) the independent photoelastic components are only P_{11}, P_{12} and P_{44} hence one can obtain the more simple formulation of vector ζ^{μ} for the cubic crystals,[31)]

$$\zeta^{\mu} = P_{44}[\ (\pi)\cdot(I_q\cdot I_E) + (\pi\cdot I_E)I_q] + P_{12}(\pi\cdot I_q)I_E$$
$$+(P_{11}-P_{12}-2P_{44}) \sum_{I'} (\pi)_{I'}(I_q)_{I'}(I_E)_{I'}I_{I'} \qquad (2.2\text{-}23)$$

where the notation are the same as the case of anisotropic crystals and errors in ref. 31 are corrected(see ref.40). In order to estimate the intensity of Brillouin scattering one has to evaluate the factor $|\xi|^2/\rho v^2$ for each experimental condition. In the next section we summarized the complete expressions of Brillouin scattering cross section according to each acoustic mode μ (T1,T2 and PL modes).

2.2.2 Brillouin Scattering Cross Sections for each Acoustic Mode

The following discussions are intended to estimate the Brillouin scattering cross section by acoustic waves propagating along a particular crystallographic direction. The acoustic modes used in the present work of CdS and ZnSe are two kinds of transverse acoustic waves (T1 and T2) and pure longitudinal mode (PL). The experimental configurations of Brillouin scattering by each acoustic mode are summarized in Table 2.I. for CdS and ZnSe.

Table 2.I. Experimental configuration for each acoustic mode in CdS and ZnSe.

[CdS]	T2-mode	$I_q \perp$ c-axis	$\pi \parallel$ c-axis	$I_E \parallel$ c-axis
	T1-mode	$I_q \perp$ c-axis	$\pi \perp$ c-axis	$I_E \perp$ c-axis
	PL-mode	$I_q \perp$ c-axis	$\pi \perp$ c-axis	$I_E \parallel$ c-axis
[ZnSe]	T2-mode	$I_q \parallel [001]$	$\pi \parallel [1\bar{1}0]$	$I_E \parallel [1\bar{1}0]$
	T1-mode	$I_q \parallel [110]$	$\pi \parallel [1\bar{1}0]$	$I_E \parallel [1\bar{1}0]$

Case (a): T2-mode.

This acoustic mode wave is piezoelectrically active and propagates in the c-plane with polarization vector parallel to the c-axis. Form Table 2.I one can easily find,

$$I_q = [\,1, 0, 0\,], \quad \pi = [\,0, 0, 1\,] \text{ and } I_E = [\,0, 0, 1\,] \tag{2.2-24}$$

In this case eq.(2.2-18) reduces to,

$$\zeta^{T2} = \frac{P_{44}}{\varepsilon_{11}^2} [\,(\varepsilon_o \cdot \pi) \cdot I_E\,]\, \varepsilon_o \cdot I_q \tag{2.2-25}$$

and electric-scattering vector ξ^{T2} is given by,

$$\xi^{T2} = P_{44}(\varepsilon_{33}/\varepsilon_{11})\, F(f_q, \lambda)\, I_\perp \tag{2.2-26}$$

where the notation $F(f_q,\lambda)=|I_k \times I_q|$ is introduced and $I_\perp$ is the unit vector perpendicular to the incident light polarization which determines the polarization direction of scattered light. The facttor $F^{T2}(f_q, \lambda)$ is determined so as to correspond to the experimental condition in the T2-mode Brillouin scattering in CdS as,

$$F^{T2}(f_q,\lambda) \doteq \{1- \frac{1}{4n_o^2} \frac{\lambda^2}{v_{T2}^2 f_q^2} [f_q^2 + \frac{v_{T2}^2}{\lambda^2} (n_o^2 - n_e^2)^2 \}^{1/2} \quad (2.2\text{-}27)$$

and finally one can find the expression of $|\xi|^2/\rho v^2$ for T2-mode acoustic waves,

$$\frac{|\xi^{T2}|^2}{\rho v_{T2}^2} = \frac{P_{44}^2}{C_{44}} (\frac{n_e}{n_0})^4 \cdot F^{T2}(f_q,\lambda) \quad (2.2\text{-}28)$$

Equation (2.2-28) is also valid in the case of ZnSe, when we use the condition; $n_o = n_e$.

Case (b) : Tl-mode.

This acoustic mode is piezoelectrically inactive, which can be generated by mode conversion at the end of the specimens. From the Table 2.I one finds,

$$I_q = [1,0,0] \quad \text{and} \quad \pi = [0,1,0] \quad (2.2\text{-}29)$$

and I_E is in the OX_2-OX_3 plane. In this case one obtains,

$$\zeta^{Tl} = \frac{P_{11}-P_{12}}{2} \quad \text{and} \quad \xi^{Tl} = \frac{P_{11}-P_{12}}{2} F^{Tl}(f_q,\lambda) I_{//} \quad (2.2\text{-}30)$$

where $I_{//}$ is the unit vector lying in the OX_1-OX_3 plane, which means that the scattered light polarization is also perpendicular to that of incident light. By an analogy to the case of T2-mode one obtains the factor $|\xi^{Tl}|^2/\rho v^2$ for Tl-mode of CdS,

$$\frac{|\xi^{Tl}|^2}{\rho v_{Tl}^2} = \frac{(P_{11}-P_{12})^2}{2(C_{11}-C_{12})} \cdot F^{Tl}(f_q,\lambda) \quad (2.2\text{-}31)$$

$$\text{with} \quad F^{T1}(f_q,\lambda) = \{1- \frac{1}{4n_d^2} \frac{\lambda^2}{v_{T1}^2 f_q^2}[f_q^2+(\frac{V_{T1}}{\lambda})^2(n_d^2-n_o^2)]^2\}^{1/2} \quad (2.2\text{-}32)$$

where n_d is the refractive index of scattered light and n_o is the ordinary refractive index of CdS. It is also found that eq.(2.2-32) is valid for the case of isotropic crystal ZnSe using the condition ; $n_d = n_o$.

Case (c) : PL-mode.

The pure longitudinal acoustic mode(PL) used in the present study propagates in the c-plane with displacement vector parallel to the propagation direction. In this case the incident lights with polarization vector parallel to the c-axis are used in the experiment and therefore one obtains;

$$I_q = [0,-1,0], \ \pi = [0,-1,0] \text{ and } I_E = [0,0,1] \quad (2.2\text{-}33)$$

By using the result listed in Table 2.I. the following equation is found for the case of PL-mode,

$$\zeta^{PL} = (\frac{\varepsilon_{33}}{\varepsilon_{11}})^2 P_{31} I_3 \quad \text{and} \quad \xi^{PL} = \frac{P_{31}^2}{C_{11}} (\frac{\varepsilon_{33}}{\varepsilon_{11}})^2 I_{//} \quad (2.2\text{-}34)$$

Finally we obtain,

$$\frac{|\xi^{PL}|^2}{\rho v_{PL}^2} = \frac{P_{31}^2}{C_{11}} \quad (2.2\text{-}35)$$

where $I_{//}$ is the unit vector parallel to the polarization of incident light and the relation; $n_i = n_d$ is taken into account. It is found in the case of PL-mode Brillouin scattering that the polarization direction of scattered light is not rotated from that of incident light. The results of Brillouin scattering cross sections and polarization relations between the incident and scattered light by the acoustic modes used in the present work are summarized in Table 2.II.

Table 2.II. Relevant photoelastic constants and polarization relations in the Brillouin scattering.

		relevant photoelastic constants	polarization-relations
[CdS]	T2-mode:	P_{44}	$I_E \perp I_A$
	T1-mode:	$P_{11}-P_{12}$	$I_E \perp I_A$
	PL-mode:	P_{31}	$I_E \parallel I_A$
[ZnSe]	T2-mode:	P_{44}	$I_E \perp I_A$
	T1-mode:	$P_{11}-P_{12}$	$I_E \perp I_A$

2.3. Basic Theory of Resonant Brillouin Scattering(Microscopic Treatment)

In the previous section we considered the scattering efficiency for each acoustic mode phonon in a perfect transparent region. In such conditions the basic treatment of scattering mechanism is considered to originate from the momentum and energy conservation laws between the photons and the relevant phonons. It is found from the macroscopic treatment that the Brillouin scattering cross section σ_B has λ^{-4}-dependence for the incident light wavelength. Then the theoretical expression of Brillouin scattering derived in section 2.2 can not explain the resonance (or antiresonance) structure in the dispersion spectra. We observed in this section a basic treatment of resonant Brillouin scattering in the photon energy region of fundamental absorption edge based upon Loudon's theory[20] are presented.

The resonant Brillouin (or Raman) effect originates from the mutual interaction between the incident and scattered photons and acoustic (optical) phonons including the electronic excitations as a intermediate virtual states. This physical explanation is, in general., treated by using the time-dependent perturbation theory.

In the first order resonant Brillouin effect, a beam of photons with frequency ω_i is incident and radiation with frequency ω_s emitted from the crystals, $|\omega_s-\omega_i|$ being the frequency of a long wavelength lattice vibration. In the present discussion all quantities refering to the incident photons have a subscript 'i' and those refering to the radiated photons have a subscript 's'. In the crystals used in the present work there is one simple process by which the resonant sscattering can occur. The process involves three virtual electronic transitions accompanied by the following photon and phonon transitions; (1) a photon ω_i is absorbed, (2) an acoustic phonon ω_q is created or destructed (3) photon $\omega_s(=\omega_i \pm \omega_q)$ is radiated. The three transition process can occur in any time-order, giving six types of process. Now we write the total Hamiltonian H_T corresppponding to the mixing system of photons, phonons and electrons,

$$H_T = H_T^o + H_I \qquad (2.3\text{-}1)$$

$$\text{with} \quad H_T^o = H^o_{photon} + H^o_{phonon} + H^o_{electron}, \qquad (2.3\text{-}2)$$

$$\text{and} \quad H_I = H_{EL} + H_{ER}$$

where H_T^o corresponds to the Hamiltonian for the unperturbed state including the photon phonon and electron, and H_I is interaction Hamiltonian, which is formally divided into two parts H_{EL} and H_{ER} corresponding to the interactions between the electrons and phonons and between the electrons and photons, respectively. Suppose that at time zero the crystal is in its electronic ground state and the photons ω_i are incident. The probability that at time T one photon ω_i is destroyed and one photon ω_s and one phonon ω_q are created, is given by,

$$P(T) = \left| \langle n_i-1, n_s+1, n_q+1 : o \left| e^{-iH_T \cdot T/\hbar} \right| n_i, n_s, n_q : o \rangle \right|^2 \qquad (2.3\text{-}3)$$

The transition probability P(T) of eq.(2.3-3) corresponds to the process of anti-stokes Brillouin effect and this is derived under the condition that the initial and final electronic states are the same. By the theory of time-dependent perturbation the transition rate P(T) is represented in the following way;[51]

$$P(T) = \frac{2}{\hbar^2} \left| \langle f|H_I|u\rangle + \frac{1}{\hbar} \sum_{m_1} \frac{\langle f|H_I|m_1\rangle\langle m_1|H_I|u\rangle}{(\omega_u - \omega_{m1})} + \right.$$

$$\left. \cdots\cdots + \frac{1}{\hbar^{n-1}} \sum_{m_1 \cdots m_{n-1}} \frac{\langle f|H_I|m_{n-1}\rangle \cdots \langle m_1|H_I|u\rangle}{(\omega_u - \omega_{m_{n-1}}) \cdots (\omega_u - \omega_{m_1})} \right|^2$$

$$\times \delta(\omega_u - \omega_f). \qquad (2.3\text{-}4)$$

In the above equation, $|m_1\rangle, |m_2\rangle \cdots |m_{n-1}\rangle$ are the intermediate virtual states of electronic excitations, $|u\rangle$ and $|f\rangle$ are the initial and final states, respectively. The part of delta-function means the energy conservation of the system.

For the direct gap-semiconductors such as CdS and ZnSe, third order term in eq.(2.3-4) plays an important role in the effect of fundamental resonant Brillouin scattering (first-order Brillouin scattering), which is given by using two intermediate virtual states,

$$P(T) = \frac{2\pi}{\hbar^8} \times \sum \left| \frac{\langle f|H_I|m_2\rangle\langle m_2|H_I|m_1\rangle\langle m_1|H_I|u\rangle}{(\omega_u - \omega_{m_2})(\omega_u - \omega_{m_1})} \right|^2$$

$$\times \delta(\omega_u - \omega_f) \qquad (2.3\text{-}5)$$

This expression is a basic formulation to analyze the first order resonant Brillouin scattering of direct gap materials, while we should use the fifth order term in eq.(2.3-4) to discuss the

resonance effect in the case of indirect gap materials such as GaP.[52] Now we consider the complete expression of each interaction Hamiltonian H_{EL} and H_{ER} in order to perform the caluculation of eq.(2.3-5). In the present analyses we will adopt the vector potential representation for the interaction Hamiltonian H_{ER} which is written by using the creation a^+ and destruction a^- operators,

$$H_{ER} = \frac{e}{m} \sum_j \sum_k \left(\frac{2\pi h}{\eta V \omega_k}\right)^{1/2} \left[a_k^- e^{ik\cdot r_j} + a_k^+ e^{-ik\cdot r_j} \right] \left(\hat{\varepsilon}_k \cdot P_j\right) \qquad (2.3\text{-}6)$$

wher P_j and r_j are the momentum and position vectors of electron j, η is the optical dielectric constant, V the crystal volume, and $\hat{\varepsilon}_k$ is the unit polarization vector of the photon k. Here it is found that the matrix element of H_{ER} between pair states $|\alpha\rangle$ and $|\beta\rangle$ can be non-vanishing only where $|\alpha\rangle$ and $|\beta\rangle$ differ either in the states of a single hole or electron.

The electron-lattice interaction was derived by taking into account the deformation potential interaction between the electrons (or holes) and acoustic phonons. For a long wavelength acoustic vibration of crystals including two atoms in the unit cell, the displacement vector U(R) at position R is given by,

$$U(R) = \left(\frac{h}{2(M_1+M_2)N\omega_{sk}} \right)^{1/2} \xi_{sk} \cdot e^{ik\cdot R} \left(b_{s-k}^+ + b_{sk}^- \right) \qquad (2.3\text{-}7)$$

where M_1 and M_2 are the masses of the atoms in the two sublattice, N is a number of unit cells and ξ_{sk} is a unit polarization vector, and b_s^+ and b_s^- are the creation and destruction operators of phonons, in the branch s, respectively. It is intuitively obvious that a uniform displacement of the whole crystal can produce no electron (or hole)-lattice interaction. One can obtain the most important term of H_{EL} by using the following strain component S_{ij},[53,54]

$$S_{ij} = \frac{\partial U_i}{\partial R_j} = i \left(\frac{\hbar}{2(M_1+M_2)N\omega_{sk}} \right)^{1/2} \xi_{sk} k_j e^{ik\cdot R} \left(b_{s-k}^+ + b_{sk}^- \right) \qquad (2.3\text{-}8)$$

$$= S_{ij}^+ + S_{ij}^-$$

The matrix element of H_{EL} is represented by using eq.(2.3-8),

$$(\alpha|\, H_{EL}\,|\beta) = \Xi^{ij}_{\alpha\beta}\cdot\bar{S}_{ij} \qquad (2.3\text{-}9)$$

where the repeated indices 'i' and 'j' refer to the coordinates axis (x, y and z) and $\bar{S}_{ij}$ is the same as S_{ij} in eq.(2.3-8) but with the exponential removed. Since H_{EL} is one electron perturbation Hamiltonian, $|\alpha\rangle$ and $|\beta\rangle$ can differ either in the hole state or in the electron state, but not in both states. It is noticeable that if we assume that all the intermediate virtual states are free electrons in the conduction band, all the matrix elements of H_{EL} are zero because of s-like wave functions in semiconductor in which we are interested. However if we assume that the virtual states are holes or excitons it is found that the matrix elements can be non zero which means that the resonant Brillouin effects can be originated through the transitions of intermediate virtual holes (or excitons).[18] The detailed discussions of deformation potential scattering of holes (or excitons) will be stated in the next section.

Here we consider the formulation of Brillouin (or Raman) tensor by taking into account of possible transition process in eq.(2.3-5). The Brillouin tensor R_{is} for the first order resonance is represented by using the six types of transition process;

$$R_{is}(-\omega_i,\omega_q,\omega_s) = \frac{1}{V}\sum_{\alpha,\beta}\{\frac{P_{o\beta}\Xi_{\beta\alpha}P_{\alpha o}}{(\omega_\beta+\omega_q+\omega_s)(\omega_\alpha+\omega_q)} + \frac{P_{o\beta}\Xi_{\beta\alpha}P_{\alpha o}}{(\omega_\beta+\omega_q+\omega_s)(\omega_\alpha+\omega_q)}$$

$$+ \frac{P_{o\beta}\Xi_{\beta\alpha}P_{\alpha o}}{(\omega_\beta+\omega_q-\omega_i)(\omega_\alpha-\omega_i)} + \frac{P_{o\beta}\Xi_{\beta\alpha}P_{\alpha 0}}{(\omega_\beta+\omega_q+\omega_s)(\omega_\alpha+\omega_s)}$$

$$+ \frac{\Xi_{o\beta}P_{\beta\alpha}P_{\alpha o}}{(\omega_\beta+\omega_s-\omega_i)(\omega_\alpha-\omega_i)} + \frac{\Xi_{o\beta}P_{\beta\alpha}P_{\alpha o}}{(\omega_\beta+\omega_s-\omega_i)(\omega_\alpha+\omega_s)}\} \qquad (2.3\text{-}10)$$

The six terms of eq.(2.3-10) arise from the six types of scattering process and it is important to choose the term which mainly contributes to the resonant Brillouin effect observed in the present work. It is found that the third term in Brillouin tensor plays the most important role in the resonant scattering. The physical interpretation of this term is represented as the following ; (1) incident photons ω_i are firstly absorbed and some kinds of electronic-excitaions can be generated in the crystals (2) one virtual state of electronic excitation interacts with the acoustic phonons and makes a transition to another virtual state, and (3) the virtual state is destroyed and scattered photon ω_s is radiated from the crystal. The signs attached to the angular frequencies in R_{is} of eq.(2.3-10) are chosen so that a negative (positive) frequency corresponds to the destruction (creation) of the appropriate photons or phonons. We define the microscopic scattering cross section σ_B by the following equation;

$$\sigma_B = \frac{N_s}{N_i} \frac{1}{L\Omega} \tag{2.3-11}$$

where N_i and N_s are the numbers of incident and scattered particles, L is the optical path length in the crystals and Ω is the solid angle determined by the detector-system. The ratio N_s/N_i is connected to the transition probability P(T) defined in eq.(2.3-4) by the relation;

$$\frac{N_s}{N_i} = \frac{P(T)L}{Tc'N_i} \tag{2.3-12}$$

where c' is the velocity of light in the crystal. After a simple calculation one obtains the expression of scattering cross section σ_B for the case of thermal acoustic phonons,

$$\sigma_B = \left(\frac{e}{\hbar mc}\right)^4 \frac{k_B T}{2\rho v_j^2} \frac{\omega_s}{\omega_i} \left| R_{is}(-\omega_i, \omega_q, \omega_s) \right|^2 \tag{2.3-13}$$

where $$R_{is} = \frac{1}{V}\sum_{\alpha\beta}\frac{P_{\beta o}\Xi_{\beta\alpha}P_{\alpha o}}{(\omega_\beta+\omega_q-\omega_i)(\omega_\alpha-\omega_i)} \qquad (2.3\text{-}13)$$

In eq.(2.3-13) $\hbar\omega_\alpha$ and $\hbar\omega_\beta$ are energies of intermediate virtual states of electronic excitations $|\alpha>$and$|\beta>$, respectively, By using the parabolic(band) approximation one can find the expression of microscopic scattering efficiency R_{is} as;

$$R_{is}^{jk} = \frac{2}{(2\pi)^2}P_{o\beta}\Xi_{\beta\alpha}P_{\alpha o}\cdot\int_{B.Z.}\frac{4\pi k^2 dk}{(\omega_{gs}+\omega_q-\omega_i+\frac{\hbar k^2}{2\mu})(\omega_{gi}-\omega_i+\frac{\hbar k^2}{2\mu})} \qquad (2.3\text{-}14)$$

where $\hbar\omega_{gi}$ and $\hbar\omega_{gs}$ are the energy gaps for incident and scattered lights and μ the effective masses of two intermediate virtual holes. Equation (2.3-14) has an important role in discussing the resonance effect near the intrinsic edge of crystals. After performance of integration in this equation, following expression is derived;[19)]

$$R_{is}^{jk} = \frac{1}{(2\pi)^2}\sum_{\alpha\beta}\left(\frac{2\mu}{\hbar}\right)^{3/2}\cdot\frac{P_{o\beta}\Xi_{\beta\alpha}P_{\alpha o}}{\omega_{g\beta}-\omega_{g\alpha}+\omega_q}$$

$$\times\left[(\omega_{g\beta}-\omega_s)^{1/2}\tan^{-1}\left(\frac{\Delta\omega_\beta}{\omega_{g\beta}-\omega_s}\right)^{1/2}-(\omega_{g\alpha}-\omega_i)^{1/2}\tan^{-1}\left(\frac{\Delta\omega_\alpha}{\omega_{g\alpha}-\omega_i}\right)^{1/2}\right]$$

..... (2.3-15)

where $\hbar\Delta\omega_\alpha$ and $\hbar\Delta\omega_\beta$ denote the combined width of energy for $|\alpha>$ and $|\beta>$ band, respectively. In the calculation of eq.(2.3-15) we assumed that the types of the critical point is M_o-type and that the effective masses of the two different pair bands are the same. Equation (2.3-15) may be approximated in the photon energy region close to the critical point of band structur,

$$R_{is}(-\omega_i,\omega_q,\omega_s) \sim \frac{1}{4\pi}\sum_{\alpha,\beta}\left(\frac{2\mu}{\hbar}\right)^{3/2}P_{o\beta}\Xi_{\beta\alpha}P_{\alpha o}$$

$$\times\frac{1}{\omega_q}\left[(\omega_{g_\beta}-\omega_s)^{1/2}-(\omega_{g\alpha}-\omega_i)^{1/2}\right] \qquad (2.3\text{-}16)$$

By using the eqs.(2.3-15) and (2.3-16) one can estimate the resonant contribution R_{is} near the direct-edge of semiconductos which is shown in Fig. 2.3. where two band model ($\omega_{g\alpha}=\omega_{g\beta}$) is used.

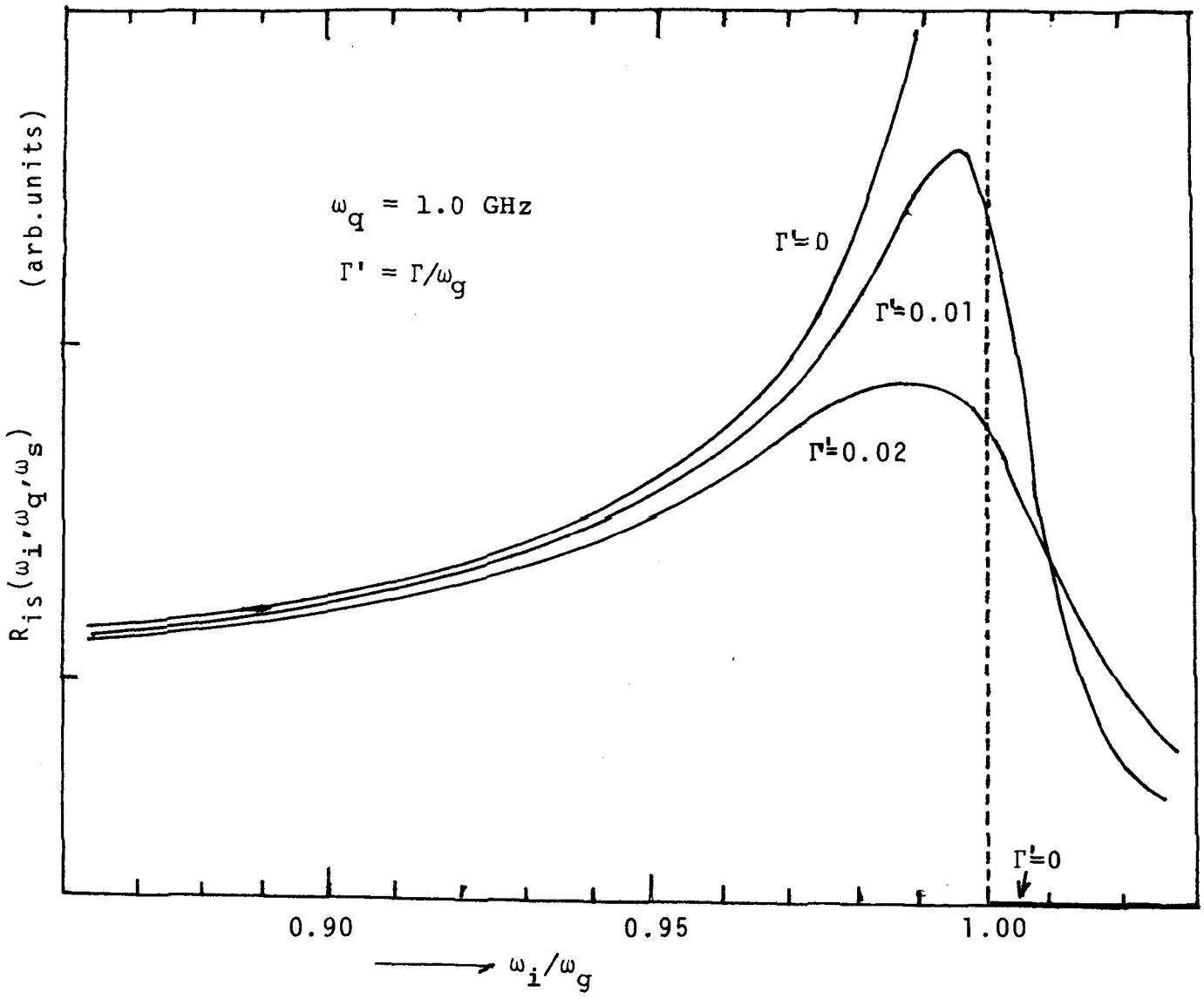

Fig. 2.3. Calculated dispersions of resonant Brillouin tensor $R_{is}(\omega_i,\omega_q,\omega_s)$ for acoustic frequency 1.0 GHz. In the calculation three kinds of broadening parameters ($\Gamma/\omega_g=0$, $\Gamma/\omega_g=0.01$ and $\Gamma/\omega_g=0.02$) are used.

It is found in Fig.2.3. that the resonant contribution R_{is} rapidly increases in the photon energy close to the intrinsic band edge of semiconductors. The total scattering efficiency σ_{BT} which is proportional to the observed dispersion curves in the present work is written by taking into account of the resonant and nonresonant contribution (R_o) by[6],

$$\sigma_{BT} = | R_{is} - R_o |^2 \qquad (2.3\text{-}17)$$

Such a theoretical treatment was first proposed byRalston et al.[6] in order to explain the structure of resonant cancellation in the Raman spectra of CdS. Provided that the treatment of eq.(2.3-16) stands for the resonance mechanism in Brillouin scattering it is found from eqs.(2.3-15) and (2.3-16) that one can observe the anti-resonance-structure in the dispersion spectra of Brillouin scattering cross section. From the present experimental results one can find that eq.(2.3-16) is very useful to analyze experimental data for the case of Brillouin scattering by the transverse phonons.

In the case of Brillouin scattering by pure longitudinal phonons (PL-mode) we do not find the antiresonance in the dispersion spectra, which is due to the fact that the sign of main resonant contribution R_{is} is the same as that of non-resonant contribution arising from the higher energy bands in the PL-mode phonon Brillouin scattering. Such analyses about the signs of resonant and non-resonant contributions are important and discussed in the latter section in connection with the analyses of deformation potential scattering.

2.4. Excitonic Resonant Brillouin Scattering

In this section we discuss a formulation of resonant Brillouin scattering, where the intermediate virtual states are the discreate and continuum excitons. The treatment of excitonic resonant-Brillouin scattering were derived by Gungly and Birman[21] by solving the third order perturbation problem in the second quantized formulation. It is also possible to show that the expression of resonant Brillouin scattering effect including the exciton contributions can be derived by using the Loudon's original formulation. First we consider the Wannier-type exciton contributions[55] to the resonant enhancement. In the parabolic band model, the energy of the exciton concerning to the conduction band (c) and valence band (v) is given by using the exciton's wave vector K,

$$E_{n,k}(c,v) = E_g + \hbar^2 K^2 /2(m_e^*+m_h^*) - \frac{R}{n^2} \qquad (2.4\text{-}1)$$

for discrete exciton states with n=1,2,3$\cdots$, and

$$E_K(c,v) = E_g + \hbar^2 K^2 /2\mu \qquad (2.4\text{-}2)$$

for the continuum states, where R is the exciton binding energy and μ is the reduced exciton mass ($1/\mu = 1/m_e^* + 1/m_h^*$). We already found that the density of states of excitons in direct-edge materials is represented by $1/(\pi a_o^3 n^3)$ for n-th discreate exciton and $\pi\alpha \cdot \exp(\pi\alpha)/\sinh\pi\alpha$ for the continuum exciton states, where a_o is Bohr radius and α is written $|R/(\hbar^2K^2/2\mu)|^{1/2}$. Here we introduce the 3-Band model as the case where $|\alpha\rangle \neq |\beta\rangle$ and thus three different bands take part in the electronic excitations. Taking into account of the 3-Band model one can obtain the excitonic scattering efficiency R_{is}^{ex} based upon the Loudon's formulation of eq.(2.3-14),

$$R_{is}^{ex} \sim \sum_{\alpha\beta} P_{o\beta}\Xi_{\beta\alpha}P_{\alpha o}\{\sum_{n}\frac{1}{\pi a^3 n^3}\frac{1}{(\omega_g - R^*/n^2-\omega_q-\omega_i)(\omega_g - R^*/n^2-\omega_i)}$$

$$+\frac{1}{(2\pi)^3}\int dK\cdot\frac{\pi\alpha e^{\pi\alpha}}{\sinh\pi\alpha}\frac{1}{(\omega_{g\beta}-\omega_q-\omega_i+\hbar K^2/2\mu)(\omega_{g\alpha}-\omega_i+\hbar K^2/2\mu)} \quad (2.4\text{-}3)$$

where $R^* = R/\hbar$ is introduced. In eq.(2.4-3) the first term corresponds to the contribution from discrete levels and the second term from the continuum electron-hole pair states. Generally, the values of $\omega_{g\alpha}$ is different fromthat of $\omega_{g\beta}$ in the 3-Band model, but in the case where the intraband transition of virtual excitations occurs through the interaction with acoustic phonons, $\omega_{g\alpha}$ is equal to $\omega_{g\beta}$. In such a case eq.(2.4-3) reduces to the same expression as that of Gungly and Birman ($\omega_{g\alpha}=\omega_{g\beta}=\omega_g$). Integrating eq.(2.4-3) one finds,[§, 76)]

$$R_{is}^{ex} \sim \sum_{\alpha\beta}\frac{P_{o\beta}\Xi_{\beta\alpha}P_{\alpha o}}{\omega_{g\alpha}-\omega_{g\beta}+\omega_q}\{\frac{1}{\pi a^3}\sum_{n}[\frac{1}{\omega_{g\beta}-R^*/n^2-\omega_q-\omega_i}-\frac{1}{\omega_{g\alpha}-R^*/n^2-\omega_i}]$$

$$+\frac{i}{4\pi}(\frac{2\mu}{\hbar})^{3/2}(4\pi^2R^*)^{1/2}\{\frac{1}{1-\exp[-(-\frac{4\pi^2R^*}{\omega_{g\beta}-\omega_s})^{1/2}]}-\frac{1}{1-\exp[-(-\frac{4\pi^2R^*}{\omega_{g\alpha}-\omega_i})^{1/2}]}\}\} \quad (2.4\text{-}4)$$

In eq.(2.4-4) the virtual states $|\alpha>$and$|\beta>$ are excitons and the summation must be performed for all the possible transition process. In the case of cubic crystals two valence bands but for the spin-orbit split off band are degenerated at the top of valence band (Γ-point), then the relation; $\omega_{g\alpha}-\omega_{g\beta}=0$ exists. In this case we can obtain more simplified formulation of excitonic resonant Brillouin scattering than the case of wurtzite materials.

---

§ We found typographycal erros in the equation derived by Gangly and Birman(ref.21) and our paper(ref.18). Correct form is given in the above equation.

2.5. Matrix Elements of Deformation Potential Scattering by Long Wavelength Acoustic Phonons.

This section is mainly devoted to determine the non-vanishing matrix elements of deformation potential scattering of holes (or excitons) in the wurtzite type crystals. In the present analyses three unperturbed wavefunctions corresponding to the three A, B and C valence bands and strain orbital Hamiltonian H_{xv} are used. The strain orbital Hamiltonian for p-like valence bands of wurtzite material at Γ-point is given by,[57-59]

$$H_{xv} = (C_1+C_3L_z^2)e_{zz} + (C_2+C_4L_z^2)(e_{xx}+e_{yy}) + c_5(L_-^2e_+ + L_+^2e_-)$$
$$+ C_6([L_zL_+]e_{-z} + [L_zL_-]e_{+z}) \qquad (2.5\text{-}1)$$

and for the electrons in the conduction band by

$$H_{xc} = d_1 e_{zz} + d_2(e_{xx} + e_{yy}) \qquad (2.5\text{-}2)$$

where the coefficients C_i and d^i are deformation potentials, the e_{ij}'s are components of strain tensor with $e_\pm=e_{xx}-e_{yy}\pm 2ie_{xy}$ and $e_{\pm z}=e_{xz}\pm ie_{yz}$, $L_i, L_\pm$ are the standard orbital angular momentum operators, and $[L_iL_j]=(L_iL_j+L_jL_i)/2$. In the case of T1- and T2-mode acoustic waves, it is obvious that deformation potential scattering of electrons in conduction band by such acoustic phonons disappears ($H_{xc}=0$). Non-vanishing strain components for the three different acoustic modes used in the present work are summarized in Table 2.III.

Table 2.III. Nonzero strain components for the three different acoustic modes in CdS.

T1-mode	e_{xx}, e_{yy}, e_{xy}	: $e_\pm = 2ie_{xy}$
T2-mode	e_{yz}, e_{xz}	: $e_{\pm z}=e_{yz}\pm ie_{xz}$
PL-mode	e_{xx}, e_{yy}, e_{xy}	

From eq.(2.5-1) and Table 2.III one can find the following expressions of strain Hamiltonian using the matrix representation,

$$H_{xv}(T1) = C_5[L_-^2 e_+ + L_+^2 e_-] = C_5[\begin{bmatrix} 0 & 0 & 0 \\ 0 & 0 & 0 \\ 2 & 0 & 0 \end{bmatrix} e_+ + \begin{bmatrix} 0 & 0 & 2 \\ 0 & 0 & 0 \\ 0 & 0 & 0 \end{bmatrix} e_-] \quad (2.5\text{-}3)$$

$$H_{xv}(T2) = \frac{C_6}{2} [(L_zL_+ + L_+L_z)e_{-z} + (L_zL_- + L_-L_z)e_{+z}]$$

$$= \frac{C_6}{\sqrt{2}} [\begin{bmatrix} 0 & 1 & 0 \\ 0 & 0 & -1 \\ 0 & 0 & 0 \end{bmatrix} e_{-z} + \begin{bmatrix} 0 & 0 & 0 \\ 1 & 0 & 0 \\ 0 & -1 & 0 \end{bmatrix} e_{+z}] \quad (2.5\text{-}4)$$

$$H_{xv}(PL) = H_{xv}(T1) + (C_2 + C_4L_z^2)(e_{xx}+e_{yy})$$

$$= H_{xv}(T1) + [C_2 \begin{bmatrix} 1 & 0 & 0 \\ 0 & 1 & 0 \\ 0 & 0 & 1 \end{bmatrix} + C_4 \begin{bmatrix} 1 & 0 & 0 \\ 0 & 0 & 0 \\ 0 & 0 & 1 \end{bmatrix}](e_{xx}+e_{yy}) \quad (2.5\text{-}5)$$

where we used,

$$L_+ = \sqrt{2} \begin{bmatrix} 0 & 1 & 0 \\ 0 & 0 & 1 \\ 0 & 0 & 0 \end{bmatrix}, \quad L_- = \sqrt{2} \begin{bmatrix} 0 & 0 & 0 \\ 1 & 0 & 0 \\ 0 & 1 & 0 \end{bmatrix} \text{ and } L_z = \begin{bmatrix} 1 & 0 & 0 \\ 0 & 0 & 0 \\ 0 & 0 & -1 \end{bmatrix} \quad (2.5\text{-}6)$$

The matrix notations of wave functions corresponding to the three valence bands[60] are described as,

$$\begin{aligned} &A: && S_+\uparrow && \cdots\cdots \Gamma_9 \\ &B: && \sqrt{2}a_BS_-\uparrow + a_cS_o\downarrow && \cdots\cdots \Gamma_7 \\ &C: && \sqrt{2}a_cS_-\uparrow - a_BS_o\downarrow && \cdots\cdots \Gamma_7 \end{aligned} \quad \text{with} \quad \begin{aligned} S_+ &= -(S_x+iS_y)/\sqrt{2} = \begin{bmatrix} 1 \\ 0 \\ 0 \end{bmatrix} \\ S_o &= S_z = \begin{bmatrix} 0 \\ 1 \\ 0 \end{bmatrix} \\ S_- &= (S_x-iS_y)/\sqrt{2} = \begin{bmatrix} 0 \\ 0 \\ 1 \end{bmatrix} \end{aligned} \quad (2.5\text{-}7)$$

where $\uparrow$ and $\downarrow$ represent spin up and down, and S_+, S_- and S_o are defined by using the p-like basic functions S_x, S_y and S_z. The coefficients a_B and a_C are determined from the parameters of the quasi-cubic model; i.e., the spin orbit splitting energy Δ_{so} and crystal field parameter Δ_c,[58]

$$a_B = [\,1 + \frac{1}{2}\,(\,2 - \frac{3}{\Delta_{so}}\,E_{BA}\,)^2\,]^{-1/2} \qquad (2.5\text{-}8)$$

$$a_C = [\,1 + \frac{1}{2}\,(\,2 - \frac{3}{\Delta_{so}}\,E_{CA}\,)^2\,]^{-1/2} \qquad (2.5\text{-}9)$$

where E_{BA} and E_{CA} are the energy difference between the A and B-, and between the A and C valence bands, respectively, and the coefficients a_B and a_C are normalized according to the relation; $a_B^2 + a_C^2 = 1$. By using the values of E_{AB} and E_{AC} derived by Cardona in the electro-reflectance measurement,[61,62] a_B=o.74 and a_C=0.67 are found. Next we define the matrix elements of deformation potential scattering by using the matrix representation,

$$< \Phi_{v\beta}\,|\,[H_{xv}]\,|\,\Phi_{v\alpha} > \;=\; \Xi_{\beta\alpha}\cdot\,[e_{ij}] \qquad (2.5\text{-}10)$$

In the above equation, $|\Phi_{v\alpha}>$ and $|\Phi_{v\beta}>$ denote the state vectors corresponding to the wave functions; $\Phi_{v\alpha}$ and $\Phi_{v\beta}$, and the subscripts α and β indicate the A, B, and C valence bands (or excitons) and $[e_{ij}]$ means the expression of appropriate non-zero strain. Substituting eqs.(2.5-3) (2.5-7) into eq.(2.5-10) one can find the following results of matrix elements by using the parameters a_B, a_C and C_i.

$$\Xi_{AB}(T1) = -2\sqrt{2}a_B C_5,\quad \Xi_{AC}(T1) = -2\sqrt{2}a_C C_5,\quad \Xi_{BC}(T1) = 0$$
$$\Xi_{\alpha\alpha}(T1) = 0 \qquad (2.5\text{-}11)$$

for the case of T1-mode and

$$\Xi_{AB}(T2) = a_C C_6/\sqrt{2},\quad \Xi_{AC}(T2) = -a_B C_6/\sqrt{2},\quad \Xi_{BC}(T2) = -C_6$$
$$\Xi_{\alpha\alpha}(T2) = 0 \qquad (2.5\text{-}12)$$

for the case of T2-mode and

$$\Xi_{AB}(PL) = -2a_B C_5,\quad \Xi_{AC}(PL) = -2a_C C_5,\quad \Xi_{BC}(PL) = a_B a_C C_4$$
$$\Xi_{AA}(PL) = C_2 + C_4,\quad \Xi_{BB}(PL) = a_B^2 C_4 + C_2,\quad \Xi_{CC}(PL) = a_C^2 C_4 + C_2 \qquad (2.5\text{-}13)$$

for the case of PL-mode.

From the above results, it is found that the intraband transitions (two band model) are only possible in the case of PL-mode, and this is due to the fact that there exist the longitudinal strain components in the crystals. Based upon the present results of matrix elements 2- and 3-Band models in the transition process of electronic virtual excitations are constructed. With the use of deformation potential constants C_2, C_4, C_5 and C_6 obtained by Rowe et al.[63] one can evaluate the matrix elements, which are listed in Table 2.IV. with the results of cubic crystals(ZnSe).

Table 2.IV. Matrix elements of deformation potential scattering in CdS and ZnSe.

[CdS]	Tl-mode:	Ξ_{AB} = -1.28 (eV)	Ξ_{AC} = -1.07	Ξ_{BC} = 0
		Ξ_{AA} = 0	Ξ_{BB} = 0	Ξ_{CC} = 0
	T2-mode:	Ξ_{AB} =0.36	Ξ_{AC} =-o.44	Ξ_{BC} =-0.8
		Ξ_{AA} 0	Ξ_{BB} = 0	Ξ_{CC} = 0
	PL-mode:	Ξ_{AB} =2.29	Ξ_{AC} =1.29	Ξ_{BC} =1.34
		Ξ_{AA} =-1.60	Ξ_{BB} =-2.80	Ξ_{CC} =-3.29
[ZnSe]	Tl-mode:	Ξ_{AB} =2.07	Ξ_{AC} =2.94	Ξ_{BC} = 0
		Ξ_{AA} = 0	Ξ_{BB} = 0	Ξ_{CC} = 0
	T2-mode:	Ξ_{AB} =-3.81	Ξ_{AC} =-4.66	Ξ_{BC} =-2.27
		Ξ_{AA} = 0	Ξ_{AC} = 0	Ξ_{CC} = 0

In the anlyses of deformation potential interaction in ZnSe the calculation of matrix elements for the two kinds of transverse acoustic mode (Tl and T2) are performed by the analogical treatment with the case of CdS. It is clear that there exists no essential difference in the deformation potential scattering

between the wurtzite and zinclende-crystals for the case of transverse acoustic phonons, where we can find that the interband transition is possible.

2.6. Construction of 2- and 3-Band Models in Resonant Brillouin Scattering

In this section we discuss the possible transition process of intermediate virtual states (holes or excitons) and determine the dominant contribution process with the help of the results in the matrix elements of deformation potential scattering derived in the previous section. First we consider the selection rules of dipole transtion in the appropriate pair bands (between the conduction and valence bands) of CdS. The selection rules of optical transition at Γ -point of CdS are given by Thomas and Hopfield.[64] Schematic representation of the selection rules in optical transition between the appropriate pair bands is shown in Fig.2.4.

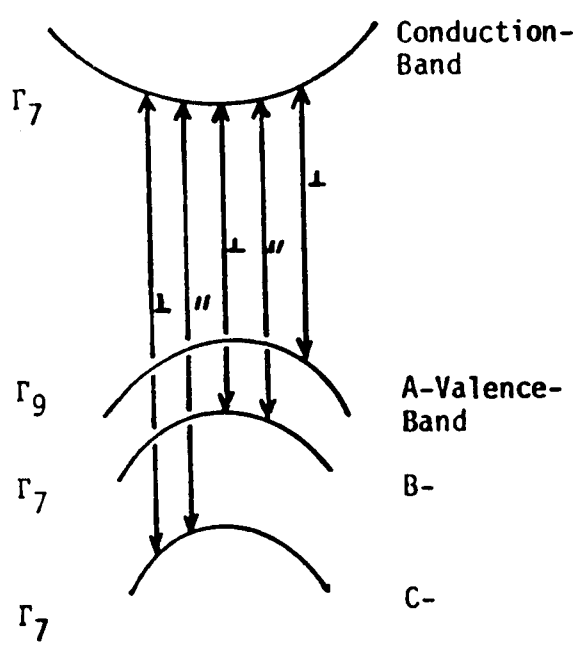

Fig. 2.4. Schematic diagram of selection rule in optical transition at Γ point

As well known, the conduction band has Γ_7-symmetry and A, B and C valence bands at Γ-point have Γ_9, Γ_7 and Γ_7 symmetry respectively. (in the case of excitons these symmetries are the same). The optical transitions of incident and scattered photons with polarization vectors perpendicular to the c-axis are all possible, while in the case of photons with polarization vector parallel to the c-axis the optical

transition between the conduction and A valence band is forbidden. In the present experiment the light beam polarized parallel to the c-axis is incident to the CdS sample in the case of T2-mode Brillouin scattering, and thus the optical gap energy for the incident light is given by E_{gB} or E_{gC} where E_{gB} (or E_{gC}) is the energy gaps between the B(or C) valence band and conduction band. This means that the initial intermediate virtual states (initial electronic excitations) are holes (or excitons) with Γ_7-symmetry. Such a condition appears in the case of PL-mode Brillouin scattering experiment, because of the experimental configuration of parallel polarization direction. On the other hand in the case of Tl-mode the polarization vector of incident light is perpendicular to the c-axis and therefore the energy gap for incident light is given by E_{gA}. In this case the initial electronic excitations have Γ_9-symmety. The analysis stated above is very important to determine another virtual state. In the determination of possible transition process of the virtual states we have to use the results of matrix elements in the deformation potential scattering discussed in the previous section. By using the selection rules of the deformation potential scattering we are able to find the dominant transition process for the corresponding acoustic mode-Brillouin scattering with help of the selection rules of the interband transitions:

[Tl-mode] : (ω_i)---➔|A-exciton> $\xrightarrow{\Xi_{BA}}$|B-exciton>----- (ω_s)

[T2-mode] : (ω_i)---➔|B-exciton> $\xrightarrow{\Xi_{AB}}$|A-exciton>----- (ω_s)

[PL-mode] : (ω_i)---➔|B-exciton> $\xrightarrow{\Xi_{BB'}}$|B'-exciton >----- (ω_s)

In the above transition process we assume that the electronic

excitations are all exciton states and $|\ \rangle$ means the virtual states and $\longrightarrow$ denotes the transition of virtual state by the relevant acoustic phonons. In Fig.2.5 the transition process for the acoustic mode-scattering, which has the dominant contribution to the Brillouin scattering efficiency are shown schematically.

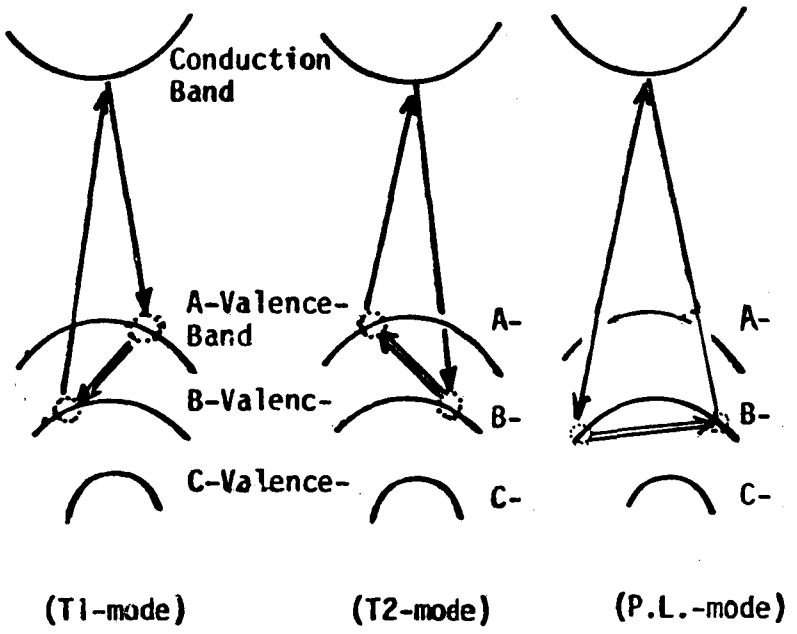

Fig. 2.5. Schematic diagram of dominant transition process for each acoustic mode in CdS.

It is fond from Fig.2.5 that 3-Band model of transition process in the virtual states is responsible for the dominant contribution to the resonant Brillouin effect for the transverse acoustic mode (T1 and T2) and 2-Band model is important for the case of PL-mode acoustic phonons. As shown in Chapter IV, these models explain the resonant behavior of scattering efficiency near the intrinsic band edge of CdS.

In the zincblende type crystals analsis is simpler because the two valence bands but for the spin orbit splitt off band (C-valence

band) are perfectly degenerate at the Γ-point in the Brillouin zone. Such a selection rule of the dipole transition as found in the case of CdS does not exist in the case of zincblende crystals. The most important factor in the determination of dominant transition process in the selection rule of deformation potential scattering derived in section 2.5.

We have already shown that the possible transition of virtual states are ; $|A\rangle \leftrightarrow |B\rangle$ and $|A\rangle \leftrightarrow |C\rangle$ for the case of Tl-mode acoustic phonons, and $|A\rangle \leftrightarrow |B\rangle$, $|A\rangle \leftrightarrow |C\rangle$ and $|B\rangle \leftrightarrow |C\rangle$ for the case of T2-mode acoustic phonons. Other diagonal matrix elements (corresponding to the intraband transitions) are all zero. If we assumed that the reduced masses of A and B excitons (or holes) are the same and the spin orbit splitting energy(Δ_{so}) is considerably large we are able to predict that the important virtual exciton states are only $|A\rangle$ and $|B\rangle$. Such a feature is quite similar to the case of CdS for the Brillouin scattering by transverse acoustic phonons.

2.7. Advance Theory of Resonant Brillouin Scattering

The treatment of resonant nonlinear optical susceptibility was first applied to the analyses of electro-reflectance(ER) effect by Aspness[65]) by taking into account of the fact that ER theory and spectra have been analyzed with the analogy of the theory of nonlinear optical coefficients. He developed the perturbation theory of ER and established thoretically a connection of the Franz-Keldysh theory[66,67] to that of nonlinear optics.[68] In this section we present the dominant resonant term in the third order nonlinear optical susceptibility caused by existing acoustic phonons and derive the micoscopic expression of photoelastic

constant P_{ijkl} of which dispersion have an important role in the resonant Brillouin scattering. The theory was first proposed by Hamaguchi and later extended by the present author. We use one-electron approximation, where the Bloch function $\Phi_{nk}(r)$ describing electron states in the crystal satisfies a time-dependent schrödinger equation;

$$H_o \Phi_{nk} e^{-i\omega_{nk}t} = ih\frac{\partial}{\partial t}\Phi_{nk}\, e^{-i\omega_{nk}t} \qquad (2.7\text{-}1)$$

where H_o is the unperturbed Hamiltonian and $E_{nk}=\hbar\omega_{nk}$ is the energy of state Φ_{nk}. Interaction Hamiltonian H_I is the same as introduced in section 2.4 but for the scalr gage-representation of electron-radiation mutual interaction, given by

$$H_{ER} = eE\,(e^{-i\omega_+ t} + e^{i\omega_- t}) = H_p^+ + H_p^- \qquad (2.7\text{-}2)$$

where $\hbar\omega_\pm=\hbar\omega\pm i\Gamma$; Γ is the broadening energy and a small positive value in the case that the field E is real. Then the total interaction Hamiltonian H_I is written,

$$H_I = H_p^+ + H_p^- + H_q^+ + H_q^- \text{ , with } (\alpha|H_q^\pm|\beta)=\Xi_{\alpha\beta}\bar{S}_{ij}^\pm \qquad (2.7\text{-}3)$$

where $H_q^\pm$ corresponds to the electron-phonon interaction Hamiltonian which includes the creation and destruction operators of phonon, and S_{ij} is the same representation as defined in eq.(2.3-8) but with the exponetial term removed. The wave function Ψ_{nk} corresponding to the perturbed state can be evaluated as a power series in the perturbation by using the Green operator,[69]

$$\Psi_{nk}(r,t) = [\,1 + (G_o H_I)^n\,]\,|\Phi_{nk}(r,t)\rangle \qquad (2.7\text{-}4)$$

where Φ_{nk} is unperturbed state and G_o is Green operator. Here the schrödinger equation to be solved is,

$$H_T \Psi_{nk}(r,t) = i\hbar \frac{\partial}{\partial t} \Psi_{nk}(r,t) \qquad (2.7\text{-}5)$$

By substituting eq.(2.7-4) into eq.(2.7-5) one can find Ψ_{nk}, and from which the polarization and dielectic constant can be calculated. The dielectric tensor ϵ_{ij} of the crystal can be calculated from the polarization P according to

$$D_i = \varepsilon_{ij} E_j = \delta_{ij} E_j + 4\pi P_i \qquad (2.7\text{-}6)$$

where
$$P = -\frac{e}{V} \sum_{vk} \langle \Psi_{vk}(r,t) | X | \Psi_{vk}(r,t) \rangle \qquad (2.7\text{-}7)$$

and $\Psi_{vk}(r,t)$ is given by eq.(2.7-4). The subscript v for the band index denotes a filled valence band. The acoustic phonon induced correction to the polarization P will have the explicit form within the limit of secondorder approximation,

$$P = \frac{e}{V} \Sigma \langle vk|X|vk\rangle$$
$$- \frac{e}{V} \Sigma \langle vk|X|G_o(q^{\pm}p^{\pm}) H_q^{\pm} G_o(p^{\pm}) H_p^{\pm}|vk\rangle \exp[-i(\omega_{\pm} \pm \omega_q)t]$$
$$- \frac{e}{V} \Sigma \langle vk|X|G_o(q^{\pm}q'^{\pm}p^{\pm}) H_{q'} G_0(q^{\pm}p^{\pm}) H_q G_o(p^{\pm}) H_p|vk\rangle \exp[-i(\omega_{\pm} \pm \omega_q \pm \omega_{q'})t]$$
$$\cdots\cdots\cdots \qquad (2.7\text{-}8)$$

where $G_o(ij\cdots)$ is Green function indicated as following,

$$G_o(ij\cdots\cdots) = \frac{1}{\varepsilon_{nk} + S_i + S_j + \cdots - H_o} \qquad (2.7\text{-}9)$$

where i, j$\cdots$ represent a particular combination of symbols(q ,p,$\cdots$) and if

$$i = \begin{bmatrix} q^+ \\ q^- \\ p^+ \\ p^- \end{bmatrix} \quad \text{then} \quad S_i = \begin{bmatrix} \hbar\omega_q \\ -\hbar\omega_q \\ \hbar\omega_+ \\ -\hbar\omega_- \end{bmatrix} \qquad (2.7\text{-}10)$$

In eq.(2.7-8) first term corresponds to the unperturbed term having no contribution to the ΔP. The second term is found to change with time in the form $\exp[i(\omega \pm \omega_q)]$ and thus one can find that this term just corresponds to the first order resonant Brillouin (or Raman) effect caused by one acoustic phonon. From this consideration it is easily understood that the third term is an expression of second order Brillouin (or Raman) effect where two phonons are involved. By using the above relation one can evaluate the change in the complex dielectric constant $\Delta\varepsilon^*$ induced by the acoustic phonons,

$$\Delta\varepsilon^*(\omega, \omega_q) = A_1 \cdot \frac{2}{(2\pi)^3} \int \frac{4\pi k^2 dk}{(\hbar\omega \pm \hbar\omega_q - \varepsilon_{cv'}(k) + i\Gamma)(\hbar\omega - \varepsilon_{cv}(k) + i\Gamma)} \qquad (2.7\text{-}11)$$

$$\text{with,} \quad A_1 = -\frac{4\pi e}{m^2\omega^2} (\hat{\varepsilon}_s \cdot P_{cv})(\hat{\varepsilon}_i \cdot P_{cv}) \left(n_q + \frac{1}{2} \pm \frac{1}{2}\right) \Xi^{kl}_{vv'} \cdot S_{kl} .$$

where $\hat{\epsilon}_i$ and $\hat{\epsilon}_s$ are the polarization vectors for incident and scattered lights, $P_{cv}, (P_{cv})$ is the matrix element of dipole transitions between the valence band v(v') and conduction band(c), $\varepsilon_{cv}(k)$ $(\varepsilon_{cv'}(k))$ is the energy difference between the valence band v (v') and conduction band (c). Using the following relation,

$$\lim_{\Gamma \to +0} \frac{1}{x + i\Gamma} = P\left[\frac{1}{x}\right] - i\pi\delta(x) \qquad (2.7\text{-}12)$$

with P is the Caucy Principal value; the complex dielectric constant $\Delta\varepsilon^*$ can be divided into real and imaginary parts,

$$\Delta\varepsilon^*(\omega, \omega_q) = \Delta\varepsilon_1(\omega, \omega_q) + i\Delta\varepsilon_2(\omega, \omega_q) \qquad (2.7\text{-}13)$$

$$\text{with} \quad \Delta\varepsilon_1(\omega, \omega_q) = A_1 \frac{2}{(2\pi)^3} \int \frac{4\pi k^2 dk}{(\hbar\omega \pm \hbar\omega_q - \varepsilon_{cv'}(k))(\hbar\omega - \varepsilon_{cv}(k))} \qquad (2.7\text{-}14)$$

and with

$$\Delta\varepsilon_2(\omega,\omega_q) = A_1 \frac{2}{(2\pi)^3}\left\{ \int \frac{4\pi k^2 dk \cdot \delta(\hbar\omega-\varepsilon_{cv}(k))}{(\hbar\omega\pm\hbar\omega_q-\varepsilon_{cv'}(k))} + \int \frac{4\pi k^2 dk \delta(\hbar\omega\pm\hbar\omega_q-\varepsilon_{cv'}(k)}{(\hbar\omega-\varepsilon_{cv}(k))} \right\}$$

..... (2.7-15)

In eqs.(2.7-14) and (2.7-15) it should be noted that the formulation of $\Delta\epsilon_1$ is valid for the incident phonon energy $\hbar\omega<E_g$, and $\Delta\varepsilon_2$ is valid for $\hbar\omega>E_g$. It is very interesting to point out that the expression of real part ε_1 in the dielectric constant perfectly corresponds to that of resonant Brillouin efficiency (R_{is}) (eq.2.3-14). From these considerations we find that resonant light scattering is closely related to the resonant enhancement of ε_1 near the critical point. The change in imaginary part ϵ_2 is found to correspond to the change in the absorption coefficient induced by acoustic phonons. Such an interpretation is very helpful to discuss the resonant features of Brillouin scattering in the higher photon energy regions (E_1 or E_2-edge) which is given in detail in Appendix I.

Now we derive the dispersion of appropriate photoelastic constant by using the 2-Band model in the case of M_o-critical point. Photoelastic constant P_{ijkl} is defined by the following equation according to the definition of Pockel,

$$\frac{(\Delta\varepsilon_1)_{ij}}{\varepsilon_{im}\varepsilon_{mj}} = - P_{ijkl}S_{kl} \qquad (2.7\text{-}16)$$

Using the following relation (see Appendix I)

$$\Delta[\varepsilon_1(\omega)-1] = -\frac{1}{\hbar e}(n_q+1/2\pm1/2)S_{KL}\Xi^{kl}\frac{d\varepsilon_1}{d\omega} \qquad (2.7\text{-}17)$$

$$\text{with} \quad \frac{d\varepsilon_1}{d\omega} \propto (\omega_g-\omega)^{-1/2} + (\omega_g+\omega)^{-1/2} \qquad (2.7\text{-}18)$$

We can find the dispersion of P_{ijkl} near the M_o-critical point,

$$P_{ijkl}(\omega,M_o) \propto (n_q+1/2\pm1/2)\ \varepsilon_{ii}\varepsilon_{jj}\frac{\Xi^{kl}}{\varepsilon}\left[(\omega_g-\omega)^{-1/2}+(\omega_g+\omega)^{-1/2}\right] \quad (2.7\text{-}19)$$

Equation (2.7-19) shows that the photoelastic constant $P_{ijkl}(\omega,M_o)$ increases drastically at the photon energy close to the fundamental absorption edge of semiconductors. It should be noted here that the photoelastic constant $P_{ijkl}(\omega,M_o)$ derived in the present analyses is not the total photoelastic constant $P_{ijkl}(T)$ which corresponds to the total Brillouin tensor $R_{is}(T)$. It is evaluated by taking into account of the nondispersive contributions with different sign by,

$$P_{ijkl}(T) = P_{ijkl}(\omega,M_o) - P_{ijkl}(NR) \quad (2.7\text{-}20)$$

where the non-resonant photelastic constant $P_{ijkl}(NR)$ is considered to arise from other critical points higher than the fundamental energy gap. From eq.(2.7-20) one can find that the total photoelastic constant $P_{ijkl}(T)$ passes through zero point while undergoing a reversal in sign as the incident photon energy comes near to the band gap. Such physical interpretation seems to correspond to a existence of resonant cancellation in the observed dispersion curves of Brillouin scattering cross section.

2.8. Summary

Basic treatment of light scattering is presented by using the phenomenological expression and quantum theory. By using the tensor formulation of photoelastic constant the expressions of Brillouin scattering cross section for the three different acoustic phonon modes are determined and the possibility of resonant enhancement

of Brillouin scattering cross section near the intrinsic band edge of semiconductors is presented based upon the time-dependent perturbation theory. From the analyses of deformation potential scattering of intermediate virtual states by acoustic phonons, it is found that the observed resonant effect is interpreted in terms of the 3-Band model. It is also found that the dispersion of $\Delta\varepsilon_1$ (real part of the chang in the complex dielectric constant) induced by the acoustic phonons corresponds to that of Brillouin tensorand from this fact one can obtain the appropriate photo-elastic constant.

Chapter III Experimental Procedure

3.1. Introduction

The intense phonon beams amplified by acoustoelectric instabilities[34-38] are very useful to investigate the dispersion spectra of the resonant enhancement and cancellation near the fundamental absorption edge of semiconductors. This advantage will be readily understood by the following fact. An application of drift velocity greater than the sound velocity in piezoelectric semiconductors results in selective acoustoelectric amplification of phonon beams travelling in a narrow frequency range near the frequency of maximum gain.[37] The phonon beams usually form so called'acoustic domain ' 1 mm wide traveling from the cathode to the anode. Amplified acoustic phonons have a intensity of the order 10^9 above the thermal equilibrium value, which is easily achieved in the frequency range 0.1 to 4 GHz. Such a frequency range of acoustic phonons is found to be most suitable for the present study of Brillouin scattering.[40] One of the advantages of the present experimental technique is that one can easily detect the optical signals (scattered light or modulated light by acoustic phonons) without using the high power tunable dye laser because of strong acoustic power. It should be noted that the high-power laser beam is important light source in the measurement of resonant light scattering by thermal phonons, where the high resolution Fabry-Perot interferometer is required.[14,74] On the other hand in the present experiment some complicated problems come out as follows, which originate from the fact that we use high density phonon flux of piezoelectric semiconductors. First we have to consider effects of alternative piezoelectric field ($\sim 10^5$ V/cm) existing in the domain on the scattering intensity. One must take into account the effect

of indirect Brillouin scattering[75,85,91] induced by such strong electric fields in the piezoelectric semiconductors such as CdS. Second problem is an existence of large strain inside the domains. The strain is found to perturb the band structure, especially in the case of longitudinal acoustic phonons where linear strain components exist. A discussion concerning this effect will be given in connection with piezobirefringence effect. In the case of semi-insulating ZnSe, acoustelectric instability cannot be achieved due to the two facts; weak electromechanical coupling constant ($K = 0.049$)[121] and small carrier concentrations. Therefore the technique of acoustic pulse injection is essential in the present investigation. It is confirmed experimentally that two kinds of transverse acoustic phonon modes (slow(T1) and fast(T2)-transverse sound waves) can be excited in the end - bonded ZnSe samples, which are mainly used to study the resonance effect of Brillouin scattering.[29]

3.2. Experimental Procedure and Sample Construction

The experimental arrangement used in the present work is shown in Fig.3.1. The arrangement was used in the measurements of resonant Brillouin scattering, transmission modulation, and Brillouin scattering with small change. A high intensity light source of a continuous spectrum is obtained from a Xe-flash tube (Ushio Type 626 Xe-flash lamp or Sunpak Strobo GTPRO 4011) and dispersed by conventional monochromator (JASCO CT-50). The resolution is about 5-10 Å in the range of present experiment. The output beams from the monochromator are focussed by a lens on the specimen with incident angle θ_i after passing a polarizer (Gran-Thomson Prism). Incident and scattered angles (θ_i and θ_d)

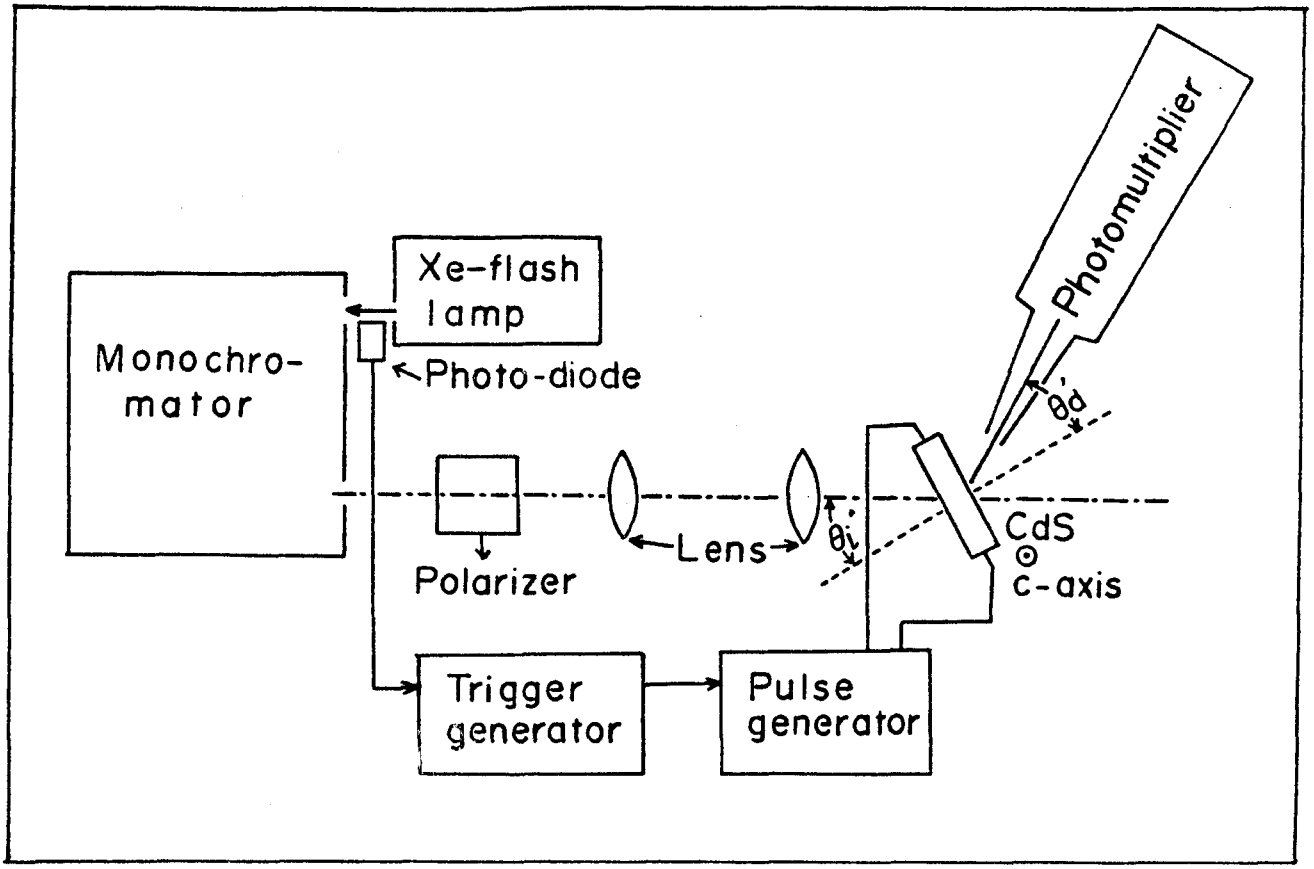

Fig. 3.1. Schematic diagram of the experimental apparatus. The specimen is mounted on the rotatable table and incident angle θ_i and scattered-angle θ_d are set to detect light scattered by phonons with a specific frequency.

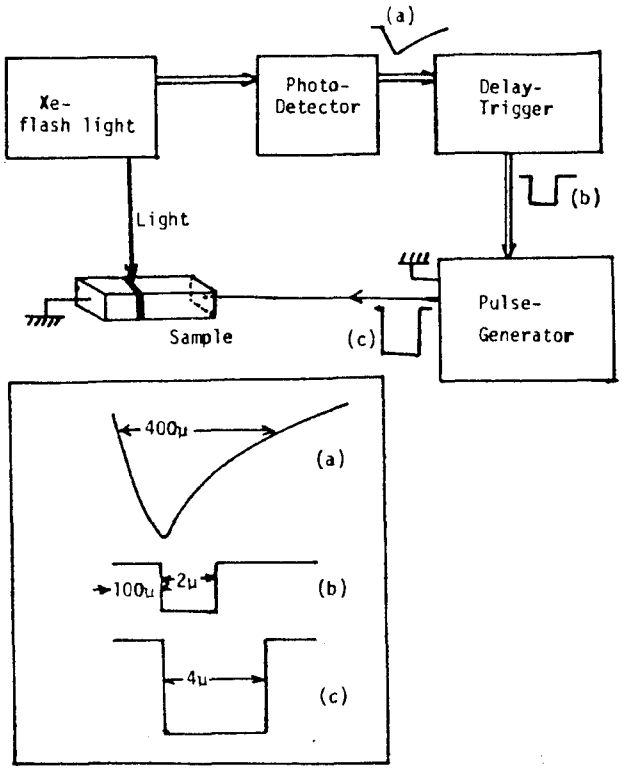

Fig. 3.2. Block diagram of trigger-system in experimental apparatus.

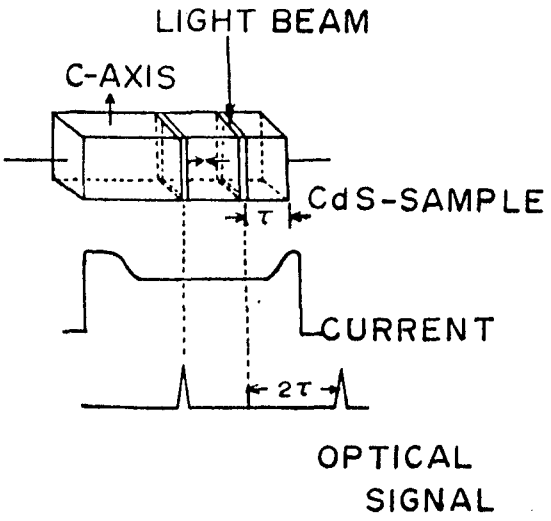

Fig. 3.3. Current waveform and typical optical signals.

are so determined as to be able to detect the light scattered by acoustic phonons with a particular frequency. The size of light is about 0.5 mm in diameter which is comparable with the width of acoustic domain. High voltage pulses are applied between both ends of the CdS in order to generate the acoustic domains. Such high voltage pulses are synchronized with the flash light so as to traverse the acoustoelectric domains at the illuminated part of the specimens. In order to obtain the strong optical signals, the travelling acoustoelectric domain is synchronized to traverse the illuminated position at the instance of the peak intensity of the light pulse. For this purpose the delayed trigger system shown in Fig.3.2 is used. The half width of the light pulse is about 400 μsec. and the delayed trigger is generated after 100 μsec from the out put pulse of photodetector. The pulse width of the high voltage generated by the Pulse Generator (Velonex Model-350) is about 4 μsec. Analyzer (Polaroid) is mounted in front of the photomultiplier. In the experiments of resonant Brillouin scattering where one has to change the incident light wavelength, the incident and scattered light angles for a given acoustic frequency were calculated as a function of light wavelength. In Fig.3.3. sample configuration, current wave form and optical signals are schematically shown. Current oscillation shows the generation of propagating acoustic domain in the specimen. Usually we can find two optical signals corresponding to the acoustic packet propagating to the anode and to the reflected acoustic packet. The CdS samples are cut in bar shapes (from Eagle Pitcher Co., and Teikoku Tsushin) and mechanically polished. In order to obtain ohmic-contacts, indium is deposited

by evaporation on the both ends of the samples at $\sim 1\times10^{-5}$ Torr, and copper wires are soldered on them. The carrier concentration and mobility of CdS are determined by the acoustoelectric currents[77] which are listed in Table 3.I. with sample dimensions.

Table 3.I. Characteristics of CdS and ZnSe Samples used in the present work.

	Sample No.	Dimensions	n	μ
[CdS]	UHP.R.1	8.0×0.8×1.9(mm)	2.9×10^{15}(cm^{-3})	330(cm^2/Vsec.)
	UHP.R.5	10.1×0.9×1.5	2.8×10^{15}	270
	UHP.R.6	9.5×0.3×1.0	2.8×10^{15}	300
	UHP.R.11	7.5×0.4×1.2	.....	....
	UHP.1	5.5×0.3×0.8	.....	....
	UHP.2	5.1×0.5×1.0	.....	....
[ZnSe]	ZR. 1	5.5×0.3×0.9	semi-insulating	
	ZR. 2	6.1×0.5×0.9		
	ZR. 5	4.7×0.5×0.8		
	Z5	7.4×0.5×0.8		

The measurements of resonant Brillouin scattering in ZnSe are made also by using the experimental set up of Fig.3.1.. The high intensity phonon flux is achieved by the technique of acoustic injection.[78,79] The typical dimensions of the semi-insulating ZnSe samples are summarized in Table 3.I. The acoustic pulse injections are carried out by the end-bonded configuration of CdS and ZnSe, which is shown in Fig.3.4 schematically.

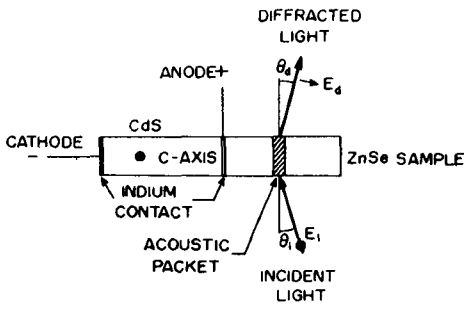

Fig. 3.4. Schematic Brillouin-scattering by an acoustic-packet introduced from semiconductive CdS into insulating ZnSe.

3.3. Resolution of Acoustic Frequency

The spatial resolution of Brillouin scattering is determined by the area of the incident light spot. A typical width of acoustic domains is about 0.5 mm in semiconductive CdS. In the present experiment the light beams are focussed by a conventional lens on the surface of the sample in a diameter of 0.5 mm, and therefore the spatial resolutions are mainly determined by the cross sectional area of the light spot. The resolution of the acoustic frequency is determined by the collection cone angles of incident and scattered lights. In the present works the focussed light beams penetrate into the sample with a finite solid angle Ω_i and scattered light is collected by a cone with solid angle Ω_s. In such a case as the measurement of dispersion of scattering efficiency it is very important to find a relation of resolution, in other words, $\Delta\delta$ vs $\Delta\omega_q$ curve with respect to the incident light wavelength, where δ is off axis angle of propagating domains and $\Delta\omega_q$ is the deviation of acoustic frequency from the observed acoustic frequency ω_q. The resolution of acoustic frequency is derived by solving the equation of momentum conservation between the incident, scattered photons and phonons. Complicated treatment of resolution in spatial and acoustic frequency is studied by Yamada[80]. At present time we will examine the wavelength dependence of $\Delta\delta$ and $\Delta\omega_q$ in the experimental region in CdS. From the calculation of resolution we find that $\Delta\delta$ and $\Delta\omega_q$ are proportional to the quantities of collection angle of the incident light; $\Delta\delta_i$ and that of the scattered light; $\Delta\delta_s$, which are determined by the experimental condition. The collection cone angles of incident and scattered lights are shown in Fig. 3.5.

After simple calculation one obtains,

$$\Delta\delta = \frac{1}{n_i^2+n_d^2-2n_in_d\cdot\cos(\theta_i-\theta_d)} \times\{\frac{\sin\theta_d}{\sqrt{n_d^2-\cos^2\theta_d}}\,[n_d^2-\cos\theta_d\cos\theta_i$$

$$-\,(n_d^2-\cos^2\theta_d)(n_i^2-\cos\theta_i)\,]\times\Delta\delta_s + \frac{\sin\theta_i}{\sqrt{n_i^2-\cos^2\theta_i}}$$

$$\times[n_i^2-\cos\theta_i\cos\theta_d-\sqrt{(n_d^2-\cos^2\theta_d)(n_i^2-\cos^2\theta_i)}\,]\times\Delta\delta_i\} \qquad (3.3\text{-}1)$$

$$\frac{\Delta\omega_q}{\omega_q} = \frac{1}{n_i^2+n_d^2-2n_in_d\cos(\theta_i-\theta_d)}$$

$$\times\{\,\sin\theta_d[\cos\theta_i-\cos\theta_d\sqrt{\frac{n_d^2-\cos^2\theta_d}{n_i^2-\cos^2\theta_i}}\,]\times\Delta\delta_s$$

$$+\,\sin\theta_i[\cos\theta_d-\cos\theta_i\sqrt{\frac{n_d^2-\cos^2\theta_d}{n_i^2-\cos^2\theta_i}}\,]\times\Delta\delta_i\,\} \qquad (3.3\text{-}2)$$

where n_i and n_d are the refractive indeces for the incident and scattered lights, θ_i and θ_d are the angles of the incident and scattered lights out side the crystals, respectively. It is found in those equations that $\Delta\omega_q$ and $\Delta\delta$ depend upon the incident lihgt wavelength, since n_i, n_d, θ_i, and θ_d are the functions of the wavelength. In Fig.3.6 $\Delta\delta$ and $\Delta\omega_q/\omega_q$ are plotted as a function of incident light wavelength. The angle of $\Delta\delta$ is found to change from 21° to 19° in the experimental wavelength region(5200 Å 5800 Å). From the fact that the half-width of propagating angle of acoustic domains in ∿10°, one finds that it is not required to perform a correction in the observed scattering intensity due to the change of off-axis angle. It is also found in Fig.3.6 that the ratio of $\Delta\omega_q$ to ω_q is nearly equal to 0.3±0.01 in the wavelength region

from 5200 to 5800 Å. For example, in the case of 1GHz acoustic frequency, the change of $\Delta\omega_q$ is smaller than 10^0 MHz and negligibly small in the wavelength range of the present experiment. These features are understood by taking into account of the fact that the present measurements of Brillouin scattering are limited to a low frequency region of acoustic waves 0.1 ~2 GHz. In the experiment of higher acoustic frequencies it is important to take inti account of the such resolution.

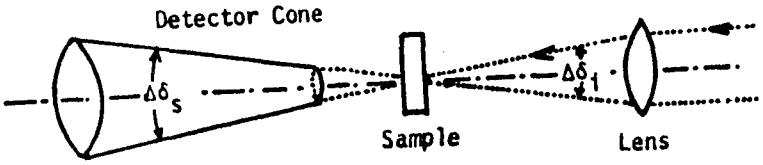

Fig. 3.5. Schematic diagram of focussed light beam and detector cone used in the present work.

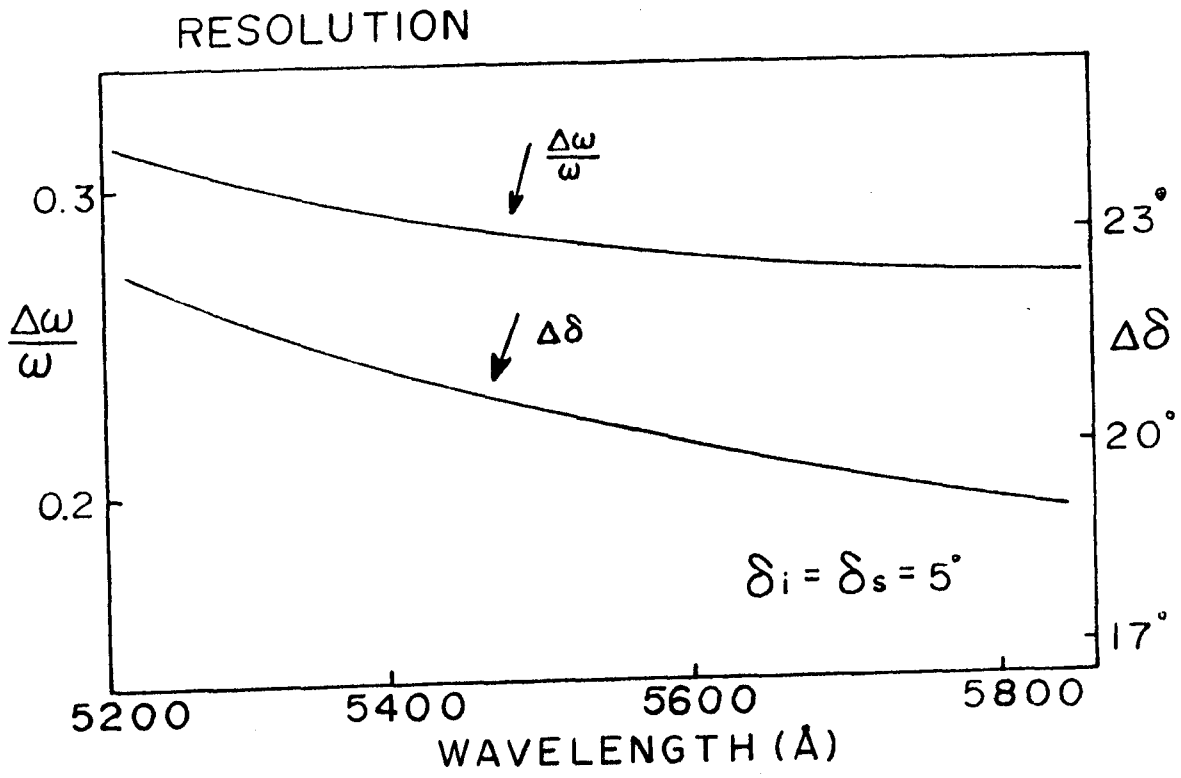

Fig. 3.6. The estimated values of $\Delta\delta$ and $\Delta\omega_q/\omega_q$ versus incident light wavelength.

3.4. Summary

Experimental arrangement and sample construction used in the present workare presented. It is pointed out that in order to obtain the strong optical signals of Brillouin scattering and optical modulation, the travelling acoustoelectric domain is perfectly synchronized to traverse the illuminated position at the instance of the peak intensity of the light pulse. Resolution of acoustic frequency $\Delta\omega_q$ and of the change in the off axis angle $\Delta\delta$ in the present measurements of resonant Brillouin scattering are discussed. One can find that it is not significant to correct the observed scattering intensities because of small changes of $\Delta\omega_q$ and $\Delta\delta$ inthe present experimental wavelength regions.

Chapter IV. Resonant Brillouin Scattering in CdS and ZnSe

4.1. Introduction

Chapter IV deals with the experimental results and discussion of resonant Brillouin scattering in CdS and ZnSe. Present measurements are mainly performed in the 'Allowed-Polarization Condition' of Brillouin scattering[81] at room temperature by using the amplified or mode converted acoustic phonons. The main features of present results are following. Steep increases in scattering cross sections for the acoustic modes investigated in the present work (T2-, T1-, and PL-modes in CdS and T2-, and T1-modes in ZnSe) are observed in the photon energy regions close to the fundamental absorption edge.[15,18,19] The structures of resonant cancellations are found at the photon energies just below the fundamental absorption edges of CdS and ZnSe in the dispersions of Brillouin scattering for the transverse acoustic waves. It is found in comparison with the theory that the structures of resonant enhancement and cancellation are well explained by the theoretical treatment of resonant scattering[18] derived in Chap.II. where 3-Band model in transition process of intermediate virtual excitons is properly taken into account so as to satisfy the experimental polarization conditions. Resonant cancellations are interpreted like the treatment proposed by Ralston et al.,[6] where the total scattering amplitude is given by a sum of the resonant and non-resonant terms of opposite sign. The physical mechanisms of non-resonant contribution arising from the higher energy bands are discussed by using the theory derived from the nonlinear susceptibility(Chap. II). In the latter part of this chapter dispersion curves of photoelastic constants are analyzed[29] by using the

theory of stress induced piezobirefringence.[58,82] From this analysis we are able to understand the antiresonance-structure in the dispersion curves of scattering cross sections.

4.2. 1. Resonant Brillouin Scattering by Piezoelectrically Active Mode Phonons in CdS.

The Brillouin scattering intensities were measured at room temperature as a function of incident light wavelength (incident photon energy). The results for piezoelectrically active shear waves (T2-mode) of 0.5, 1.0 and 2.0 GHz are shown in Fig.4.1, where the ratios of the scattered light intensity I_s to the incident light intensity I_o is used. The general features are similar to the results of n-GaAs[15] if we take into account the strong absorption of the incident and scattered lights near the fundamental absorption edge. The scattering efficiency has narrow and deep minimum at 5620 Å (2.22 eV). The decrease of the scattering intensity near the edge is caused by the strong absorption of the incident and scattered lights due to the sharp increase in the absorption coefficients. In order to deduce the intrinsic-Brillouin scattering efficiency from the present data of I_s/I_o, one has to take into account not only the absorption of incident and scattered light but also the depletion of the light from various Brillouin components. In the case of isotropic crystals; GaAs, the correction of such strong absorption is made by using the relation;[15]

$$I_s/I_t = \sigma_B b' d\Omega \qquad (4.2\text{-}1)$$

where I_t is transmitted light intensity, b' is the optical path length, and $d\Omega$ is the solid angle in which the light is scattered. Equation (4.2-1) is valid in an estimation of the scattering

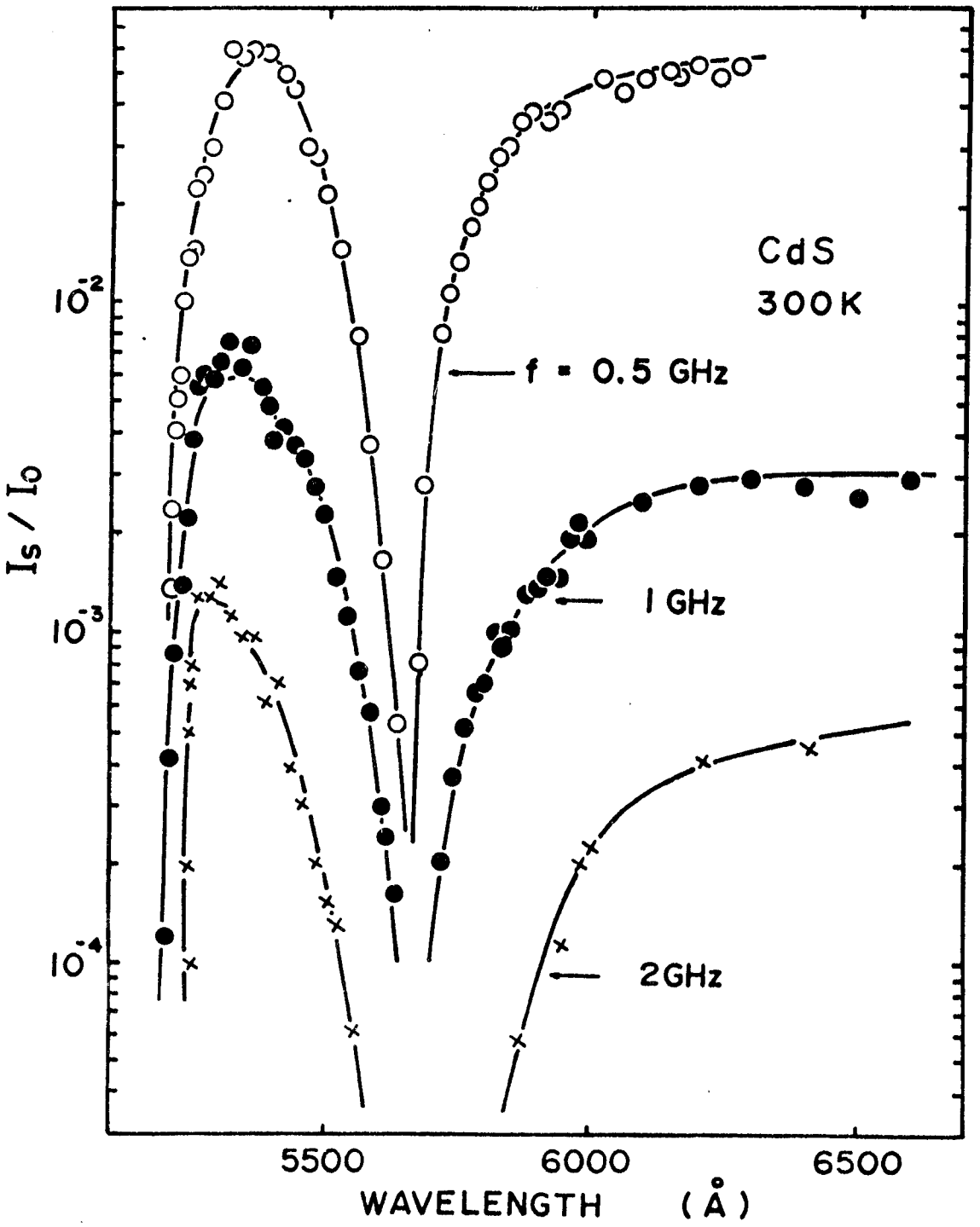

Fig. 4.1. Brillouin scattering signals for T2-mode phonons in CdS. The ratios of Brillouin scattered light intensity I_s to the incident light intensity I_o are plotted as a function of incident light wavelength.

efficiency of ZnSe, which is shown in the nextsection. In the case of CdS, however, one must take into account the optical anisotropy to obtain the intrinsic Brillouin scattering dispersion. A simple analysis which includes the effect of the difference in the absorption coefficients (see APPendix II) gives the following relation,

$$\frac{I_s}{I_o} = \frac{\sigma_B d\Omega_s}{\alpha_i - \alpha_d \cdot \frac{n_i}{n_i}} \exp\left(-\frac{\alpha_d b}{\cos\theta_d}\right) \times \left\{1 - \exp\left[-\left(\alpha_i - \alpha_d \frac{n_d}{n_i}\right)\frac{b}{\cos\theta_d}\right]\right. \qquad (4.2\text{-}2)$$

where α_i and α_d are the absorption coefficients for the incident and scattered lights, and b is the width of the sample in the scattering plane. The refractive indices n_i and n_d refer to the incident and scattered lights, and the angle θ_i and θ_d are determined by the momentum conservation at the fixed point of the photon energy. At longer wavelength far from the band edge the values of α_i and α_d are so small that we can approximate eq.(4.2-2) by,

$$\frac{I_s}{I_o} = \frac{\sigma_B b}{\cos\theta_i} \exp\left(-\frac{\alpha_d + \sigma_T}{\cos\theta_d}\right) d\Omega_s \qquad (4.2\text{-}3)$$

where σ_T is the total scattering coefficient defined in the Appendix II. It is evident that eq.(4.2-1) can be derived by assuming equal optical path lengths for the scattered and unscattered lights; $b/\cos\theta_i = b/\cos\theta_d = b'$. Near the band edge however, the condition; $(\alpha_i - \alpha_d n_d/n_i)b \ll 1$ is not satisfied and thus we have to use the expression of eq.(4.2-2) in order to compute the Brillouin scattering cross section from Fig.4.1. By making use of the absorption coefficient data of Dutton[83] and the refractive index data of

Bienieski and Czyzak[84] we calculated the dispersions of the scattering cross section, which are shown in Fig.4.2.

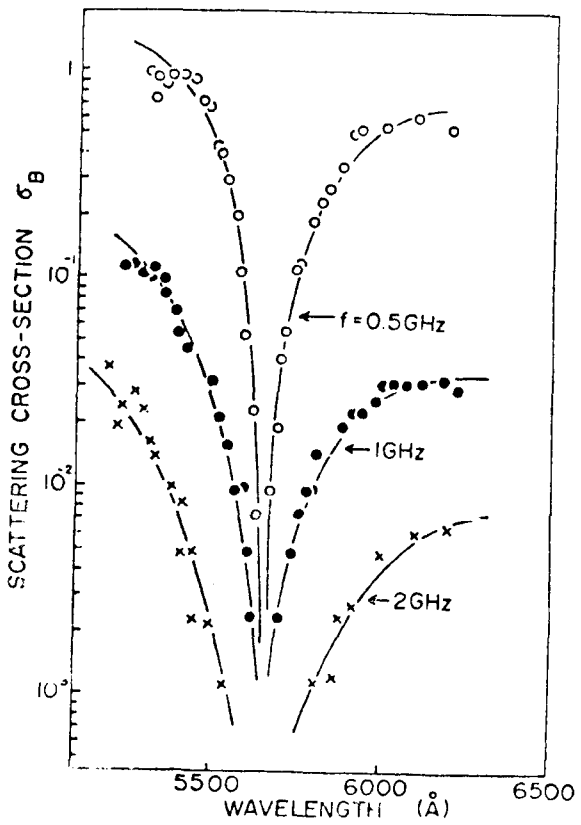

Fig. 4.2. Brillouin scattering cross section plotted as a function of incident light wavelength in CdS.

The magnitude of the scattering cross section is proportional to the energy density of the amplified phonons and thus depends on the applied electric field. Therefore we plot the results in arbitrary units in Fig.4.2. The general features of the three dispersion curves for 0.5, 1.0 and 2.0 GHz phonons are quite similar but for the absolute scattering intensity. We find that in the long wavelength region the scattering cross sections approach to the nonresonant Brillouin scattering, namelly Brillouin scattering predicted from the photoelastic effect of macroscopic theory. The usual wavelength dependence λ^{-4} is not found in the present result because of narrow wavelength range of the incident photons. We find a deep and narrow minimum at 2.22 eV and a steep increase in the higher photon energy region beyond the minimum. These data indicate an existence of the resonant enhancement and cancellation near the fundamental absorption edge in CdS.

We estimate here the dispersion spectra of the Brillouin scattering by using the microscopic theory derived in Chap. II. First we use Loudon 's formulation without exciton effects. As stated in Chapter II. the scattering cross section in the microscopic treatment have the form,

$$\sigma_B = \left(\frac{e}{\hbar mc}\right)^4 \frac{k_B T}{2\rho v_j^2} \frac{\omega_s}{\omega_i} |R_{is}|^2 \qquad (4.2\text{-}4)$$

where the most dominant term of Brillouin tensor R_{is} is givn by,

$$R_{is} = \frac{1}{V} \sum \frac{P_{o\beta} \Xi_{\beta\alpha} P_{\alpha o}}{(\omega_\beta - \omega_s)(\omega_\alpha - \omega_i)} \quad \text{with} \quad \omega_s = \omega_i \pm \omega_q \qquad (2.4\text{-}5)$$

where the notations are same as those introduced in eq.(2.3-13) of Chapter II. From the analyses of deformation potential scattering of virtual state by acoustic phonons we have found that the 3-Band model of transition process including the virtual holes of B- and A valence bands is significant to estimate the dispersion of resonant light scattering by T2-mode phonons in CdS. In the present case , therefore, we should use the deformation potential matrix element Ξ_{AB} instead of $\Xi_{\alpha\beta}$ in eq.(2.15). Taking into account the difference in the optical band gaps for the two different light polarizations in CdS, one can obtain the expression of R_{is} for T2-mode,

$$R_{is}(T2) = \frac{2}{(2\pi)^2} \left(\frac{2\mu}{\hbar}\right)^{3/2} \frac{P_{oA} \Xi_{AB} P_{Bo}}{\omega_{gA} - \omega_{gB} + \omega_q}$$

$$\times \left[(\omega_{gA} - \omega_s)^{1/2} \tan^{-1}\left(\frac{\Delta\omega_A}{\omega_{gA} - \omega_s} \right)^{1/2} - (\omega_{gB} - \omega_i)^{1/2} \tan^{-1}\left(\frac{\Delta\omega_B}{\omega_{gB} - \omega_i} \right)^{1/2} \right]$$

$$\cdots\cdots\cdots \qquad (4.2\text{-}6)$$

where μ is the reduced mass, which is assumed to be equal for the $|B\rangle$ and $|A\rangle$ pair-states for simplicity, $\hbar\omega_{gB}$ and $\hbar\omega_{gA}$ are the optical band gaps for the pair-states $|B\rangle$ and $|A\rangle$ corresponding to the incident and scattered light, respectively, and $\hbar\Delta\omega_B$ (or $\hbar\Delta\omega_A$) is the combined width of the conduction and B-(or A-) valence band. Equations (4.2-5) and (4.2-6) indicate that the

scattering cross sections increase as the incident photon energy approaches the band gap $\hbar\omega_{gB}$ or $\hbar\omega_{gA}$. This results in a resonant Brillouin scattering. The cancellation is explained in terms that the resonant contribution (R_{is}) to the scattering efficiency is opposite in sign to the nonresonant contribution ($-R_o$). In other words the scattering cross section is given by,

$$\sigma_B \sim |R_{is} - R_o|^2 \qquad (4.2\text{-}7)$$

Here we will consider the term of nonresonant contribution, which has the non-dispersive λ^{-4} dependence. R_o is usually considered as the contributions from other far-off critical points in the band structure. It is obviously evident that the resonant contribution R_{is} originates from M_o-type critical point. However, the type of critical point resulting in the non resonant term cannot be easily determined, although it is important to discuss the mechanism of Break-down of selection rule in Brillouin scattering stated in Chap. VI. We have studied the behaviors of resonant effect in the higher photon energy regions for the three dimensional M_1, M_2, and M_3- critical points in semiconductors, which is shown in Appendix I. It is found that the scattering efficiencies arising from the M_1 and M_3-critical points change drastically when the incident photon energies pass through the energy region corresponding to the critical point and never show the exponential tail in the low photon energy regions(see Fig.AI). On the other hand the resonant feature of Brillouin efficiency arising from the M_2-critical point is found to behave similar in form to M_o-critical point except the sign, where the scattering efficiency has the slowly changing exponential tail-structure in the photon energy regions lower than the critical points. It means that the non resonant contribution

observed in transparent regions is closely related to the contribution from M_2-critical point. One can explain qualitatively the antiresonance structure observed at photon energy 2.22 eV in CdS, by assuming that the energy gap of M_2-critical point is $\sim$ 1 eV larger than M_o-gap and that the factor of matrix element; $P_{o\beta}\Xi_{\beta\alpha}P_{\alpha o}$ is about three times larger than the factor $P_{o\beta}\Xi_{\beta\alpha}P_{\alpha o}$ in M_o-critical point. Using eqs.(4.2-6) and (4.2-7) we calculated the total scattering cross section for the T2-mode phonons. In present calculation we used values of $\hbar\Delta\omega_B$(or $\hbar\Delta\omega_A$) in the range of 0.1 eV to 10 eV and we fond that the results are weakly dependent on the values. We adjusted the value R_o and energy gaps to fit the experimental curve. We found that the calculated curve is fitted to the experimental data when we used $\hbar\omega_{gB}$=2.40 eV and $\hbar\omega_{gA}$=2.38 eV. The results are shown in Fig.4.3 by the dotted curve. Similar analysis was made by Gelbart anf Many[17], who found that the best fit to the data was obtained by using the energy gap $\hbar\omega_g$ =2.41 eV, which is in good agreement with the present result. It should be noted that they plotted I_s/I_t as a function of incident photon energy and that such plot does not give correct values of σ_B near the band edge due to the reason stated earlier. The energy gap obtained in the above analyses is much smaller than the value 2.53 eV deduced from reflectance measurements by Cardona and Harbeke.[61] The values of energy gaps are also estimated from electro-reflectance data made by Cardona et al.[62], who found peaks in the electro-reflectance spectra at 2.452 eV, 2.466 eV and 2.525 eV. If we take into account the exciton effects by using the theory of Blossey[86] have higher energy gaps by exciton binding energy (28 meV) than the peak values obtained by Cardona et al.[62] (see Fig.8 of ref.62)

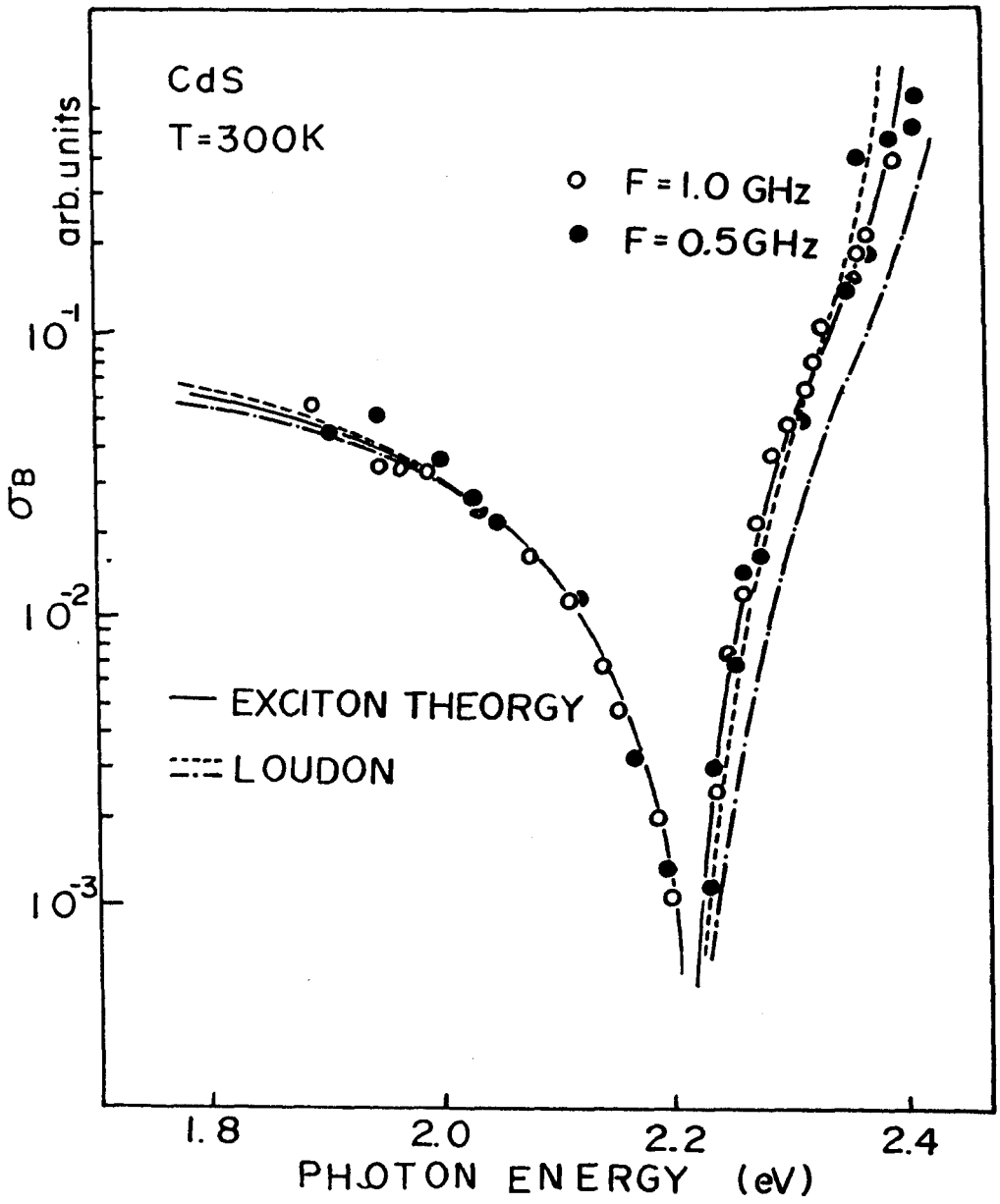

Fig. 4.3. Dispersion curves of Brillouin scattering cross section for 0.5 amd 1.0 GHz phonons. Solid curves are calculated by taking into account the exciton effects with optical band gap: E_{gi}=2.494 eV for the incident light and optical band gap; E_{gs}=2.480 eV for the scattered light. Dotted and dashed curves are estimated by Loudon's theory with Bnad gaps; E_{gi}=2.40 eV, and E_{gs}=2.38 eV, and with E_{gi}=2.494 eV, E_{gs}=2.480 eV,respectively.

; therefore, we obtain $\hbar\omega_{gA}$=2.480 eV, $\hbar\omega_{gB}$=2,494 and $\hbar\omega_{gC}$=2.553 eV. Absorption coefficients at $\hbar\omega_{g\alpha}$= 2.4 eV anf $\hbar\omega_{g\beta}$=2.38 are estimated from Dutton's data to be about 10^2 cm^{-1}. Such large values at lower photon energies than the band gaps can be explained by the exciton effect. As we mentioned in Chapter II, the Coulomb interaction is always present between the excited electrons and holes, and thus it seems to be reasonable to assume that the virtual intermediate electronic excitations are the exciton states. As it is well known, the three valence bands labeled A, B and C in conjunction with the Γ_7-conduction band gives rise to A, B and C series of exciton states, respectively. The selection rule for the momentaum matrix element is is the same as that of band to band transition. In this case we take into account the A and B exciton states for the virtual intermediate states because the dominant contribution R_{is} to the resonant enhancement comes from the bands with the band gap close to the incident or scattered photon energy. In the present calculation of R_{is} we use the representation of excitonic resonant Brillouin scattering derived in Chap. II.(eq.(2.4-4)), where we use the values; $\hbar\omega_{g\alpha}$=$\hbar\omega_{gB}$=2.494 eV and $\hbar\omega_{g\beta}$=$\hbar\omega_{gA}$=2.48 eV . The exciton binding energy is reported to be 28 meV in CdS[86] and we used this value for the both states. Only the adjustable parameter is R_o which is determined to give a minimum of the scattering cross section at 2.22 eV in the dispersion spectra. The calculated result is shown by the solid curve in Fig.4.3, where we find a better and excellent agreement with the experimental results in the whole range of the present investigation.

It should be noted here that there exist d.c. electric field (5×10^3 V/cm) and a.c. field ($\sim10^4$/cm) associated with the piezoelectric potential in the acoustic domain. When the electric fields

are capable of ionizing the exciton, the analysis made is not correct. However, we find that the ionization field of the exciton in CdS is about 1.4×10^5 V/cm[61] which is much higher than the d.c or a.c field associated with the domain. Thus we can conclude that the electric fields do not dominate the Coulomb potential and that the present treatment is adequate.

4.2.2. Resonant Brillouin scattering by Mode-Converted Phonons in CdS.

In this chapter we present dispersion curves of resonant Brillouin scattering for the two kinds of mode-converted phonons (Tl- and PL-modes). The mode conversion was achieved by reflection of the intense phonon beams at the end of the specimen and thus piezoelectrically inactive transverse mode(Tl-mode) and pure longitudinalmode(PL-mode) were generated effectively. Tl-mode phonons are also excited by using the acoustic injection into an end-bonded specimen with proper crystal orientation. In Fig.4.4. the observed dispersion curves of Brillouin scattering for 0.8 GHz and 1.0 GHz Tl-mode phonons are shown. The dispersion curves plotted by (O) and (●) are obtained by using the mode converted phonon beams by reflection and the curves of solid dispersions are obtained by using the injected phonon beams. The experimental results obtained by both methods agree well with each other in the experimental region and show a resonant behavior in the scattering efficiency near the fundamental absorption edge. In the case of Tl-mode one finds from the phenomenological analyses that the scattering efficiency is proportional to the factor $(P_{11}-P_{12})^2$, (P_{11} and P_{12} are the photoelastic constants). Piezobirefringence measurement by Yu and Cardona[58] predicted that the absolute value

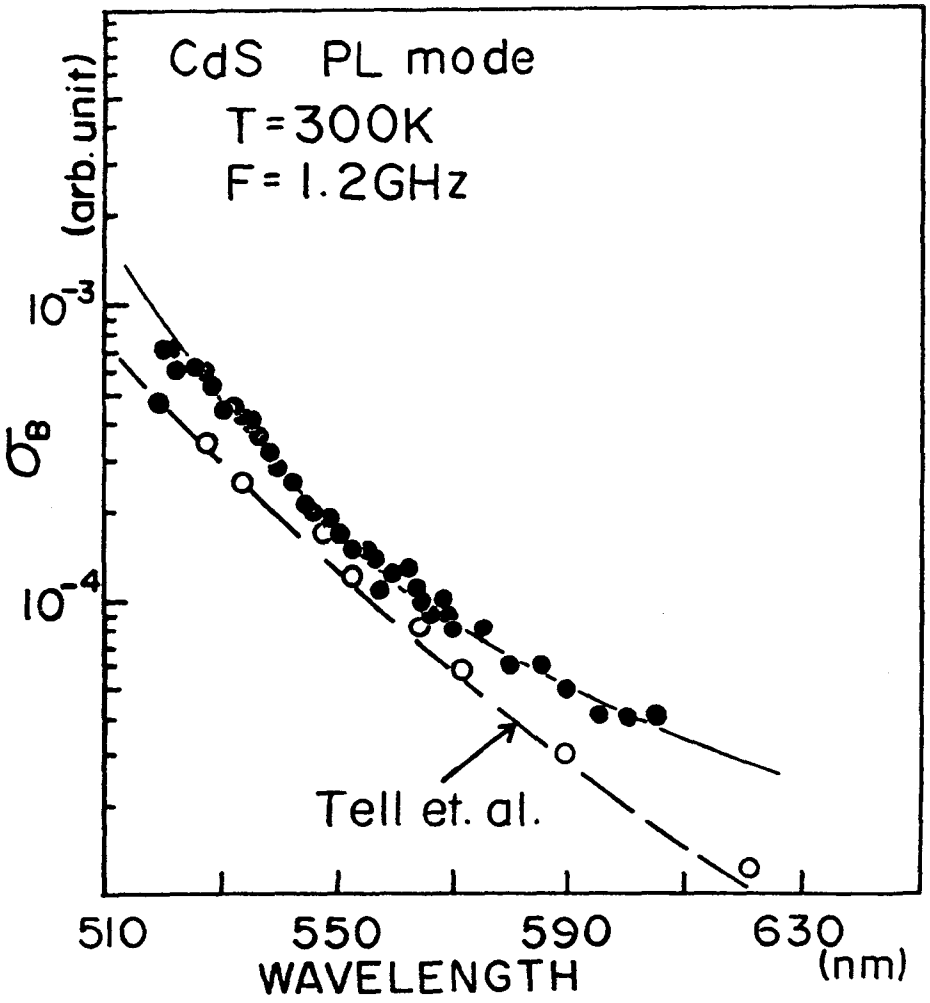

Fig. 4.5. Dispersion curve of Brillouin scattering cross section for PL-mode phonons in CdS. For comparison the dispersion curve observed by Tell et al. is also plotted.

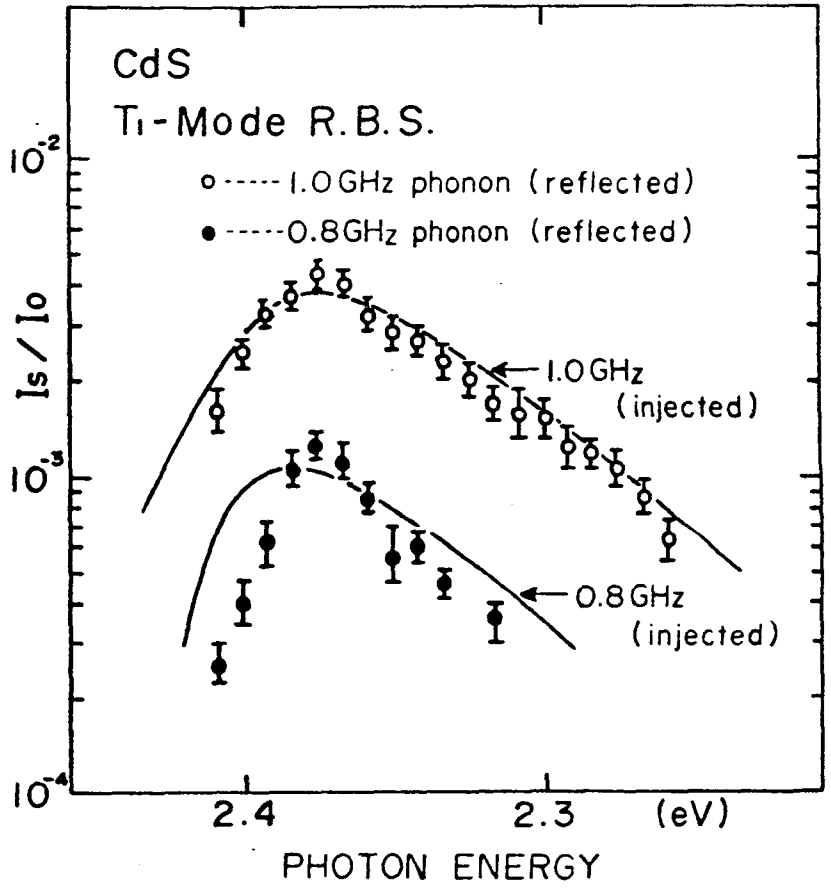

Fig. 4.4. Brillouin scattering signals for T1-mode phonons in CdS. Data points (○) and (●) are obtained by the phonon beams reflected at the end of the specimen and the solid lines are obtained by the phonon beams injected into the end-bonded specimen.

of $P_{11}-P_{12}$ passes through zero at 2.22 eV while undergoing reversal in sign. This experimental result means that the resonant cancellation can be also observed in the dispersion curves of Brillouin scattering cross section for T1-mode phonons. However, one cannot find the structure of resonant cancellation around 2.22 eV in the present work because of weak optical signals.

The decrease in scattering intensity is due to the strong absorption and depletion of incident and scattered light. Using eq.(4.2-2) we estimated the scattering cross sections which are shown in Fig.4.5 along with theoretical dispersion. Dispersion of Brillouin scattering efficiency by pure longitudinal phonons (1.2 GHz) is plotted in Fig.4.6 . In this figure the observed scattering efficiency I_S is normalized by the transmitted light intensity. Such a normalization is valid in the case of PL-mode phonons because the incident light polarization vector(I_E) is parallel to that of the scattered light and thus optical anisotropy does not exist. PL-mode phonons used in the present measurement are generated by reflection of acoustic domain at the end of the specimen and propagates in the c-plane with acoustic displacement vector parallel to the propagating direction. Based upon the above condition it is easily found that the scattering efficiency by PL-mode phonons is proprtional to P_{31}^2. It is interesting to point out that the dispersion spectra of PL-mode Brillouin scattering is quitely different from the resonant feature for the transverse acoustic phonons (T2- and T1-modes). In Fig.4.5 one cannot find a resonant cancellation around 2.22 eV, while in this photon energy region the scattering efficiency changes monotonically. Such experimental results are

interpreted as follows. The sign of resonant contribution in Brillouin scattering efficiency by PL-mode phonons arising from the M_o-critical point is equal to the sign of non-resonant contribution from the far off critical point(M_2-critical point).

A comparison of observed dispersion curve of scattering efficiency for mode-converted phonons with theoretical dispersion is performed by using the formulation of resonant Brillouin scattering derived in Chap.II. In order to fit the theoretical dispersion with that of experimental curves in Fig.4.5(Tl-mode) we assumed the total scattering efficiency $\sigma_{BT}(Tl)$ for Tl-mode as given by,

$$\sigma_{BT}(Tl) = |R_{is}(Tl) - R_o(Tl)|^2 \qquad (4.2\text{-}9)$$

Here $R_o(Tl)$ (non-resonant term) is an adjustable parapeter which is determine by using the results of Berkowicz et al.[23] We estimate the total scattering efficiency $\sigma_{BT}(Tl)$ by using the dip energy 2.20 (the dip energy is also derived by extrapolating the present data to the low photon energy region), which is shown in Fig.4.5 by solid line, where the intermediate A- and B-excitons are taken into account. In the calculation we used the values oscillator strengths reported by Thomas and Hopfield.[64] Band parameters used in the present analyses are summarized in Table 4.I.

Table 4.I. Parameters used in the calculation of resonant enhancement of the Brillouin scattering cross sections for the mode-converted phonons in CdS.

$\hbar\omega_{gA}$	$\hbar\omega_{gB}$	$\hbar\omega_{gC}$	$\Xi_{AB}(Tl)$	$\Xi_{BC}(PL)$	$\Xi_{BB}(PL)$	$\Xi_{CC}(PL)$
2.480 (eV)	2.494	2.553	-1.28 (eV)	1.34	-2.80	-3.29

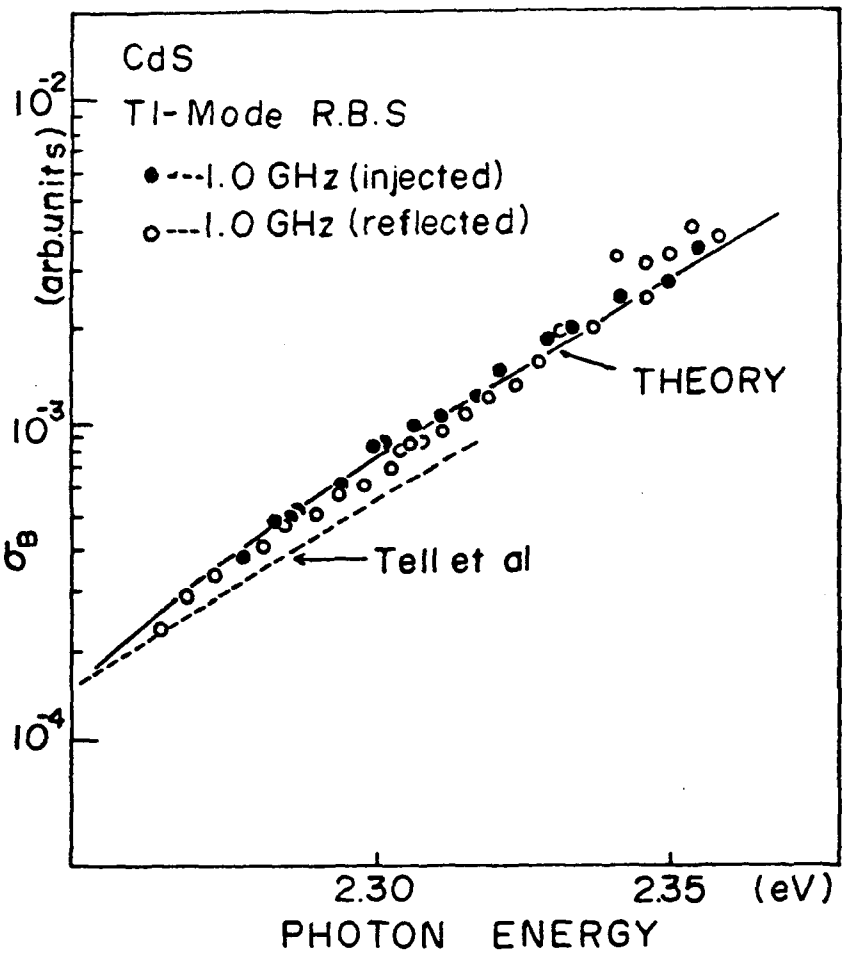

Fig. 4.6. Comparison of experimental data with theoretical dispersion curves of resonant Brillouin scattering by Tl-mode phonons in CdS.

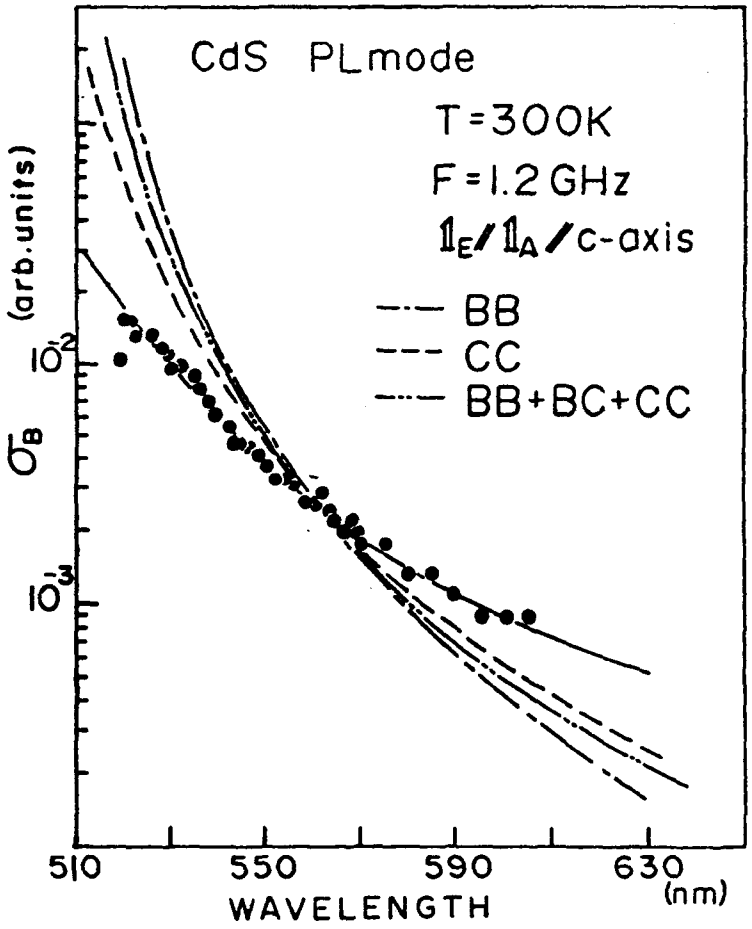

Fig. 4.7. Comparison of experimental data with theoretical dispersion curve of resonant Brillouin scattering by PL-mode phonon in CdS.

We find in this figure a good agreement between the experimental and theoretical dispersions.

In the case of PL-mode, it is found from the analyses of Chap. II. that all the interband and intraband transitions of intermediate electronic excitations are allowed and several kinds of resonant contributions from allowed transition process should be considered. However, it should be noted that the intermediate A-excitons (or holes in A-valence band) does not take part in the present effect because of the forbidden dipole transitions. Calculated dispersion curves by taking into account of the B-exciton(dash dotted line), C-exciton(broken line) and the sum of all the possible excitations(two dash dotted line) are shown in Fig.4.7. In this estimation we used the following relation;

$$\sigma_{BT}(PL) \propto | R_{is}(PL)|^{2} \qquad (4.2\text{-}10)$$

assuming that the non-resonant term R_o is zero. In Fig.4.7 we do not obtain an excellent agreement between the experimental and theoretical curves for the case of PL-mode Brillouin scattering,which seems to be due to the following two reasons. First reason is that one cannot estimate the adjustable parameter R_o(non-resonant term) because of a lack of cancellation point in the dispersion spectra. Second reason is attributed to the fact that we use the unperturbed band parameters shown in Table-4.I. although there exists a considerably strong perturbation by longitudinal strain components in the crystal in the case of PL-mode. In the present case it is very difficult to obtain the correct band parameters (such as band gaps or dipole matrix-elements) because accurate value of strains cannot be evaluated.

4.3.1. Resonant Brillouin Scattering by Injected Phonons in ZnSe

In this section we present a study of resonant Brillouin scattering in semi-insulating ZnSe by making use of injected acoustic waves.[29] Acoustoelectric instability cannot be achieved in ZnSe sample used in the present work because of weak piezoelectricity and small carrier concentration. Therefore the thechnique of acoustic injection is very profitable in the present investigation. From the analyses based upon the acoustic matching theory[78,87] discussed in Chap.VII one can expect that three kinds of acoustic mode excited in an end-bonded specimen; quasi-longitudinal(QL), quasi-transverse(QT) and pure-transverse (PT) modes. We confirmed by Brillouin scattering experiment that two kind of transverse acoustic modes are excited in ZnSe. Our experimental results of sound velocities are V_s(T1)=1670 m/s, for slow TA mode and V_s(T2)=2710 m/s for fast TA mode, which are in good agreement with those of pulse echo method.[89] Schematic arrangement of injected acoustic packet in ZnSe for studying the resonant Brillouin scattering is shown in Fig.4.8.

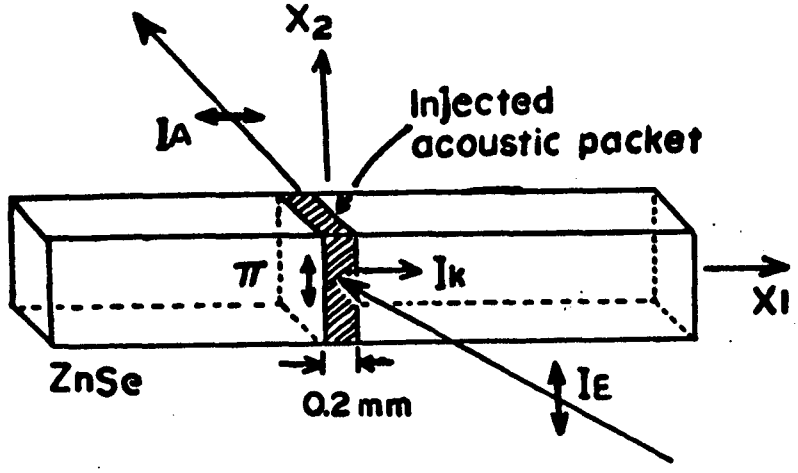

Fig. 4.8. Schematic arrangement for studying resonant Brillouin scattering in ZnSe.

We show the experimental dispersions of Brillouin scattering cross sections for anti-stokes scattering process of T1-mode acoustic phonons in Fig.4.9, in which experimental results are plotted by taking into account the depletion of the incident and scattered light.[15,18] Appropriate phonon frequencies are 0.2 and 0.3 GHz.

Features of such dispersions are almost independent of these acoustic frequencies. This can be understood from the fact that the relative intensity of the scattering efficiency depends upon the frequency spectrum in the acoustic packet and upon the factor $\cos\theta_i$ (this factor depends on the relevant acoustic frequency due to the momentum conservation). The general shape of the experimental dispersion is similar to the results of GaAs[15] and CdS.[18] In the case of ZnSe the scattering cross section has narrow minimum at about $\sim$2.5 eV and shows a sharp increase in the region close to the band edge. Figure 4.10 shows the dispersions of scattering efficiency due to the T2-mode phonons at room temperature. Relevant phonon frequencies are 0.2 and 0.8 GHz and the main feature is almost the same as the results of T1-mode except for the dispersions in the cancellation region. Such a difference in the dispersions comes from the variation on the positions of the minima for the scattering by T1 and T2-mode phonons.

We are able to estimate the position of the minimum, corresponding to the photon energy where the scattering efficiency is just zero, with the help of the following interpretation; (a) relevant photoelastic constant, $P_{11}-P_{12}$ for T1-mode and P_{44} for T2-mode undergo reversal in sign at the corresponding cancellation points, (b) Brillouin scattering intensities for T1 and T2-modes are

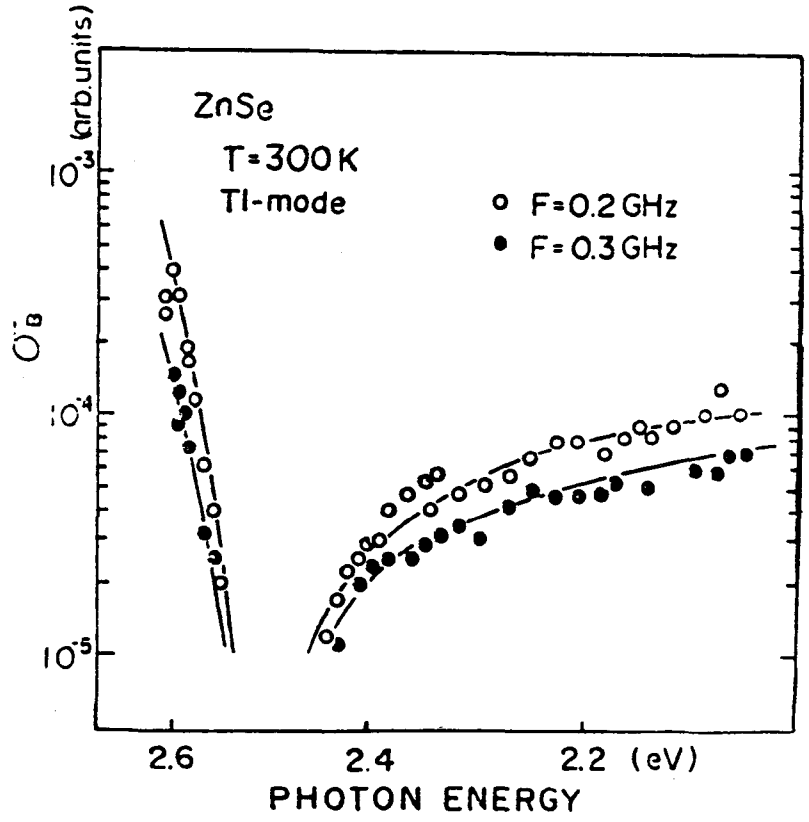

Fig. 4.9. Brillouin scattering dispersion curves for 0.2 and 0.3 GHz Tl-mode phonons in ZnSe. Experimental points are normalized by transmitted light intensity I_t.

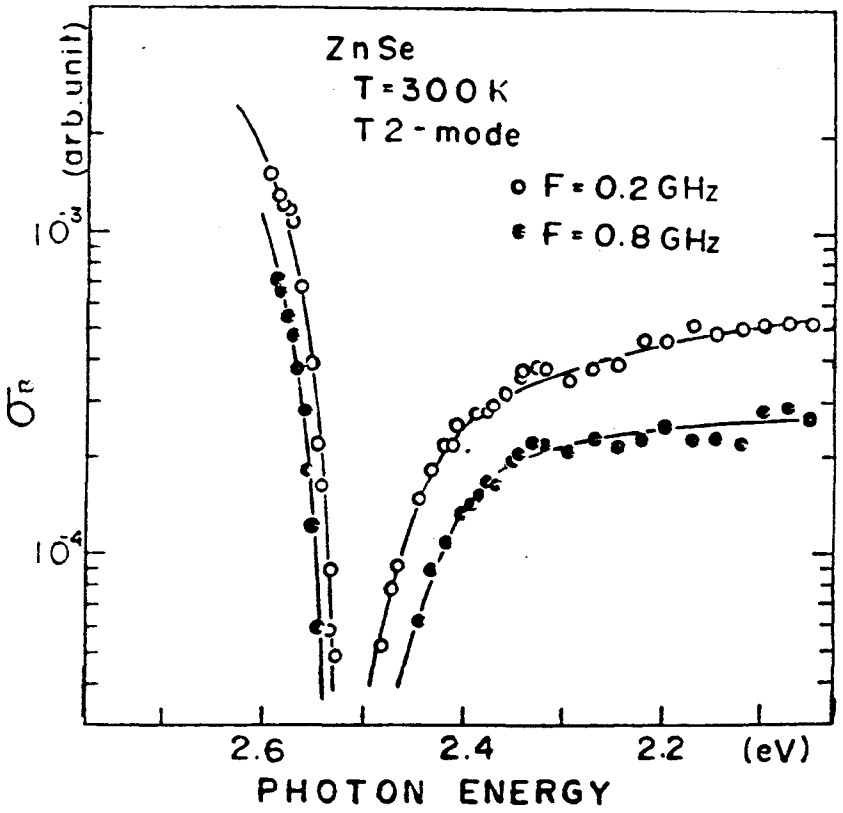

Fig. 4.10. Brillouin scattering dispersion curves for 0.2 and o.8 GHz T2-mode phonons in ZnSe. Experimental points are normalized by transmitted light intensity I_t.

accurately proportional to the factor of $(P_{11}-P_{12})^2$, P_{44}^2, respectively. We plotted the square root of $I_s(T1)/I_t(T1)$ and $I_s(T2)/I_t(T2)$ by taking into account the reversal in sign in Fig.4.11 where $I_s(T1)$ and $I_s(T2)$ are Brillouin scattering intensity. From Fig.4.11 one finds sign reversal at 2.48 eV for T1 and 2.50 eV for T2-mode acoustic phonons by extraporation. Such a phenomenological treatment that the relevant photoelastic constant undergoes a reversal in sign will be discussed in latter section in connection with the piezobirefringence theory.

From the analyses of deformation potential scattering described in the previous Chapter, we find that the transitions between the virtual states associated with the A and B valence bands and between the B and C valence bands are allowed through the interaction of holes and T1-mode phonons and that in the case of T2-mode phonon scattering all the interband transitions between the virtual states associated with the A, B and C valence bands are possible. From eq.(4.2-6) we find that the main contribution comes from the excitation corresponding to the smallest band gap, and thus from the transition between the virtual

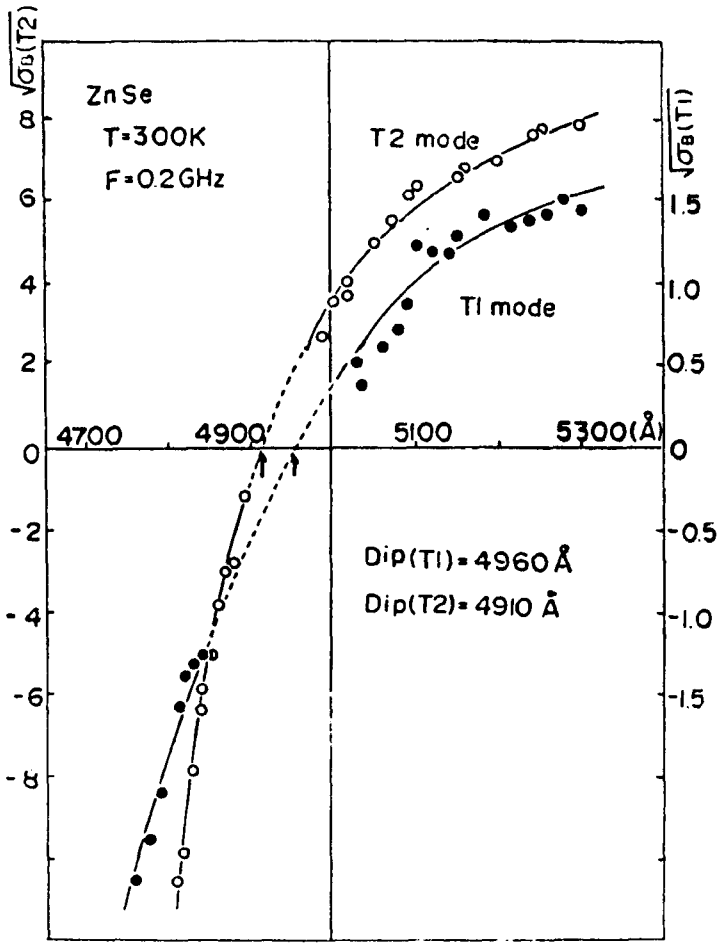

Fig. 4.11. The plots of $\sqrt{\sigma_B}$ versus incident light wavelength for T1- and T2-mode phonons.

states associated with the A and B valence bands. Since the A and B valence bands are degenerate at the Γ-point of Brillouin zone, we can put $\omega_{gA}-\omega_{gB}=0$ in eq.(4.2-6).

As pointed out in the previous section the exciton effect plays an important role in the resonant enhancement. The effect is taken into account by using the formula of eq.(2.4-4) presented in Chap.II.

Now we calculate the Brillouin scattering cross section σ_{BT} by assuming that the resonant contribution R_{is} to the scattering efficiency is opposite in sign to the non-resonant contribution R_o. With this assumption we obtain the total resonant scattering cross section in the form $\sigma_{BT}=|R_{is}-R_o|^2$, where R_o is the adjustable parameters and determined to fit the calculated curve with the experimental. The calculation of σ_{BT} is performed by using the parameters given in Table 4.II. In the estimation we assumed $P_{o\beta}=P_{\alpha o}$ for the momentum matrix elements. The calculated curves for T1 and T2-modes acoustic phonons are shown in Fig.4.12 and 4.13, respectively along with the experimental data. In Fig.4.12 and 4.13 the solid curves are calculated from eq.(4.2-6) neglecting the exciton effect, whereas the dashed curves are obtained by taking into account the exciton effect. We find that the general shapes of both dispersions are quite similar except the cancellation and resonant regions. As shown in Fig.4.12 and 4.13, the cross sections

Table 4.II. Values of parameters used in the calculation of total scattering cross section for T1 and T2-mode phonons. Superscripts(1) and (2) correspond to the strong and weak contribution to the scattering cross section, respectively.

	$\hbar\omega_{gi}^{(1)}$	$\hbar\omega_{gi}^{(2)}$	$\hbar\omega_{gs}^{(1)}$	$\hbar\omega_{gs}^{(2)}$	$\hbar\Delta\omega_{\alpha\beta}$	$\Xi_{\alpha\beta}^{(1)}$	$\Xi_{\alpha\beta}^{(1)}$	f
T1-mode:	2.68 (eV)	2.68	2.68	3.11	5.0	2.07	2.94	0.2GHz
T2-mode:	2.68 (ev)	2.68	2.68	3.11	5.0	-3.81	-2.70	0.2GHz

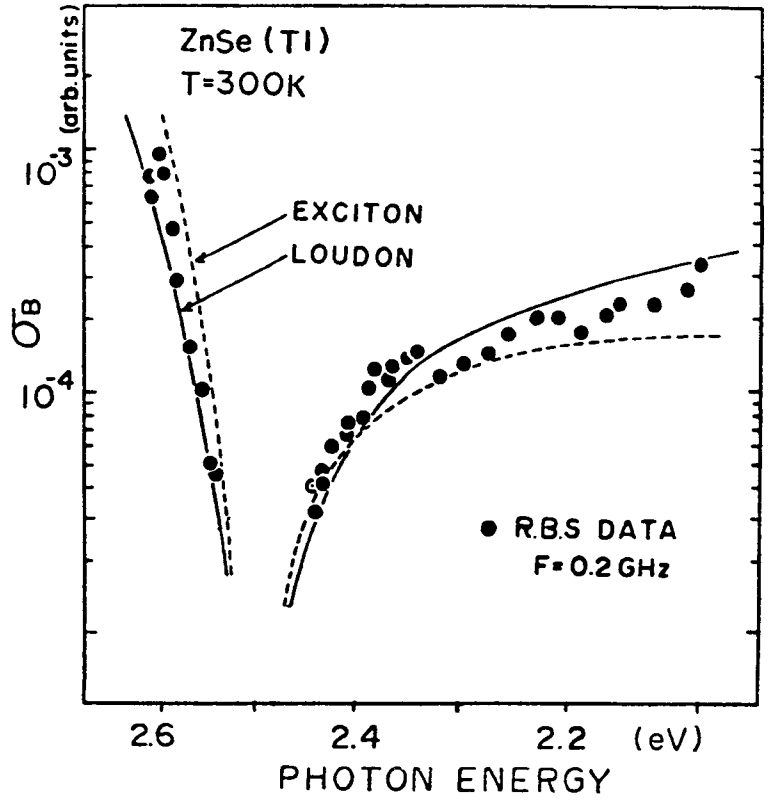

Fig. 4.12. Comparison of experimental with theoretical dispersion curves for T1-mode phonons. Solid curves are obtained by using the Loudon's theory and dashed lines are obtained by taking into account the excitons.

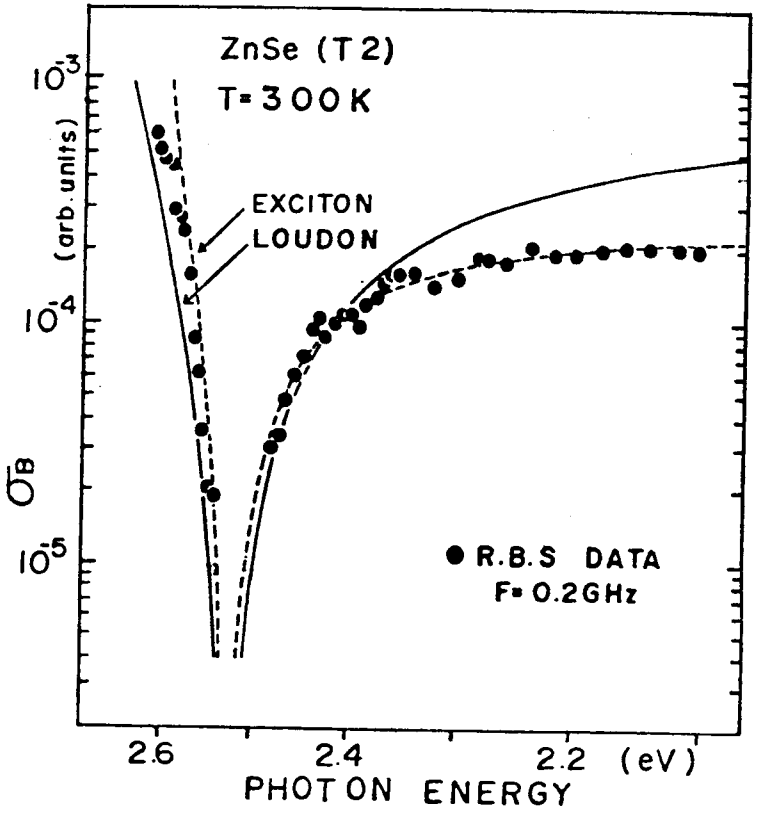

Fig. 4.13. Same as Fig. 4.12. but for the T2-mode phonons.

estimated from the Loudon's formulation are smaller than those of experimental data near the fundamental edge for both T1 and T2-mode phonons. On the other hand the dispersion curves calculated from eq.(2.4-4) show a reasonable agreement with the experimental results for both T1 and T2-mode phonons in the whole energy regions. We can easily find that non-zero strain components exist in the specimen in the presence of T1 and T2-mode acoustic phonons, however, such strains do not effectively perturb the band structure. Therefore one can just estimate the total scattering cross section (including the exciton effect) by using the zero order unperturbed wave functions. These physical features are important in discussion of hole (or exciton)-acoustic phonon interaction. Same interpretation as mentioned above is also possible in the case of wurtzite materials such as CdS and CdSe.

4.3.2. Derivation of Relevant Photoelastic Constants from Static Birefringence Theory.

In this section we derive the dispersions of relevant photelastic constants near the fundamental edge of ZnSe from the stress-induced birefringence theory.[58, 82] In the piezobirefringence experiments static stress is applied to produce a change in the dielectric constant, whereas in the Brillouin scattering experiments stress associated with a strain of injected acoustic wave, induces a change in the dielectric constant. Therefore two phenomena are equivalent and analyzed with the use of the same photoelastic constant P_{ijkl}. In the presence of stress component X_{kl} in the crystal change in the dielectric constant tensor ε_{ij} is given by,

$$-\frac{\Delta\varepsilon_{ij}}{\varepsilon_{ii}\varepsilon_{jj}} = P_{ijkl}S_{klmn}X_{mn} \qquad (4.3\text{-}1)$$

where ε_{ij}, P_{ijkl} and S_{klmn} are the dielectric constant(in the absence of the stress) photoelastic and elastic compliance constants, respectively. In the case of isotropic crystal all the diagonal elements of dielectric constant tensor are equal ($\varepsilon_{11}=\varepsilon_{22}=\varepsilon_{33}$) and other off-diagonal components are zero. The photoelastic constant tensor has the following form,

$$\begin{bmatrix} P_{11} & P_{12} & P_{12} & 0 & 0 & 0 \\ P_{12} & P_{11} & P_{12} & 0 & 0 & 0 \\ P_{12} & P_{12} & P_{11} & 0 & 0 & 0 \\ 0 & 0 & 0 & P_{44} & 0 & 0 \\ 0 & 0 & 0 & 0 & P_{44} & 0 \\ 0 & 0 & 0 & 0 & 0 & P_{44} \end{bmatrix} \qquad (4.3\text{-}2)$$

and the elastic compliance constant tensor [S] has also the same form as eq.(4.3-2). When the stress X is applied in the [100] direction of the crystal, we obtain piezobirefringence coefficient $\alpha(T1)$ from eqs.(4.3 -1) and (4.3-2),

$$\alpha(T1) = \frac{\Delta\varepsilon_{\parallel} - \Delta\varepsilon_{\perp}}{X} = -\varepsilon_{11}^2 (P_{11}-P_{12})(S_{11}-S_{12}) \qquad (4.3\text{-}3)$$

where $\Delta\varepsilon_{\parallel}$ and $\Delta\varepsilon_{\perp}$ are the changes in the dielectric constants, defined with respect to the stress direction: that is, the light polarization parallel to the[100] and [010] directions, respectively. Comparing eq.(4.3-3) with eq.(2.2-31) we find that this configuration corresponds to the Brillouin scattering by T1-mode phonons. In the case of stress applied to the [110] direction, nonvanishing stress components are $X_{xx}=X_{yy}=X_{xy}=X_{yx}=x/2$, where X is the stress magnitude. Therefore the birefringence coefficient $\alpha(T2)$ is

$$\alpha(T2) = \frac{\Delta\varepsilon_{\parallel} - \Delta\varepsilon_{\perp}}{X} = -\varepsilon_{11}^2 P_{44} S_{44} \qquad (4.3\text{-}4)$$

In eq.(4.3-4), $\Delta\varepsilon_{\parallel}$ and $\Delta\varepsilon_{\perp}$ are the changes in the dielectric constants for the light polarization parallel to the [110] and [1$\bar{1}$0]

directions, respectively. We find that this configuration corresponds to the Brillouin scattering by T2-mode acoustic phonons.

Microscopic treatments of intrinsic piezobirefringence have been carried out by Higginbotham et al.[82] using an interband one electron model for the optical constants, which include the effects of the dispersions of the E_o, $E_o+\Delta_o$, E_1, $E_1+\Delta_1$ and E_2 gaps. Taking the types of critical points into account we obtain the real part of the dielectric constant ε_1 from the Kramers-Kronig transformation. The contribution to ε_1 can be written as

$$[\varepsilon_1(\omega)]_{//,\perp} - 1 = A|P_{//,\perp}|^2 \omega_o^{-3/2} f(x_o) \qquad (4.3\text{-}5)$$

where $A=(2e^2\hbar^{1/2}/m^2)(2m^*/\hbar^2)^{3/2}$, $f(x)=[2-(1+x)^{1/2}-(1-x)^{1/2}]/x^2$. In eq.(4.3-5) $x=\omega/\omega_o$ ($\hbar\omega_o=E_o$), m^* is the combined density of state mass and $P_{//,\perp}$ is the matrix element of the component of momentum polarized either parallel or perpendicular to the stress according to the subindex. The change in $\varepsilon_1(\omega)$ with stress-application can be written including two degenerate v_A, v_B valence bands as

$$\Delta\varepsilon_1(\omega) = \sum_{v_A,v_B} \left[\frac{\partial\varepsilon_1}{\partial M} \Delta M + \frac{\partial\varepsilon_1}{\partial\omega_o} \Delta\omega_o \right] \qquad (4.3\text{-}6)$$

The change in energy gaps to first order in stress are given[89] by

$$\Delta(E_c-E_{vA}) = \begin{cases} -b(S_{11}-S_{12})X & \cdots\cdot \text{for T1-mode} \\ -d/4\cdot S_{44}X & \cdots\cdot \text{for T2-mode} \end{cases} \qquad (4.3\text{-}7)$$

$$\Delta(E_c-E_{vB}) = \begin{cases} b(S_{11}-S_{12})X & \cdots\cdot \text{for T1-mode} \\ d/4\cdot S_{44}X & \cdots\cdot \text{for T2-mode} \end{cases} \qquad (4.3\text{-}8)$$

$$\Delta(E_c-E_{vC}) = 0 \qquad \cdots\cdot \text{for T1 and T2-mode} \qquad (4.3\text{-}9)$$

where we neglected the term due to the hydrostatic deformation potential, since we are concerned with a comparison with the

Brillouin scattering and the hydrostatic term disappears due to the fact that $e_{xx}+e_{yy}+e_{zz}=0$ for both T1 and T2-mode phonons. Substituting the relations of eqs.(4.3-7) (4.3-9) and values of ΔM estimated by Pollak and Cardona[89] into the eq.(4.3-6), one obtains expressions of Birefringence-coefficients $\alpha(T1)$, and $\alpha(T2)$. In a similar fashion we can include the contribution to $\alpha(T1)$ and $\alpha(T2)$ from other energy gaps. In the following analysis, however, we include only the contribution of E_o and $E_o+\Delta_o$ gaps and take into account of the exciton effect (discrete exciton contribution, n=1). After simple manipulation dispersion of the relevant photoelastic constants $P_{11}-P_{12}$ is given by[26]

$$P_{11}-P_{12}=C(T1)\{-g(\omega/\omega_o)+4\frac{E_o}{\Delta_o}[f(\omega/\omega_o)-(\omega/\omega_{os})^{3/2}f(\omega/\omega_{os})]\}$$

$$+C_{ex}(T1)\{\frac{3-x_{ex}^2}{(1-x_{ex}^2)^2}+\frac{E_{ex}}{\Delta_o}(\frac{1}{1-x_{ex}^2}-(\frac{E_{ex}}{E_{ex}+\Delta_o})^3\frac{1}{1-x_{exs}^3}\}+D(T1) \qquad (4.3\text{-}10)$$

with

$$g(x)=[2-(1+x)^{-/2}-(1-x)^{-1/2}]/x^2$$

$$C(T1)=-(3m^*/2)^{3/2}P^2b\omega_o^{-5/2}/((S_{11}-S_{12})\varepsilon_{11}^2)$$

$$C_{ex}(T1)=-3(4\pi Nf_1)b/(E_{ex}^2(S_{11}-S_{12})\varepsilon_{11}^2)$$

where Δ_o is spin orbit splitting energy, $\hbar\omega_{os}=E_o+\Delta_o$, $x_{ex}=\omega/E_{ex}$, $x_{exs}=\omega/(E_{ex}+\Delta_o)$, E_{ex} exciton energy, N the number of molecules per unit volume and f_1 is the oscillator strength. In eq.(4.3-10) the first term corresponds to the contribution of E_o and $E_o+\Delta_o$ gaps. In a similar manner we can calculate the dispersion of P_{44}, which is given by replacing C(T1), $C_{ex}(T1)$, and D(T1) in eq.(4.3-10) with C(T2), $C_{ex}(T2)$, and D(T2) where $C(T2)=-(3m^*/2)^{3/2}P^2\omega_o^{-5/2}/(8S_{44}\varepsilon_{11}^2)$ and $C_{ex}(T2)=-3(4\pi Nf_1)d/(8E_{ex}^3S_{44}\varepsilon_{11}^2)$.

Dispersions of the appropriate photoelastic constants were calculated in the energy region near the fundamental absorption edge by using the parameters shown in Table 4.III. In this table the values of minimum positions in σ_B (or cross over points of the photoelastic constants) for T1 and T2-mode are estimated from experimental data and the adjustable parameters D(T1) and D(T2) are determined so that these minimum positions agree with the cross over point of the relevant photoelastic constants. Taking into account the exciton contribution we calculated the dispersions of $P_{11}-P_{12}((P_{11}-P_{12})^2)$ and $P_{44}((P_{44})^2)$ which are shown in Fig.4.14 and 4.15 by dashed (dash-dotted) curves, along with the experimental points. These experimental points for T1 and T2-mode phonons in Fig.4.14 and 4.15 are estimated from Fig.4.11 and plotted to fit the calculated curves at a fixed point with an arbitrary scaling factor. We find that the photoelastic constants undergo a reversal in sign and that the calculated curves are in good agreement with the experimental dispersions.

Table 4.III. Values of parameters used in the calculation of dispersions of photoelastic constant from static piezobirefringence theory.

T1-mode($P_{11}-P_{12}$)	T2-mode(P_{44})
$C(T1)=5.7\times10^{-3}$ (a)	$C(T2)=2.24\times10^{3}$ (a)
$C_{ex}(T1)=3.1\times10^{-5}$ (a)	$C_{ex}(T2)=1.72\times10^{-5}$ (a)
$D(T1)=-3.6\times10^{-2}$ (b)	$D(T2)=-1.72\times10^{-2}$ (b)
Dip(T1)=2.50 eV (b)	Dip(T2)=2.52 eV (b)

(a) P. Y. Yu and M. Cardona : in ref.58.
(b) Estimated from the present experimental data, 'Dip' stands for the photon energy corresponding to the minimum in the Brillouin scattering cross sections.

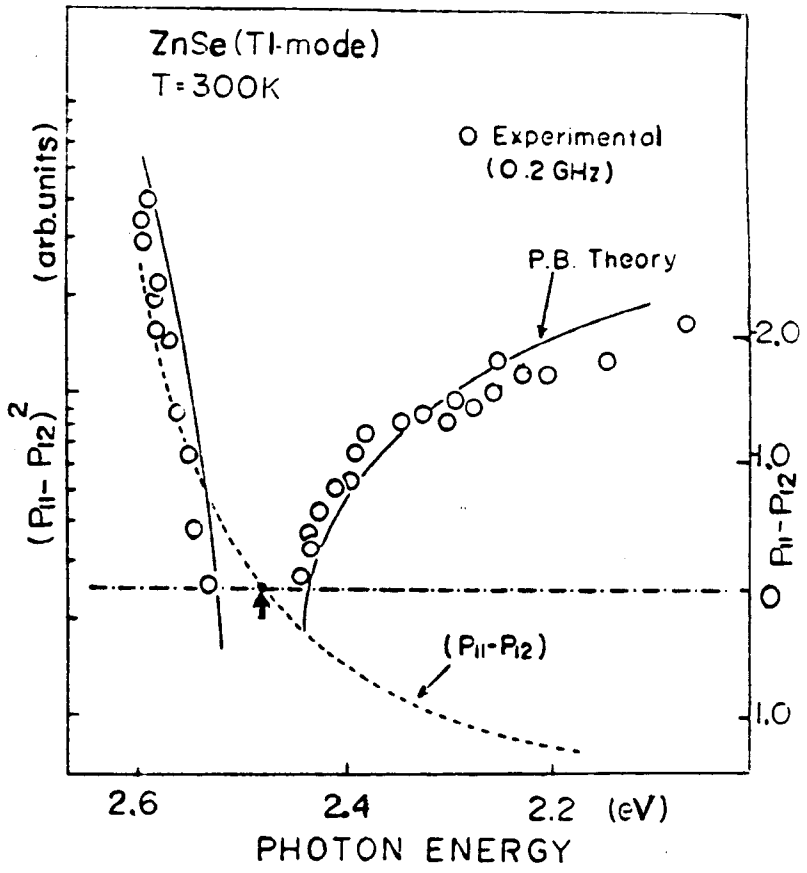

Fig. 4.14. Experimental points and fitted curves of $(P_{11}-P_{12})^2$ and $(P_{11}-P_{12})$ calculated from the P.B.-theory in ZnSe.

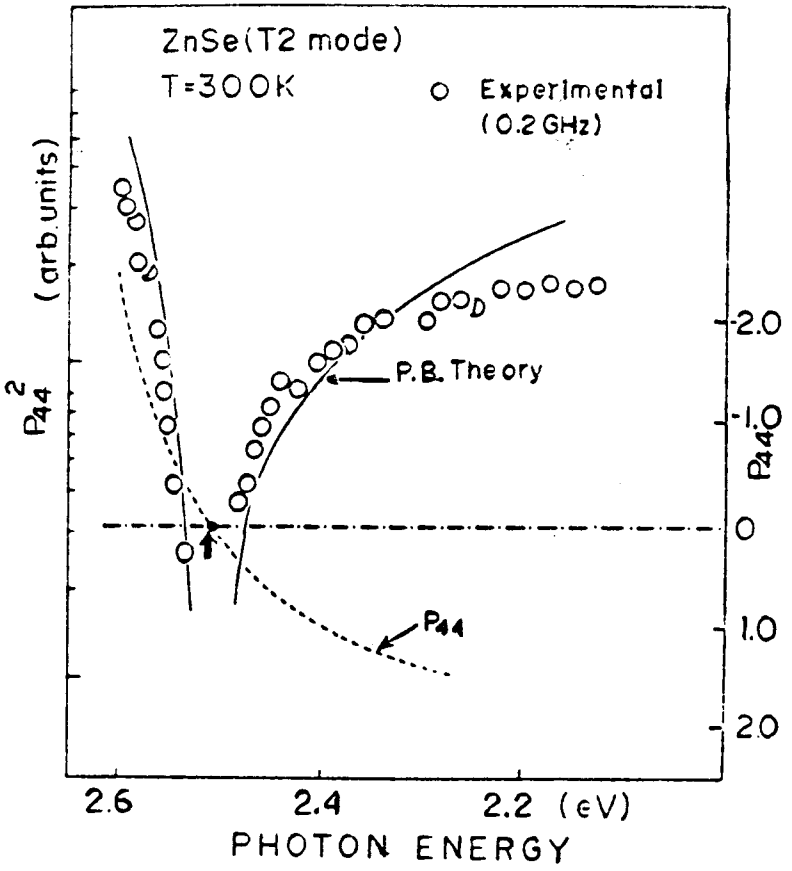

Fig. 4.15. Same as Fig. 4.14. but for the T2-mode and P_{44} and $(P_{44})^2$.

4.4. Summary

We have investigated the dispersion spectra of the Brillouin scattering cross sections by making use of intense acoustic phonons amplified through acoustoelectric effect in CdS. A deep and narrow minimum at the incident photon energy 2.22 eV and a steep increase in the higher photon energy region beyond the minimum are observed in the dispersion spectra . It is found that the observed dispersion curve of Brillouin scattering cross section for the PL-mode phonons is quite different from that for the transverse mode phonons and antiresonance structure around 2.22 eV does not exist. The dispersion spectra are well explained if we take into account of the transition of intermediate virtual states associated with the p-like valence bands and of exciton effects. It has been shown that the matrix elements for the transition of the virtual states between the B and A valence bands(interband-transition) are nonvanishing and has a dominant contribution to the resonant enhancement of transverse mode phonons, while the intraband transitions of virtual states are important for the resonant Brillouin effect of PL-mode phonons. The experimental dispersion curves of resonant Brillouin scattering due to the two kinds of injected acoustic phonons(T1 and T2-modes)into ZnSe are also presented where we found a resonant enhancement and cancellation similar to the case in semiconductive CdS. Dispersions estimated from the static P.B.-theory shows a fairly good agreement with present experimental results of ZnSe. From the present analyses we find that relevant photoelastic constant shows a sign reversal and that the cross-over point coinsides with the minimum position in the Brillouin scattering cross sections.

Chapter V. Optical Modulation and Resonant Brillouin scattering in CdS

5.1. Introduction

The large modulation of the optical transmission near the intrinsic absorption edge by acoustic doamins has been observed in GaSb,[92] GaAs[93-95] and CdS.[95-102] This chapter is devoted to show the excess optical modulation induced by acoustoelectric domains. Until now many theoretical interpretations of domain induced optical modulation (O.M.) are presented. For example in the case of n-GaAs, Spears et al.[92,94] predicted that optical modulation observed near the intrinsic absorption edge are closely connected to the edge-modulation effect by piezoelectric field inside the domain through so called Franz-Keldysh effect.[104,105] In fact there exists a large longitudinal electric field (3×10^4 V/cm in GaAs and $\sim10^5$ V/cm in CdS) associated with the amplified acoustic flux, which induces Franz-Keldysh effect resulting in optical modulation. In the semiconductive CdS measurements of O.M. have been performed in detail by many investigators.[95-101] It should be noted, however, that the experimental results of optical modulation in CdS revealed several different features. Yamamoto et al.[97] proposed that optical modulation signals are still increasing after the magnitude of electric d.c.-field existing inside the acoustic domain saturated (It is shown in Fig. 5.1.). They examined the relation between the O.M. signal and d.c.-electric field, and found that O.M. signals do not depend upon the magnitude of d.c. field. This means that the domain induced O.M. is not related to the existing d.c. electric field inside the domain. On the other hand Hata et al.[102] pointed out that the peak values of O.M. signal are observed at a

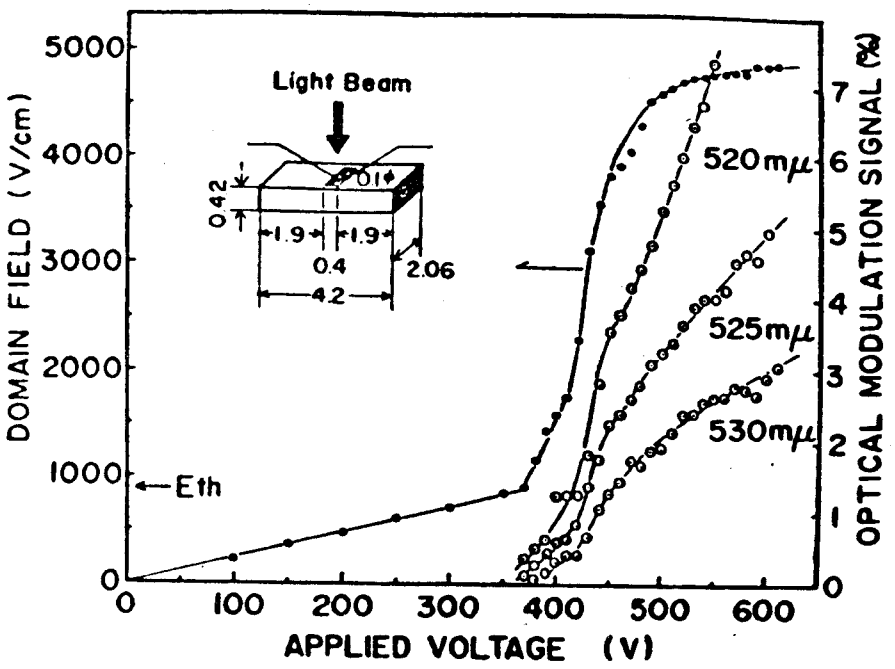

Fig. 5.1. Field dependence of O.M in CdS. O.M. signals are obtained by using the light with wavelength: 5200, 5250 and 5300 A.

slightly different position from the maximum point of piezoelectric fields in the crystals. This is due to the fact that the acoustic flux propagates in advance from the high field daomin in the specimen. Those two experimental results are inconsistent with the interpretation of O.M. in GaAs proposed by Kohn[98] and Spears.[93] Our experimental results presented in this chapter claim the explanation of domain induced-optical modulation in terms of the Franz-Kedysh effect due to the high electric fields. We observed a strong modulation signal not only in the region near the fundamental edge but also in the transparent region far from the edge.[101,103] It is found that the dispersion of optical modulation ; $\Delta I_t/I_t$ (ΔI_t is the domain induced change in the transmitted light intensity and I_t is the transmitted light intensity in the absence of domain)has a deep minimum at a photon energy below the intrinsic edge of CdS. The magnitude of the modulation increases as the incident photon energy shifts to the low photon energy region. It is very interesting to point out that the photon energy giving the minimum point in the dispersion of O.M. corresponds to the dip energy in

the dispersion spectrum of resonant Brillouin scattering presented in the previous chapter. From this result we speculate that the optical modulation induced by the propagating acoustic domain in CdS is not originated from the effect of d.c. or a.c.-electric fields. We performed a comparison of dispersion spectra of O.M. with that of resonant Brillouin scattering and found that both the dispersion spectra are quite similar in the shape in the whole experimental region as shown in this chapter. In addition we found that optical modulation is induced by piezoelectrically inactive T1-mode phonons. From these facts we would like to point out a possibility that the observed optical modulation induced by propagating acoustic domains in CdS may be explained in terms of the effect of resonant light scattering.

5.2. Experimental Results and Discussions.

Figure 5.2 shows a schematic diagram of the light polarization configurations for two kinds of acoustic domains(piezoelectrically active and inactive phonons). In Fig.5.2 I_o is the incident light intensity and I_t' is the transmitted light intensity in the presence of acoustic domain. The normalized optical modulation is defined, as mentioned before, as the ratio of the change in transmitted light intensity ΔI_t to the unperturbed light intensity I_t; $\Delta I_t/I_t$,

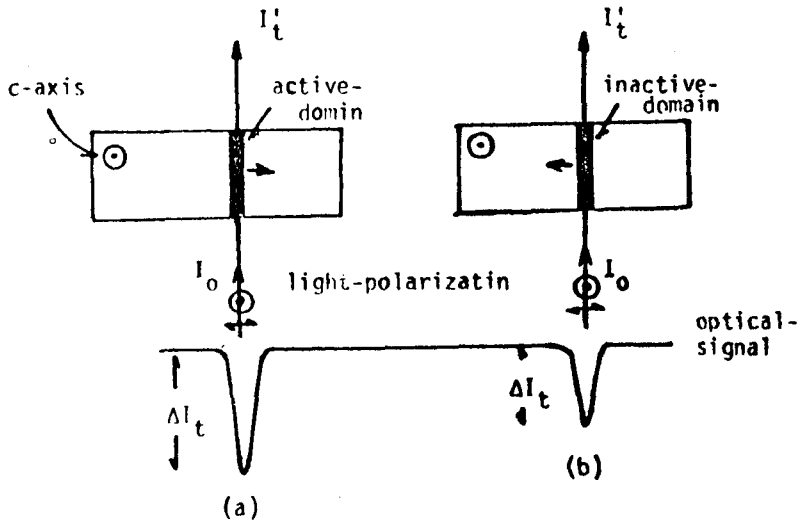

Fig. 5.2. Schematic diagram of Polarization-conditions and optical signals in the measurement of O.M in CdS. Optical signal(a) originates from the active domain and (b) originates from the inactive(reflected-) domain.

where the relation $I_t = I'_t + \Delta I_t$ exists. In the measurement of O.M. by using the piezoelectrically active domains two polarization conditions are used ; that is , (a) incident and scattered light polarizations (I_E and I_{tA}) are parallel to the c-axis and (b) incident and transmitted light polarizations (I_E and I_{tA}) are both perpendicular to the c-axis of CdS. In the case of inactive phonons the polarization condition of (a) is used. Fig. 5.3 shows dispersion spectra of normalized-optical modulation observed under the two polarization conditions; (a) ($I_E // I_{tA} // c$-axis) and (b) ($I_E // I_{tA}$) $\perp$ c-axis

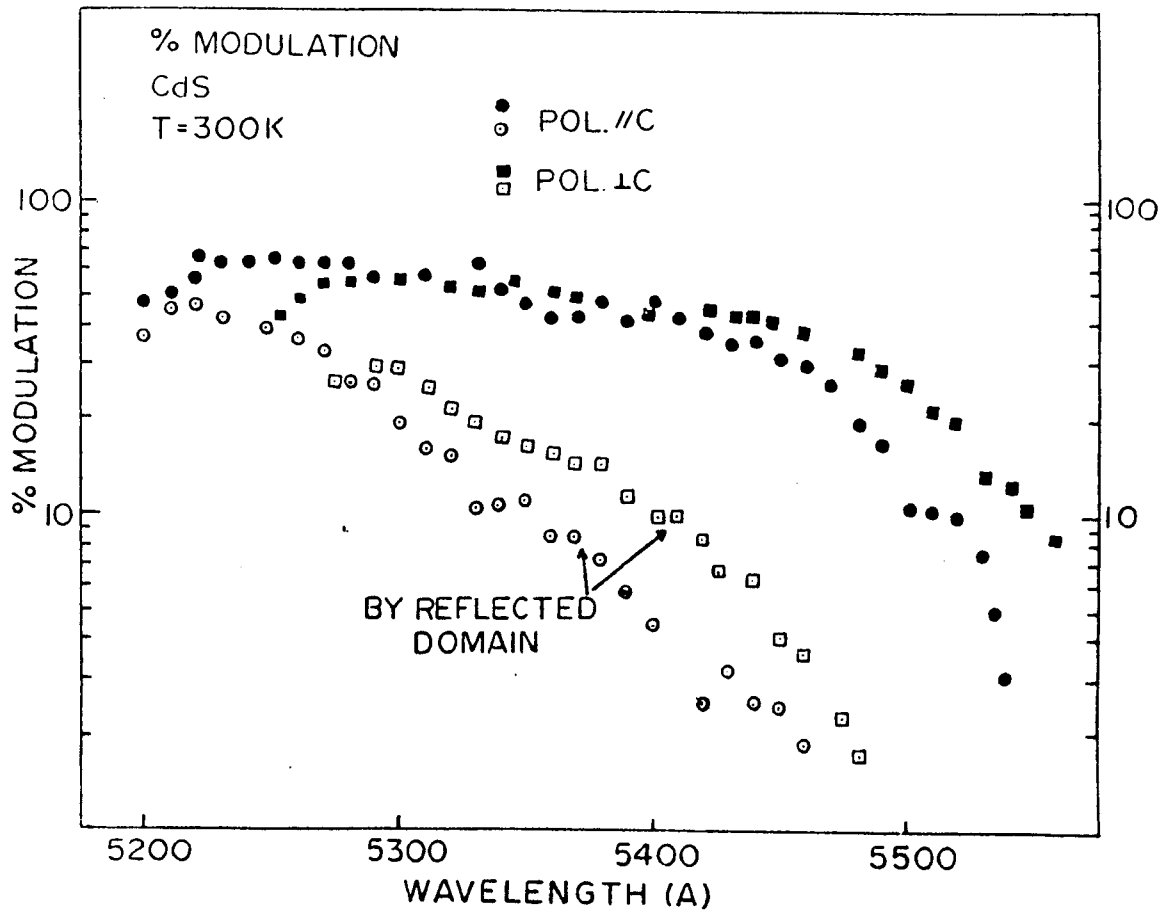

Fig. 5.3. Dispersion spectra of O.M observed under the two polarization conditions: (a) $I_E // I_{TA} //$ c-axis and (b) ($I_E // I_{TA}$) $\perp$ c-axis near the fundamental absorption edge of CdS. The data points of (●) and (■) are obtained by using the active domains and (⊙) and (⊡) are obtained by using the inactive (reflected-) domain.

near the intrinsic absorption edge of CdS at room temperature. Experimental data obtained by using the piezoelectrically active domains are shown by (●) and (□), those obtained by using the piezoelectrically inactive(reflected) domains are shown by (⊙) and (⊡). As shown in Fig.5.3 maximum optical modulation observed under the polarization condition(a) is ~70 % and drastically decrease as incident light wavelength passes through the photon energy region of 5600 Å. It is found that the O.M.signals can be also observed in the measurement using the reflected domain (consisting piezoelectrically inactive phonons) and that the maximum modulation reaches~50 % near the intrinsic edge of the specimen. The dispersion spectra of O.M.observed in the lihgt wavelength region from 5200 Å to 6500 Å are shown in Fig. 5.4 along with the dispersions of resonant Brillouin scattering by 1.0 GHz acoustic phonons. The plots of (O) refer to the polarization condition (a) and (●) to the polarization condition (b). One can find in Fig.5.4 two interesting features ; (1) there exist a considerably strong optical modulation signals in the wavelength region far from the edge and (2) a deep and narrow minimum in the O.M.-dispersion appears at the phonon energy corresponding to the position of the dip in the Brillouin scattering cross section. We find that the dispersion spectra of O.M. for both (a) and (b) polarization conditions are quite similar to that of resonant Brillouin scattering in the experimental photon energy region. As mentioned before the physical interpretation of present O.M.spectra by using th Franz-Keldysh effect (F.K.effect) through the piezoelectric field is not valid, because the effective edge-modulation by F.K.effect can be

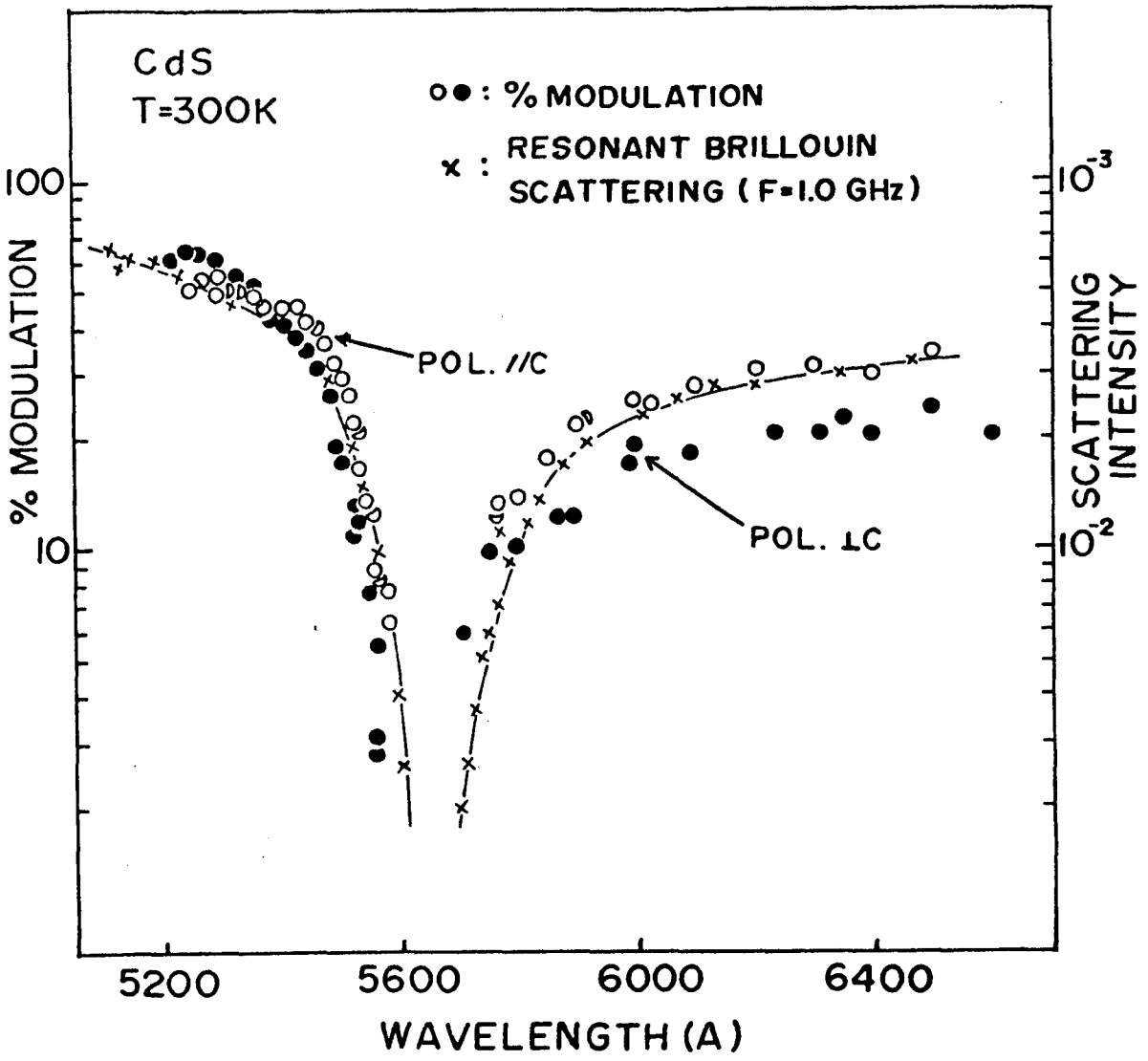

Fig. 5.4. Dispersion spectra of O.M. in the wavelength region from 5200 to 6500 A in CdS. observed under the two polarization conditions (a) (○) and (b) (●). For comparison the resonant dispersions of Brillouin scattering by 1.0 GHz phonons are Plotted.

expected only in the photon energy region close to the intrinsic edge. We obtain the O.M. signals of several tenths near the edge when we assume that the change $\Delta\alpha$ in absorption coefficient α is induced by the electric field ($\sim 10^4$ V/cm). However, it is well known that the optical modulation induced by the electric field decreases remarkably when the incident light wavelength becomes longer and that a structure of deep minimum is not observed far

from the edge. Moreover, in the case of O.M. induced by inactive acoustic domains we cannot expect any possibility of electric field-modulation because of the absence of piezoelectric field in the domains. Therefore we conclude that the present results of O.M. effect in CdS cannot be fully understood in terms of such a field modulation effect. We present a tentative explanation of acoustic domain induced optical modulation by making use of the resonant light scattering. In order to carry out the comparison between the optical modulation and resonant Brillouin scattering we calculate a change in the transmitted light intensity caused by the depletion due to the light scattering. The change in the transmitted light intensity ΔI_t due to the Brillouin scattering is represented by,

$$\Delta I_t(/\!/,\perp) = I_o \exp[-\alpha(/\!/,\perp) - I_o \exp[(\alpha(/\!/,\perp)+\sigma_{BT})b] \qquad (5.2\text{-}1)$$

where I_o is the incident light intensity, σ_{BT} is total Brillouin scattering cross section and $\alpha(/\!/)$ and $\alpha(\perp)$ are the intrinsic absorption coefficients for the light with polarization vectors parallel and perpendicular to the c-axis, respectively. Equation (5.2-1) can be rewritten in more convenient form,

$$\frac{\Delta I_t}{I_t} = 1 - \exp(-\sigma_{BT} b) \qquad (5.2\text{-}2)$$

where I_t is transmitted light intensity in the absence of acoustic domain and the ratio $\Delta I_t/I_t$ corresponds to the normalized modulation defined before. It is found from eq.(5.2-2) that the dispersion spectra of the modulation show a feature similar to that of Brillouin scattering. We have already shown that the general feature of the resonant Brillouin scattering is independent

of acoustic phonon frequency. Therefore total Brillouin scattering cross sections σ_{BT} arising from various acoustic frequencies seems to show a similar shape of the resonant Brillouin spectrum arising from a particular acoustic frequency. Taking these facts into account we estimate optical modulation, $\Delta I_t/I_t$, for both (a) and (b)-polarization conditions and the results are shown in Fig.5.5. In this figure the broken lines are estimated by using eq.(5.2-2) in which the dispersion curves of resonant Brillouin scattering by 1.0 GHz acoustic phonons are used instead of σ_{BT}. We adjust the value σ_{BT} to fit the dispersion estimated from eq.(5.2-2) to the experimental dispersion of O.M. at the longer wavelength region, since the optical modulation is undoubtedly caused only by light scattering in the long wavelength region. It is found in Fig.5.5 that the estimated dispersion by using eq.(5.2-2) for the case of polarization vector parallel to the c-axis agrees well with observed dispersion of O.M. in the whole experimental region, while a slight difference exists between the two dispersion curves for the case of Polarization condition (a); (the polarization vectors of incident and transmitted light are both perpendicular to the c-axis). However, general feature of the modulation is well explained in terms that the depletion of light due to the resonant Brillouin scattering results in the optical-modulation. Similar analysis was carried out for the case of O.M. induced by the piezoelectrically inactive domains which are shown in Fig.5.6, where we find a good agreement between the observed modulation spectra and estimated dispersion spectra by using the Brillouin scattering. In this case modulation effect is considered to originated only from the light scattering effect.

The slight difference between the dispersion of O.M. and

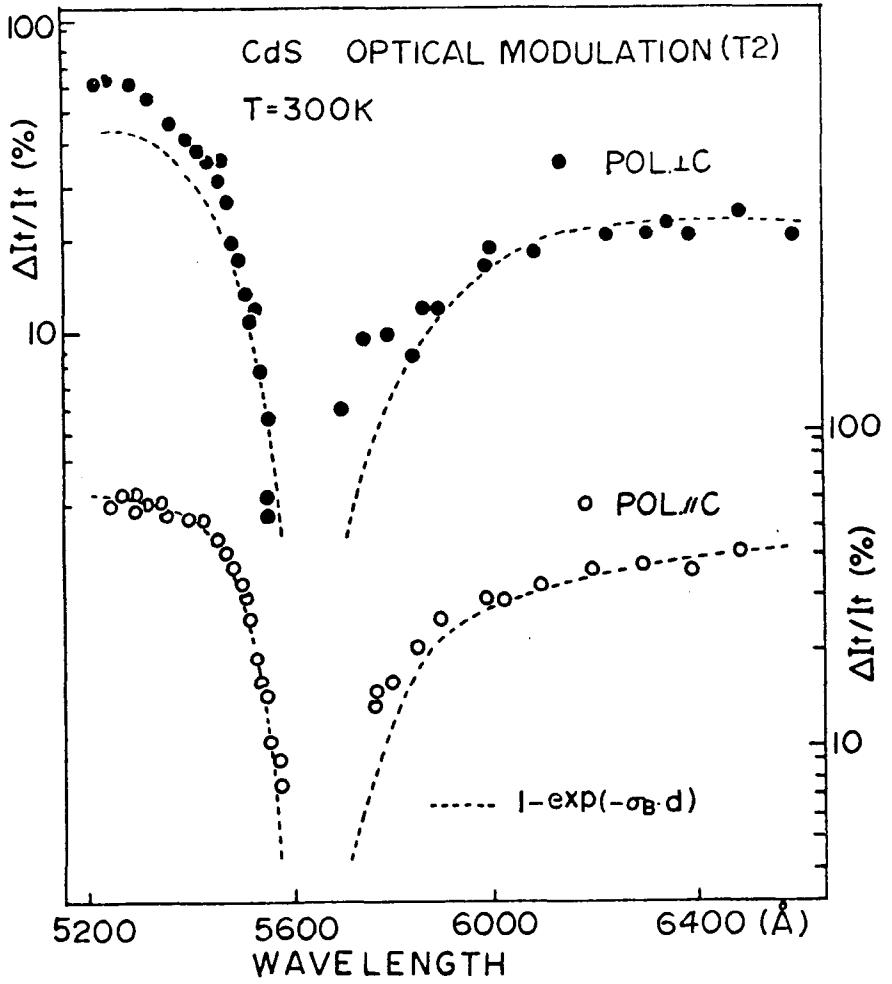

Fig. 5.5. Comparison of experimental dispersions of O.M. induced by the active acoustic domain with estimated dispersions from resonant light scattering.

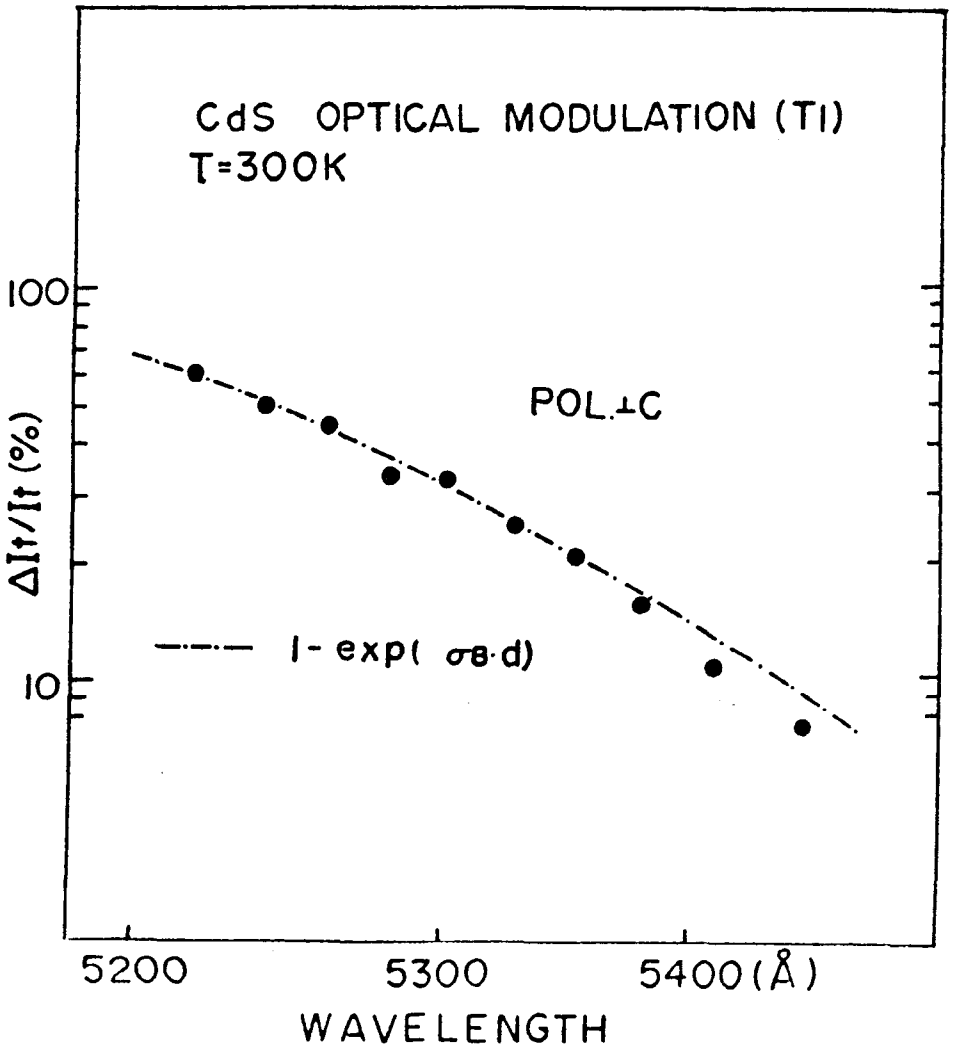

Fig. 5.6. Same as Fig. 5.5. but for the inactive acoustic domain.

estimated curves in the polarization condition(b) in Fig.5.4 is interpreted by taking into account of the electric field modulation mentioned above. By using the data of electric field induced changes in appropriate band gaps reported by Williams[106] we estimate an approximate change in absorption coefficients $\Delta\alpha(//)$ and $\Delta\alpha(\perp)$, where $(//)$ and $(\perp)$ refer to the light polarization vector parallel and perpendicular to the c-axis. Assuming the electric field $\sim 10^5$ V/cm one find that $\Delta\alpha(//)$ is 4.0(cm^{-1}) and $\Delta\alpha(\perp)$ is 16.8 (cm^{-1}) at the light wavelength 5200 Å. By substituting these values into the following relation;

$$\left.\frac{\Delta I_t}{I_t}\right|_{\text{field}} = 1 - \exp(-\Delta\alpha \cdot b) \qquad (5.2\text{-}3)$$

The modulation caused by the electric field is fond to be $(\Delta I_t/I_t)(:\text{field}) \fallingdotseq 80$ % for the polarization condition(b) and $(\Delta I_t/I_t)(:\text{field}) \fallingdotseq 20$ % for the polarization condition(a). For the light wavelength longer than 5300 Å these values of $(\Delta I_t/I_t)$ rapidly decrease to few percent. It is found from a simple calculation described above that the contribution of field-modulation effect in the case of (b) is larger than that ot Polarization condition(a). Such a feature of field modulation effect seems to explain the difference in the optical modulation between the two condition(a) and (b), where we find the modulation for (b) is larger than for(a)(This feature is shown in Fig.5.2 and 5.4). If we take into account of the contribution of field modulation effect to the present analysis we can explain qualitatively such a polarization dependence of modulation. It is obvious that the slight difference between the observed dispersion spectra of optical modulation and dispersion curves estimated from eq.(5.2-2) in the polarization condition (b) arises from an existence of

polarization dependence of modulation. We can conclude that the polarization dependence of O.M. near the intrinsic edge is due to effect of field modulation. The contribution of field-modulation through the F.K. effect is significant only in the photon energy region close to the edge. However there remains a problem that estimated modulation(≒80 %) by using the F.K.-type modulation is very larger than that of expected values.(10∿20 %) The difference seems to be caused by a wrong estimation of magnitude of existing electric field inside the domain. The value of piezoelectric field $\sim 10^5$V/cm used in above discussion is estimated by using the relation between the strain[107] and piezoelectric constant. In the present time we must consider that the effective piezoelectric coefficient can be considerably smaller because of screening effect by free carriers. Taking into account such screening effect, the effective electric field about~5×10^3V/cm wasderived by Berkowicz,[109] which gives a reasonable value of electric field induced modulation for the polarization condition (b), while few contribution of electric field to the total optical modulation are found in the polarization condition(a).

5.3. Summary

The dispersion spectra of optical modulation $\Delta I_t/I_t$ are observed under the two polarization conditions; (a) $I_E // I_{tA} //$ c-axis and (b) $(I_E // I_{tA}) \perp$ c-axis in CdS. The general feature of the observed dispersion spectra is considerably different from that of n-GaAs. We find a deep and narrow minimum around 5600 Å in the dispersion curves of O.M. by using the piezoelectrically active acoustic domain. Observed structure cannot be explained in terms

of the Franz-Keldysh type optical modulation. A comparison of observed O.M. spectra with dispersion of resonant Brillouin scattering is carried out and it is confirmed that the O.M. signals observed in the present work are mainly caused by the depletion of incident light through the resonant light scattering. The polarization dependence of optical modulation is explained by taking into account of the contribution of electric field-modulation, which is significant in the photon energy region close to the intrinsic band edge of CdS.

Chapter VI Break Down of Selection Rule in Resonant Brillouin Scattering in CdS.

6.1. Introduction

We have studied in previous section the resonance effects of Brillouin scattering cross section near the M_o-critical points in CdS and ZnSe. Those measurements are mainly performed under the condition of allowed transitions by setting proper polarization direction, where the polarization vector of the scattered light I_A is rotated by 90° from the direction of incident light polarization (I_E) in the transverse mode phonon scattering(see chapter II). The selection rule in light scattering is generally determined by the crystal symmetry, which predicts the polarization relation between the incident and scattered lights. In this chapter we present experimental results and discussion on the break down of the selection rule of Brillouin scattering in the region near the band edge. In the present measurement we observed a strong resonance enhancement of scattering efficiency near the intrinsic band edge of CdS under a configuration of the polarization where the Brillouin tensor is expected to be zero. In the experiments of Raman scattering, the resonance enhancements of forbidden-Raman scattering by LO phonons were measured in several semiconductors. The forbidden scattering in resonant Raman effect was studied intensively at the E_0-edge of CdS[110-113] and also at the E_1-critical point of a group of III-V semiconductor compounds including InSb,[114,115] InAs,[116] and GaSb.[115] It was found that the intensities of forbidden scattering by LO phonons result in much larger resonance enhancement than those of allowed scattering near the band edge. Above experimental results on the resonance enhancement of forbidden Raman scattering by 1-LO phonon are generally interpreted by taking into

account of the electron (or exciton)-phonon coupling via the intraband Frölich interaction.[117,118] In the case of Cu_2O the resonant enhancement of forbidden Raman scattering which was observed at the dipole forbidden 1s yellow exciton series of this material has been explained in terms of the electric quadrapole and magnetic dipole terms. On the other hand it was proposed by Klein et al.[12] that impurity states modify the selection rule in Raman (or Brillouin) scattering because they break the translational and point symmetry of crystals. It is also pointed out in the impurity effects that the impurity-induced scattering is independent of scattering angle and should lead to dispersive broadening of the one phonon line since the phonon momentum is not fixed. In the present work we have observed an abnormal resonant enhancement of Brillouin scattering cross section by using the high intensity phonons of piezoelectrically active TA mode and inactive TA mode in the forbidden configurations of following; (a) the incident and scattered light polarization vectors(I_E and I_A) are both parallel to the c-axis and (b) both perpendicular to the c-axis. As mentioned before those polarization conditions are perfectly forbidden from the classical analyses (Chap.II) because corresponding photoelastic constants are all zero. We can find a sharp resonant enhancement near the intrinsic band edge for both (a) and (b)-polarization conditions. In the analysis of interaction between the excitations of the electronic intermediate states and acoustic phonons we found that the deformation potential scattering of virtual excitons (or holes)plays an important role in determining the selection rule of the Brillouin scattering cross section. From such an analysis we find a possibility of resonant enhancement of Brillouin scattering which is forbidden from the

symmetry induced selection rule.

6.2. Experimental Results and Discussions

Present measurements are performed by using the similar arrangement in Chap. III. Because of parallel polarization condition we need not to take into account the optical anisotropy of CdS, and thus incident and scattered light angles (θ_i,θ_d) are determined by using a relation derived in the case of isotropic crystals. In Fig.6.1 we plot Brillouin scattering signals measured with 1 GHz piezoelectrically active transverse acoustic phonons propagating in the c-plane as a function of polarization angle θ for a fixed light wavelength, where θ is an angle between the incident and scattered light polarization directions. Three kinds of light wavelengths 5300, 5620, and 5900 Å are chosen so as to investigate the polarization dependence in the resonant region(5300 Å), in the antiresonance region(5620 Å) and in the nonresonant region(5900 Å). In the case of transparent region (5900 Å) θ-dependence of Brillouin scattering intensity is found to reflect the selection rule arising from the crystal symmetry. We find a strong scattering signal in the case of $\theta=0$ ($I_E \perp I_A$) and the scattering signal decreases with decreasing of θ to zero ($I_E // I_A$). In the case of 5620 Å one cannot find any optical signal under the perpendicular polarization condition($\theta=90^\circ$) because of the resonant cancellation. However, it is found in the figure that the scattering intensity drastically increases as the angle θ changes from 90° to 0°. The θ-dependence of the scattering intensity at 5300 Å is quite abnormal, where the most largest optical signal is detected when we set the parallel polarization condition($I_E // I_A$) which is perfectly forbidden configuration in Brillouin scattering by TA phonons. Those experimental data mean that there exists

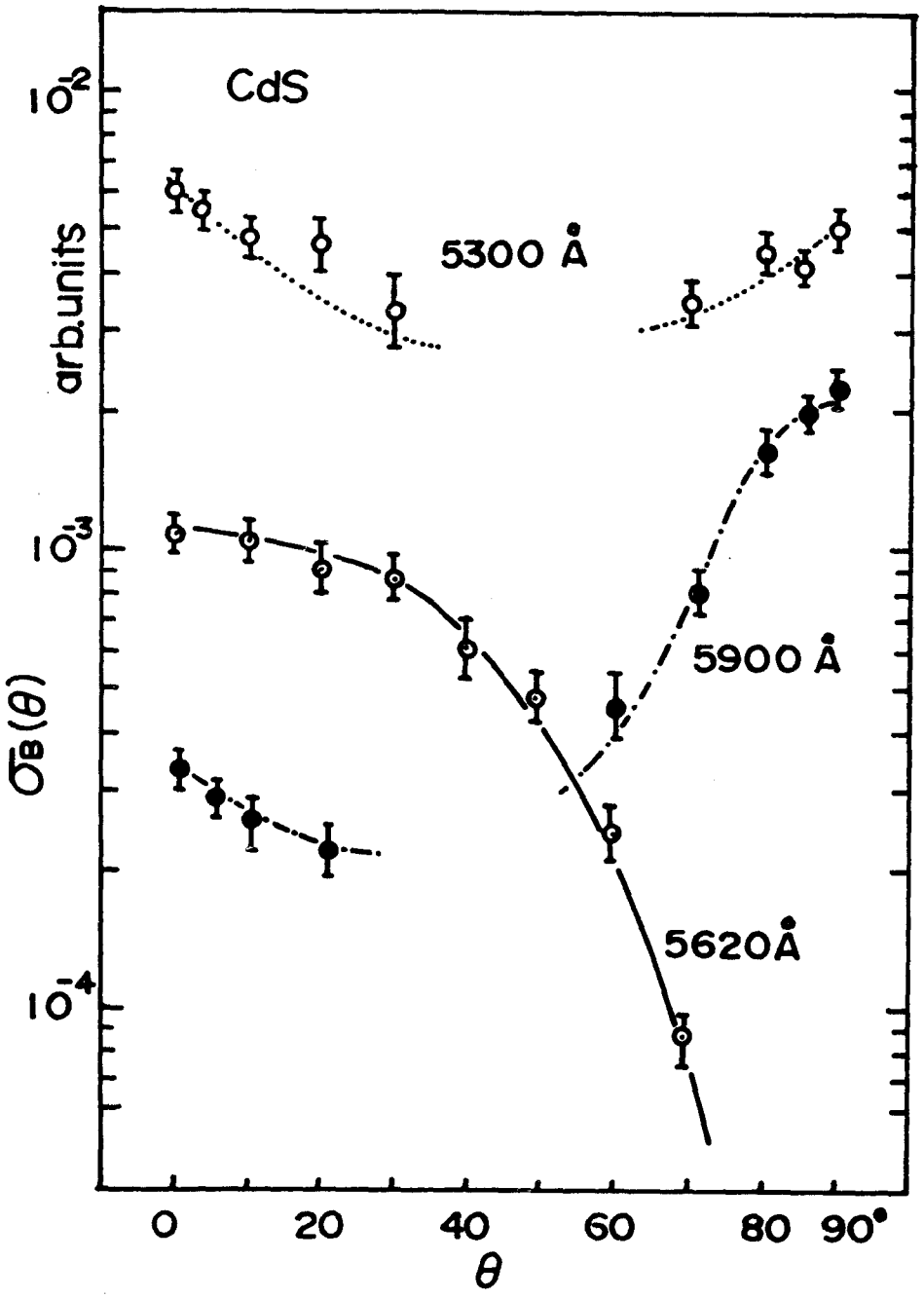

Fig. 6.1. Brillouin scattering signals versus polarization angle θ for each incident light wavelength. The angle $\theta=0^{\circ}$ refers to the polarization condition $I_E // I_A$ and $\theta=90^{\circ}$ to that of $I_E \perp I_A$.

abnormal feature in the resonant region, which cannot be predicted from the phenomenological treatment in the light scattering. The resonant dispersion of Brillouin scattering cross section observed under the forbidden configuration($I_E /\!/ I_A /\!/$ c-axis) by the piezoelectrically active TA phonons at 300 K are shown in Fig.6.2, where normal resonant curves observed under the allowed polarization condition($I_E \perp I_A$) are also plotted for comparison. In the measurements the incident and scattered light angles(θ_i and θ_d) are set to detect the Brillouin scattering signals due to a appropriate acoustic frequency(0.5 GHz). It is found in Fig.6.2 that the observed dispersion spectrum under the forbidden configuration never shows an antiresonance structure around the phonon energy 2.2 eV but shows a steep resonant enhancement near the critical point. Decrease in scattering intensity at higher energy region is caused by strong absorption of the incident and scattered lights. Correction of the effect can be made by normalizing the scattered light intensity I_s with the transmitted light intensity I_t. Dispersion spectra of scattering cross sections are shown in Fig.6.3, where the corresponding acoustic frequencies are 0.5(◐) and 0.8 GHz(●). As seen in Fig.6.3 the dispersion curves of Brillouin scattering cross section for the normal configuration $R_{is}(\perp)$ (plotted by (○) for 0.5 and (⊙) for 0.8 GHz) show a characteristic feature of resonant cancellation and enhancement, where the resonant enhancement occurs in a convex upward manner as the incident photon energy increases to the energy of fundamental absorption edge. On the other hand the dispersion curves for the configuration of forbidden Brillouin scattering shows a quite different feature from the dispersion curves of the normal configuration. As mentioned above the

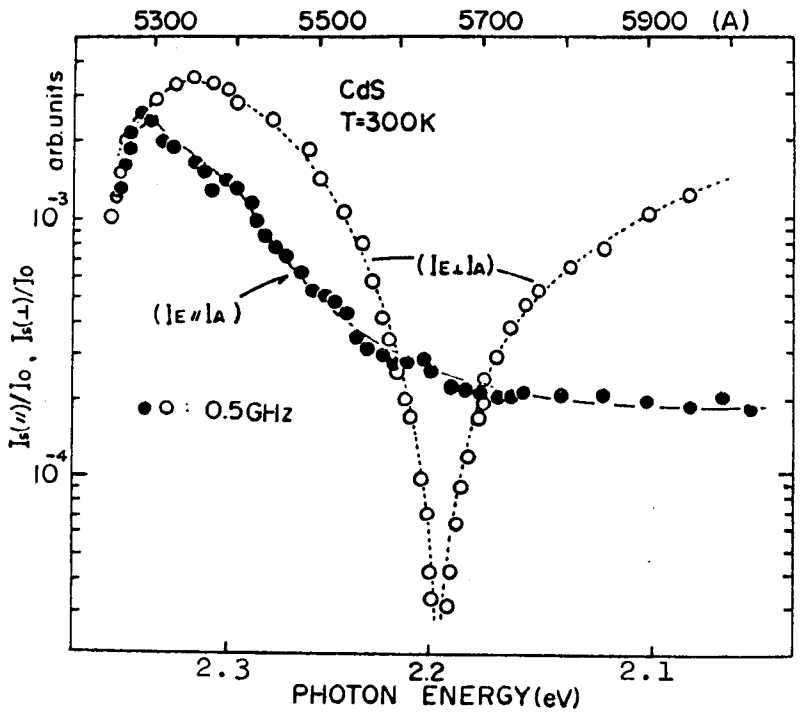

Fig. 6.2. Brillouin scattering signals for forbidden polarization condition; $I_E//I_A$ by 0.5 GHz piezoelectrically active TA phonons. For comparison dispersion spectrum of normal Brillouin scattering cross section observed under the allowed polarization condition is plotted.

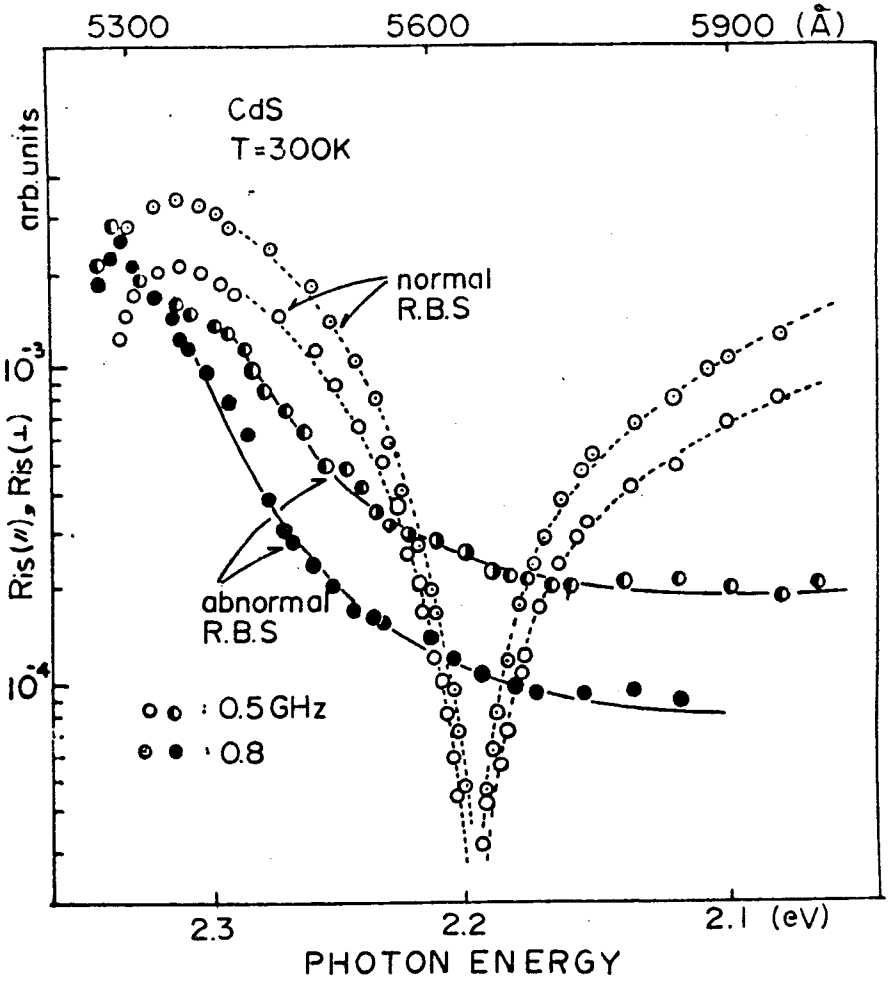

Fig. 6.3. Dispersion curves of Brillouin scattering cross sections for normal ($I_E \perp I_A$) condition and forbidden ($I_E//I_A$) conditions by 0.5 and 0.8 GHz piezoelectrically active TA phonons.

Brillouin scattering by the piezoelectrically active TA phonons under the forbidden configuration is expected to vanish. Such expectation is satisfied only at long wavelength regions. Near the intrinsic band edge of CdS, however, a strong resonance enhancement is observed on the contrary to the expectation of the classical treatment.

The experimental dispersions observed under the forbidden polarization conditions at 77 K are shown in Fig.6.4, where the dispersion curves observed at 300 K are plotted for comparison with the present experimental results at 77 K. We find in Fig.6.4 that a steep resonant enhancement occurs under the forbidden scattering condition for 0.5(●) and 0.6(○) GHz TA phonons. Stronger resonant enhancement observed at77 K than that at room temperature is due to a smaller brodening energy at 77 K. Total dispersion spectra at 77 K are found to shift to high energy region from those at 300 K, which is interpreted in terms of temperature dependence of the energy gap(∿0.1 eV larger at 77 K). Next we discuss resonance effect of forbidden Brillouin scattering by piezoelectrically inactive TA phonons. Measurements were made by using two kinds of inactive TA phonons; the one is so called Tl-mode phonons propagting in the c-plane with displacement vector perpendicular to the c-axis and the other propagates in the direction 45° off the c-axis. Such inactive phonon packets can be obtained making use of mode conversion in the reflection of acoustic domains. A weak resonance enhancement of Brillouin scattering by the inactive TA phonons are observed under the forbidden configuration($I_E // I_A \perp$c-axis) at 300 K which is shown in Fig.6.5, where dispersion curve of the allowed Brillouin scattering by the inactive TA phonons is also shown for comparison. The observed dispersions in the forbidden Brillouin scattering

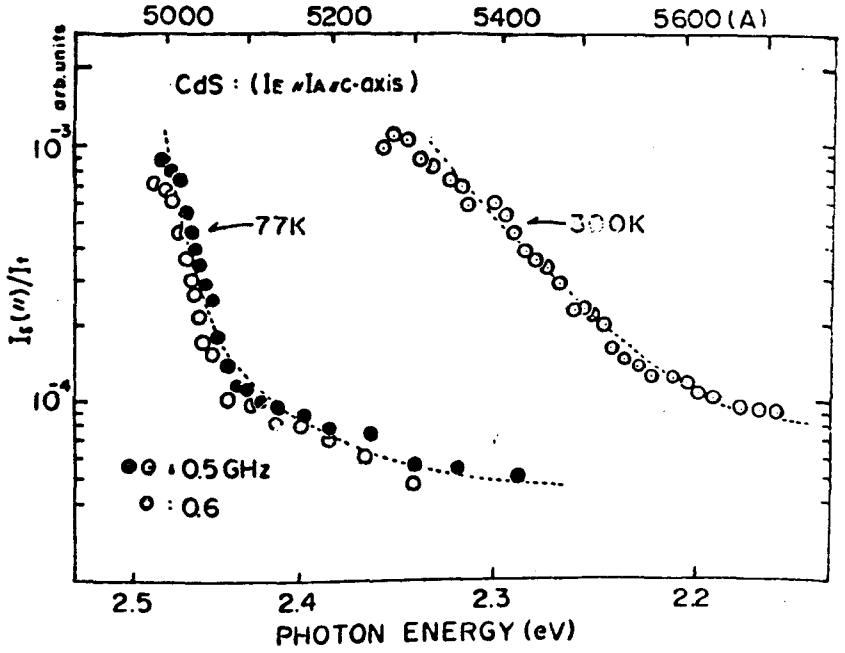

Fig. 6.4. Dispersion curves of Brillouin scattering cross section observed under the forbidden condition at 300 K and 77 K in CdS.

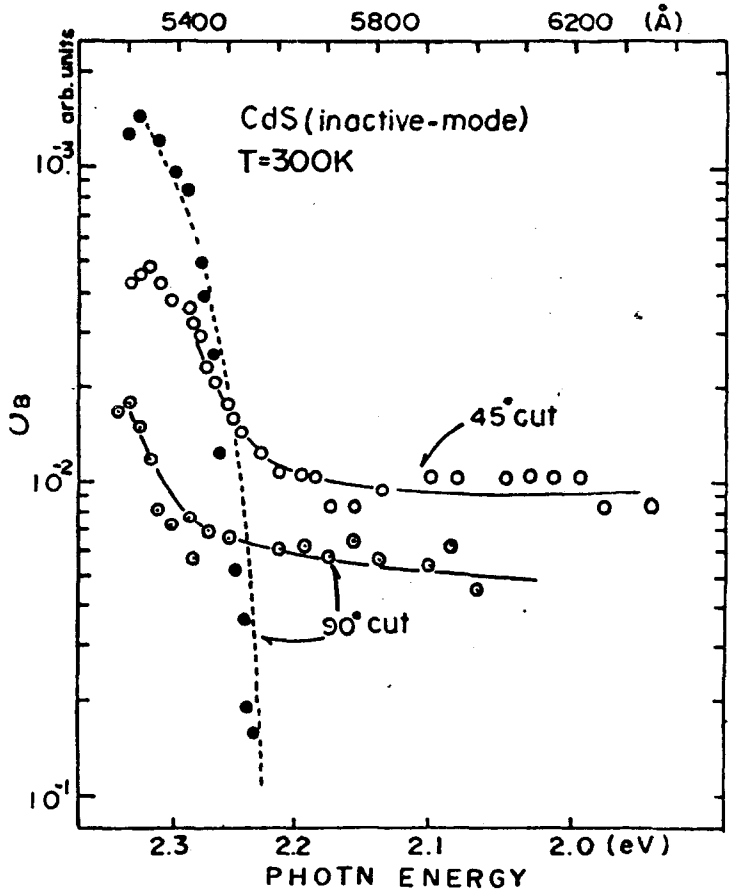

Fig. 6.5. Dispersion curves of Brillouin scattering cross section by piezoelectrically inactive TA phonons observed under the forbidden polarization condition.

show no structure of antiresonance around the 2.2 eV, while the Brillouin scattering intensity observed under the allowed polarization condition drastically decreases in this photon energy region. The two kinds of inactive phonon packets have a similar character, and are not acompanied with d.c. or a.c. electric feilds. Therefore the present observation of the resonant enhancement in forbidden scattering by inactive phonons in CdS suggests that the Break down of selection rule in Brillouin scattering is not associated with an existence of high electric field. Similar resonant enhancements are also reported in Raman scattering by inactive 1-LO phonon.[119)]

3-Band Model

We have already shown that the present results obtained under the condition of forbidden polarization conditions cannot be explained by an existing phenomenological theory derived from the crystal symmetry. Therefore we consider here a possible interpretation of resonance enhancement of forbidden scattering efficiency by taking into account of the deformation potential scattering of intermediate virtual excitons, based upon the analysis which was first made by Ando and Hamaguchi for the case of allowed Brillouin scattering. In the previous chapter we pointed out that the selection rule of deformation potential scattering of virtual electronic excitations by phonons plays an important role in the resonance enhancement. We briefly describe a procedure to construct 3-Band model of possible transition process. First we consider a polarization-relation of incident and scattered lights from the phenomenological treatment of Brillouin scattering, where the crystal symmetry is introduced in the formulation of photoelastic tensor. It is possible to conclude that the derived photoelastic constant corresponds to the nonresonant term R_{is}(nonresonant) in the micro-

scopic theory. Second we consider the resonant term of R_{is}, which is given by

$$R_{is} = \Sigma \frac{P_{o\beta} \Xi_{\beta\alpha} P_{\alpha o}}{(\omega_\beta - \omega_s)(\omega_\alpha - \omega_i)} \qquad (6.2\text{-}1)$$

where the notations are the same used in the Chap.II. The Brillouin tensor R_{is} is interpreted as resonant contribution arsing fromthe electronic transition process ;$|0\rangle$—$|\alpha\rangle$—$|\beta\rangle$—$|0\rangle$, where $|0\rangle$ refers to the electronic ground states,$|\alpha\rangle$ and $|\beta\rangle$ to the virtual states. In the treatment possible state of electronic excitation $|\alpha\rangle$ is determined from the optical selection rule of dipole transitions. Here the matrix elements $\Xi_{\beta\alpha}$ plays an important role in constructing intra- or inter-band transition of the virtual states(2- and 3-Band transition process). In Fig.6.6 the schematic diagram of optical transition and acoustic transitions of intermediate virtual excitations at Γ-point in CdS is shown. One consider the forbidden scattering by active TA phonons, where the incident and scattered light polarization vectors(I_E and I_A) are both parallel to the c-axis. In this case the corresponding photoelastic constants in the longer wavelength region are P_{34}, P_{35} and then we obtain; $P_{34}=P_{35}=0$ from the analysis based upon the crystal symmetry(see eq.(2.2-14). Therefore the nonresonant term R_o(nonresonant) is zero. The result is consistent with the present observation that the Brillouin scattering signal under the above condition disappears in the long wavelength region(far from the band edge). On the other hand the scattering signals appear at wavelengths near the band edge and increase as the wavelength approaches to the band edge. It is easily found that the electronic virtual state associated with A valence band(or A excitons) does not contribute to the light scattering

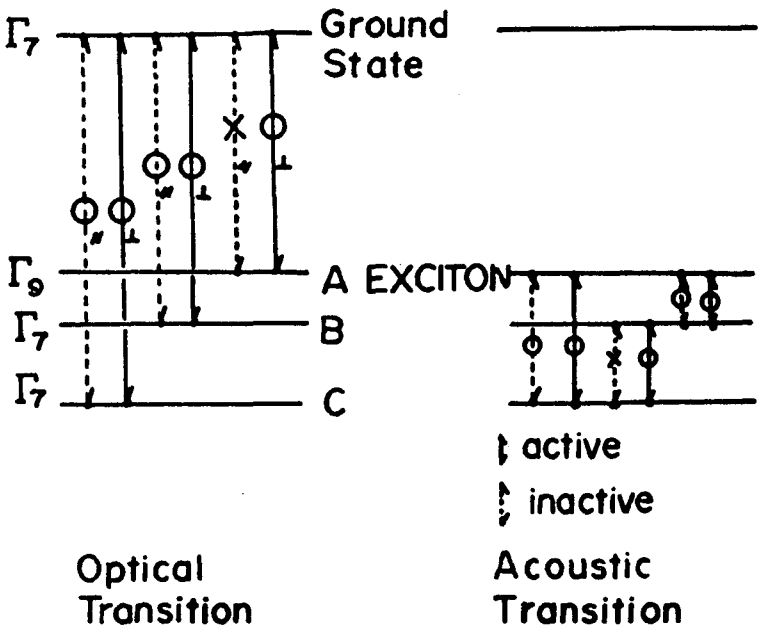

Fig. 6.6. Schematic diagram of optical and acoustic transitions of intermediate virtual excitations in CdS.

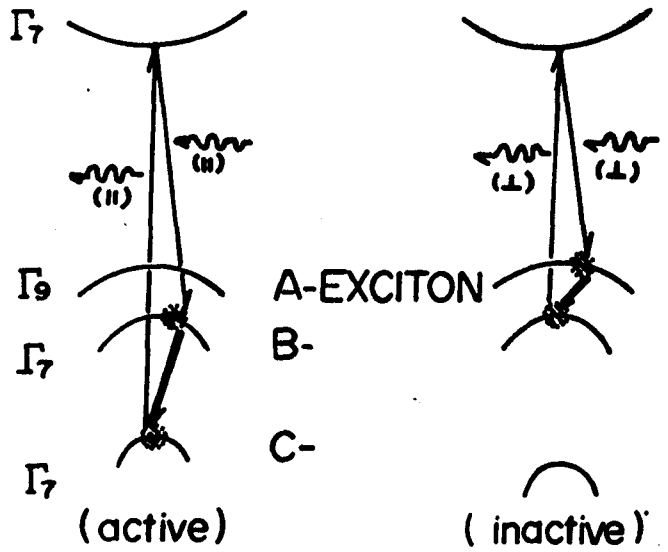

Fig. 6.7. Schematic diagram of dominant transition process of virtual states in the case of forbidden resonant light scattering by piezoelectrically active and inactive TA phonons in CdS.

in this configuration. In the following we consider the virtual states as excitons. From the experimental conditions the symmetry of initial intermediate electronic excitations are found to correspond to that of B excitons(or holes in B valence band) having Γ_7-symmetry. By making use of selection rule of acoustic transition shown in the right hand of Fig.6.6 we find that the electronic virtual state with the Γ_7-symmetry can transit to another Γ_9-symmetry virtual states corresponding to the C excitons(or holes in C valence band). The electrons and holes of C excitons recombine to radiate the phonons with polarization vector parallel to the c-axis because of Γ_7-symmetry. Consequently we obtain the following transition process in the resonant region; $|0\rangle \rightarrow |\Gamma_7\rangle \rightarrow |\Gamma_7\rangle \rightarrow |0\rangle$ in the case of forbidden scattering by the active TA phonons. In the above analysis we find that 3-Band transition process results in a dominant resonant contribution to the total Brillouin scattering cross section, which is shown schematically in Fig.6.7. Here the notations $\rightarrow$ and $\Rightarrow$ refer to the optical and acoustic transitions of virtual states. Next we consider the case of forbidden Brillouin scattering by piezoelectrically inactive TA mode phonons(T1-mode). From the present experimental condition we easily find that the corresponding photoelastic constants are P_{16} and P_{26} which are zero in the transparent region(long wavelength region). Therefore we conclude that the nonresonant term vanished at long wavelength region. The result is consistent with the present observation and also with the phenomenological(macroscopic) theory derived from the analysis of crystal symmetry. From the analysis of the macroscopic theory we find that the following transition of 3-Band process contribute to the resonant term in the photon energy region close to the band edge;

$|0\rangle \rightarrow |\Gamma_9\rangle \rightarrow |\Gamma_7\rangle \rightarrow |0\rangle$.

Such a dominant 3-Band process is shown in Fig.6.7. We estimate Brillouin scattering cross sections in the forbidden conditions by using the above results. The total scattering cross section σ_{BT} is written as,

$$\sigma_{BT}(\text{forbidden}) \propto |R_{is}(\text{resonant}) + R_{o}(\text{nonresonant})|^{2} \qquad (6.2\text{-}2)$$

with $R_{o}(\text{nonresonant})=0$ because of the reason stated above. We are able to predict from eq.(6.2-2) that antiresonance structure does not appear in the dispersion spectra of forbidden scattering cross section,which is consistent with the present experimental results shown in Figs.(6.2)-(6.5). In Fig.6.8 we show the estimated dispersion curve of Brillouin scattering efficiency for 0.5 GHz active TA phonons in the forbidden condition($I_E // I_A // c$-axis), by broken line, where the virtual states of $|B>$- and $|C>$-excitons are taken into account. The parameters used in the present calculation are summarized in Table 6.I. It is fond in Fig.6.8 that the experimental dispersion spectra of scattering efficiency shows a good agreement with that of theoretical dispersion.

Table 6.I. Parameters used in the estimation of forbidden-resonant Brillouin scattering in CdS.

piezoelectrically-active TA-phonons	[300 K]:	[77 K]
	E_{gi}=2.494 (eV)	E_{gi}=2.552 (eV) (a)
	E_{gs}=2.553	E_{gs}=2.640 (a)
	Ξ_{CB}=-0.8	Ξ_{CB}=-0.8
piezoelectrically-inactive TA-phonons	[300 K]	
	E_{gi}=2.480 (eV)	
	E_{gs}=2.494	
	Ξ_{BA}=-1.28	

(a): Cardona et al. ref.(30)

A comparison of experimental curves with theoretical curves at 77 K is shown in Fig.6.9. The experimental data are observed under the polarization condition of $I_E // I_A // c$-axis by using the amplified TA-phonons with frequencies 1.0(○) and 1.4 GHz(●). The theoretical curves are calculated by taking into account of the intermediate virtual states of $|B\rangle$- and $|C\rangle$ excitons, where band parameters at 77 K reported by Cardona et al.[30] are used(Table 6.I.). It is found from the comparison that the experimental results are well explained by the present model. Calculated curve of forbidden scattering by piezoelectrically inactive TA phonon is shown by solid line in Fig.6.10, along with experimental results, where the theoretical calculation was carried out by taking into account of the deformation potential scattering of $|A\rangle$ and $|B\rangle$ -virtual excitons. The comparison of experimental results with theoretical curve shown in Fig.6.10 is performed only in the case of inactive TA phonons propagating in the c-plane(90°-cut crystal). The observed resonant feature near the fundamental edge is found to be well explained by the theoretical dispersion. Although the experimental dispersions of forbidden scattering by piezoelectrically active and inactive TA phonons show resonant enhancement in the photon energy region, and a reasonable agreement with the theoretical curve, we find that the present experimental data indicates a saturation or slight decrease near the photon energy region very close to the intrinsic band gap, while the theoretical curves of the scattering efficiency still increase. This effect is interpreted by broadening effect.[124] By taking into account such a broadening effect we are able to explain the saturation behavior of observed dispersion spectra in the present work.

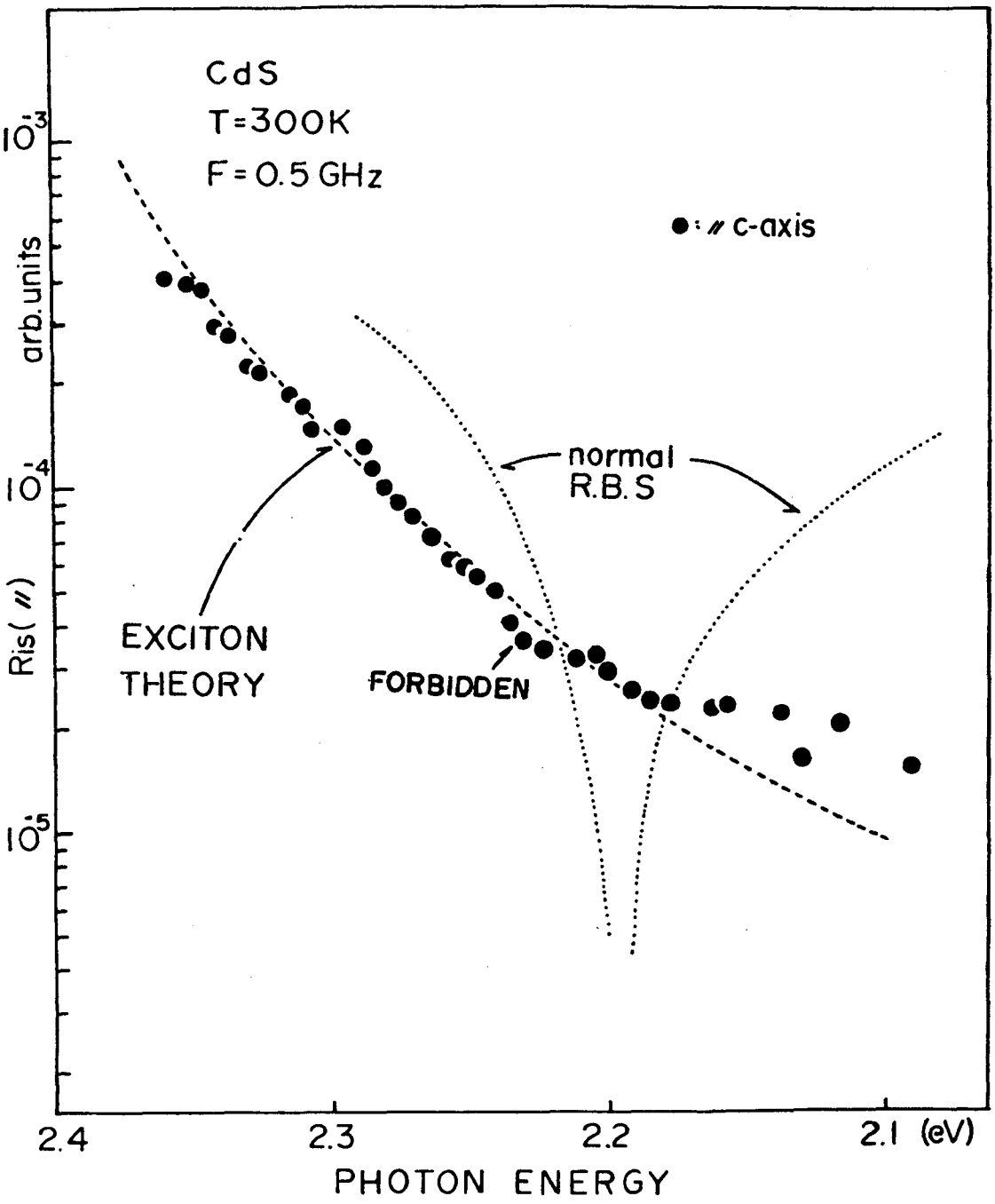

Fig. 6.8. Comparison of experimental dispersion of forbidden Brillouin scattering by piezoelectrically active TA phonons with the theoretical dispersion at 300 K. Solid line is estimated by taking into account of B and C virtual excitons.

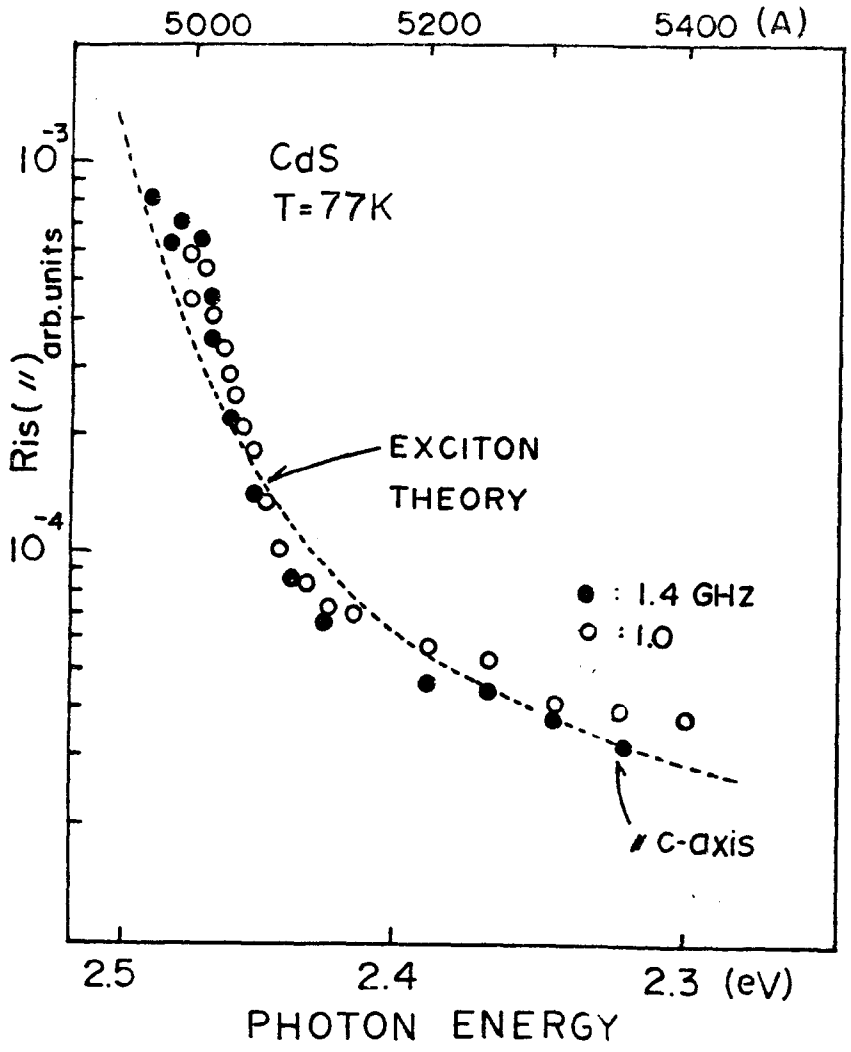

Fig. 6.9. Comparison of experimental dispersion of forbidden-Brillouin scattering by active TA phonons with the theoretical dispersion at 77 K. Broken-line is estimated by taking into account of the B- and C-virtual excitons.

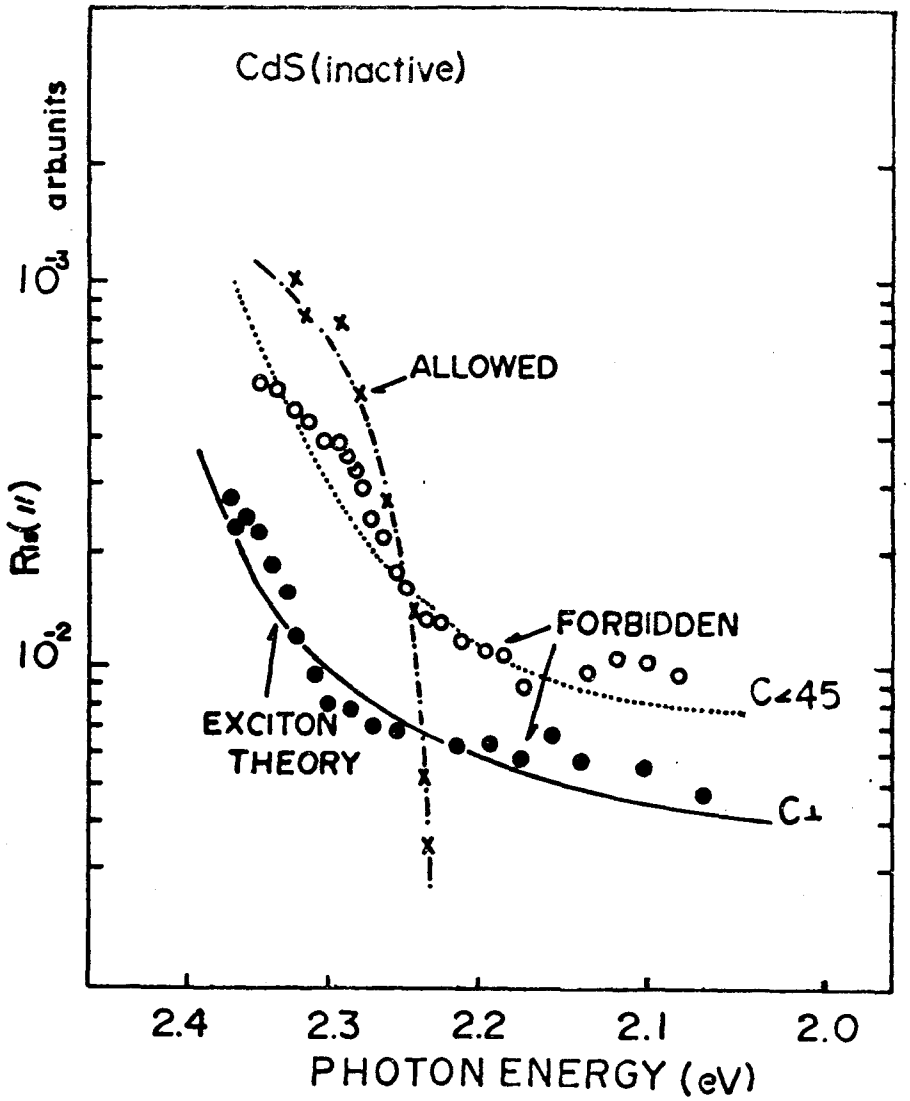

Fig. 6.10. Comparison of experimental dispersion of forbidden-Brillouin scattering by inactive TA phonons with the theoretical dispersion at 300 K. Solid line is calculated by taking into account of the A- and B-virtual excitons.

6.3. Summary

We observed resonant enhancement of forbidden Brillouin scattering efficiency in CdS. It is found in the present work that the observed-forbidden Brillouin scattering efficiency shows a resonant increase as the photon energy increase to the fundamental absorption edge, where phenomenological theory(macroscopic theory) predicts no scattering under the present configurations. Such a resonance effect is considered as the intrinsic bulk effect and explained by taking into account of the electronic contributions to the Brillouin scattering. From the present analyses of selection rules in optical transition and deformation potential scattering it is found that the intermediate virtual excitations associated with the spin orbit split off band(or C-excitons) play an important role in the resonant-forbidden scattering by piezoelectrically active TA phonons (T2-mode phonons) in CdS. We also found a resonant enhancement of forbidden Brillouin scattering by piezoelectrically inactive TA phonons(T1-mode phonons), where the selection rule of macroscopic Brillouin scattering breakes down and the scattering efficiency shows a resonant increase near the fundamental edge. We conclude that the selection rule of Brillouin scattering derived from the crystal symmetry breakes down in the photon energy region near the band edge and that the resonant light scattering is explained by taking into account of proper transition process of intermediate virtual excitons.

VII Application of Acoustic Pulse Injection into Semiconductors

7.1. Introduction

We have already shown in previous chapters that an intense acoustic domain excited in piezoelectric semiconductor CdS can be injected into different materials and by making use of such injected phonons packets one can investigate the resonance effect in Brillouin scattering by propagating acoustic flux in many kinds of semiconductors.[28,29] We found such an acoustic injection technique has a very useful application to a study of acoustic propagation and mode conversion in various semiconductors. In the present work firstly we make use of such injected sound waves in study of resonant Brillouin scattering of semi-insulating ZnSe(shown in Chap. IV) . Since such an acoustic injection technique has been used successfully for an investigation of elastic properties of propagating acoustic flux in the semiconductors[25,26]. Theoretical analysis given in this chapter is indebted to K. Yamabe(See K. Yamabe;M.S. thesis(March,1977) and K. Yamabe, K. Ando and C. Hamaguchi,Japan J.Appl.Phys.(submitted)). We describe a theoretical analysis of injection efficiency of acoustic flux by assuming an ideal bonding of CdS with ZnSe and ZnTe samples.

The reflection and transmission efficiencies of the acoustic waves are calculated by solving elastic equation under a proper boundary condition. From such analyses one can find the acoustic modes excited in the end-bonded ZnSe and ZnTe samples.[79] In the latter part of this chapter some applications of acoustic injection technique are presented,where elastic properties such as phase velocity, elastic stiffness constants(C_{11}, C_{12} and C_{44}) and propagation loss in ZnSe and ZnTe are determined by using the Brillouin scattering technique. It should be noted that the injected acoustic flux consists of an considerably wide frequency range from 0.1 to 2 GHz and therefore

such an acoustic injection can be applied not only to the present measurements of elastic properties but also to more various investigations of electron-phonon interaction in semiconductors.

7.2. Acoustic Field Equations and Transmission efficiency

As well known, there are two basic-field equations between the strain(S_{ij}), displacement(U_i) and stress(T_{ij}) in a crystal. The relation between strain and displacement is given by,

$$S_{ij} = \frac{1}{2}\left(\frac{\partial u_i}{\partial r_j} + \frac{\partial u_j}{\partial r_i}\right) \qquad (7.2\text{-}1)$$

and equation of motion is

$$\frac{\partial}{\partial r_j} T_{ij} = \rho \frac{\partial^2 u_i}{\partial t^2} - F_i \qquad (7.2\text{-}2)$$

where r_i is the orthogonal coordinate, ρ is the mass density and F_i is the external force. By introducing the particle displacement velocity[v_i] defined by the first derivative of atomic displacement with respect to time t, these two equations are reduced in following convenient form;

$$\frac{\partial}{\partial r_j} T_{ij} = \rho \frac{\partial v_i}{\partial t} \qquad (7.2\text{-}3)$$

$$\frac{\partial}{\partial t} T_{ij} = C_{ijkl} \frac{\partial v_k}{\partial r_l} \qquad (7.2\text{-}4)$$

where we droped the term of external force in eq.(7.2-1) and the elastic stiffness constant C_{ijkl} is introduced. Now we define the acoustic Poynting vector $[P]_{ac}$ with an analogy to the case of electromagnetic field,

$$[P]_{ac} = -\frac{1}{2}\sum_{i,j} (I_i) v_j^* T_{ij} \qquad (7.2\text{-}5)$$

where (I_i) is the unit vector of i-direction in the coordinate orthogonal system and v_j^* stands for the complex conjugate of V_j.

One can determine the mode of acoustic waves by solving eqs.(7.2-3) and (7.2-4) and acoustic power propagation is estimated by using the field parameters $[v_i]$ and $[T_{ij}]$. Here we consider the boundary conditions which is very important to solve the acoustic field-equations. The boundary condition of $[v_i]$ is obtained by assuming that the particle displacement velocity v is continuous at the boundary surface(bonded-surface), which is expressed by,

$$[v_i]_1 = [v_i]_2 \tag{7.2-6}$$

where the subscripts '1' and '2' refer to the specimen 1 and 2 in Fig.7.1, respectively.

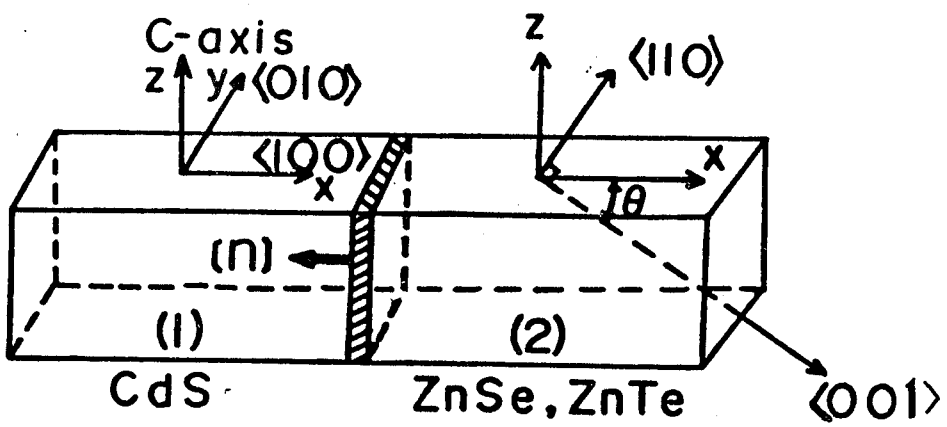

Fig. 7.1. Schematic arrangement of acoustic-wave injection for CdS-ZnSe and CdS-ZnTe systems where θ is the angle between the propagation vector of injected sound wave and [001] crystal direction in the $(1\bar{1}0)$ plane.

We also assume that motion of the boundary is ignored and that the external traction force is continuous at the interface surface between the two bonded specimens. From the above assumptions one can obtain the boundary condition of stress component T_{ij} as,

$$[T_{ij}]_1 \cdot [n] = [T_{ij}]_2 \cdot [n] \tag{7.2-7}$$

where [n] is the unit vector normal to the interface surface. Procedures to obtain the transmission and reflection coefficients of the acoustic energy are as follows. First we solve eqs.(7.2-3) and (7.2-4) using the boundary condition (7.2-6) and (7.2-7). Next we evaluate the acoustic poynting vector $[P_{ac}]$ for incident, reflected and transmitted waves. Finally we calculate the reflection and transmission coefficients. In the present we carried out such calculations for the case of CdS-ZnSe and CdS-ZnTe bonded systems. Now we estimate the transmission and reflection coefficients of acoustic waves in the special case of CdS-ZnSe (CdS-ZnTe) system. We adopt the Cartesian coordinate system with X-axis normal to the interface surface. The c-axis of CdS is fixed and parallel to the Z-direction, while the bonded specimens are cut so that the X-axis (long-dimension) makes an arbitrary angle θ with the [001] crystal direction in the $(1\bar{1}0)$ plane. The elastic stiffness constant matrix of CdS with 6mm symmetry is givn by,

$$\begin{bmatrix} C_{11} & C_{12} & C_{13} & 0 & 0 & 0 \\ C_{12} & C_{11} & C_{13} & 0 & 0 & 0 \\ C_{13} & C_{13} & C_{33} & 0 & 0 & 0 \\ 0 & 0 & 0 & C_{44} & 0 & 0 \\ 0 & 0 & 0 & 0 & C_{44} & 0 \\ 0 & 0 & 0 & 0 & 0 & C_{66} \end{bmatrix} \quad \text{with} \quad C_{66}=(C_{11}-C_{12})/2 \qquad (7.2\text{-}8)$$

The bonded crystals (ZnSe and ZnTe) belong to the class $\bar{4}3m$ and the matrix of elastic constants is given by,

$$\begin{bmatrix} C_{11} & C_{12} & C_{12} & 0 & 0 & 0 \\ C_{12} & C_{11} & C_{12} & 0 & 0 & 0 \\ C_{12} & C_{12} & C_{11} & 0 & 0 & 0 \\ 0 & 0 & 0 & C_{44} & 0 & 0 \\ 0 & 0 & 0 & 0 & C_{44} & 0 \\ 0 & 0 & 0 & 0 & 0 & C_{44} \end{bmatrix} \qquad (7.2\text{-}9)$$

As illustrated in Fig.7.1, however, the crystal axis of bonded specimen is rotated in the $(1\bar{1}0)$ plane. Therefore the matrix given by eq.(7.2-9) cannot be used directly in the case of the coordinate system. In such a case, it is very advantageous to apply a transformation of the matrix to the coordinate system in Fig.7.1. The detail of the transformation is given in Appendix III and the final result is

$$\begin{bmatrix} C''_{11} & C''_{12} & C''_{13} & 0 & C''_{15} & 0 \\ C''_{12} & C''_{22} & C''_{23} & 0 & C''_{25} & 0 \\ C''_{13} & C''_{23} & C''_{33} & 0 & C''_{35} & 0 \\ 0 & 0 & 0 & C''_{44} & 0 & C''_{46} \\ C''_{15} & C''_{25} & C''_{35} & 0 & C''_{55} & 0 \\ 0 & 0 & 0 & C''_{46} & 0 & C''_{66} \end{bmatrix} \tag{7.2-10}$$

Where C''_{ij}'s are given by eq.(AIII-7) in Appendix. In the present configuration, the acoustoelectric domain consists of shear waves, and thus we can put $[v]_I=[0,0,v_{zI}]$ for the atomic displacement velocity and $[k]_I=[k_I,0,0]$ for the wave vector of the incident acoustic waves. For simplicity we sssume that the incident wave is expressed by a plane wave; that is,

$$[v(x)]_I = [z]A_z\exp\{i(-k_Ix+\omega t)\} \tag{7.2-11}$$

where bracket is used for vector quantity and [z] is the unit vector in the z-direction. In a similar fashion we can describe the reflected and transmitted waves in the following forms;

$$[v(x)]_R = ([x]B_x+[y]B_y+[z]B_z)\exp\{i(k_Rx+\omega t)\} \tag{7.2-12}$$

$$[v(x)]_T = ([x]D_x+[y]D_y+[z]D_z)\exp\{i(-k_Tx+\omega t)\} \tag{7.2-13}$$

where k_R and k_T are the wave vectors of the reflected and transmitted waves, respectively. Using these expressions we can derive the stress for the incident, reflected or transmitted waves by substituting eqs.(7.2-11),(7.2-12) or(7.2-13) into eq.(7.2-4).

The coefficients B_i and D_i are determined by using boundary condition eqs.(7.2-6) and (7.2-7) which can be rewritten as,

$$[v_i(0)]_I + [v_i(0)]_R = [v_i(0)]_T \qquad (7.2\text{-}14)$$

$$[T_{ij}(0)]_I + [T_{ij}(0)]_R = [T_{ij}(0)]_T \qquad (7.2\text{-}15)$$

The results are summarized in Table 7.I, where the particle displacement velocity[v], phase velocity V_p, stress T_{ij} and complex acoustic Poynting vector $[P_{ac}]$ are given for the incident(acousto-electrically excited), reflected and transmitted waves. In general, the reflected waves consist of one pure longitudinal(PL) and two pure transverse(PT) mode acoustic waves, while the transmitted waves are pure transverse(PT), quasi longitudinal(QL) and quasi transverse (QT) mode coustic waves. In Table 7.I we used contracted notation for stress and

$$\alpha_{\pm} = \frac{1}{2}\{C''_{55}+C''_{11} \pm ((C''_{55}-C''_{11})^2+4C''_{15}{}^2)1/2\} \qquad (7.2\text{-}16)$$

$$\beta_{\pm} = (C''_{11}-\alpha_{\pm})/C''_{15} \qquad (7.2\text{-}17)$$

From the obtained particle velocity vector [v] we can calculate polarization angle ϕ_- and $\phi_+=\phi_--90°$ for the QT and QL waves excited in ZnSe and ZnTe, where the angles are defined by the angles between the propagation direction and the particle displacement. In Fig.7.2 the angle ϕ_- is shown as a function of the angle θ which is defined in Fig.7.1. The solid(ZnSe) and broken(ZnTe) curves in Fig.7.2 are calculated by using the elastic stiffness constant obtained by the present work (which will be shown later section). Acoustic Poynting vectors for the reflected and transmitted waves are calculated by substituting [v] and $[T_{ij}]$ for each acoustic mode into eq.(7.2-5). The reflection and transmission coefficients are defined

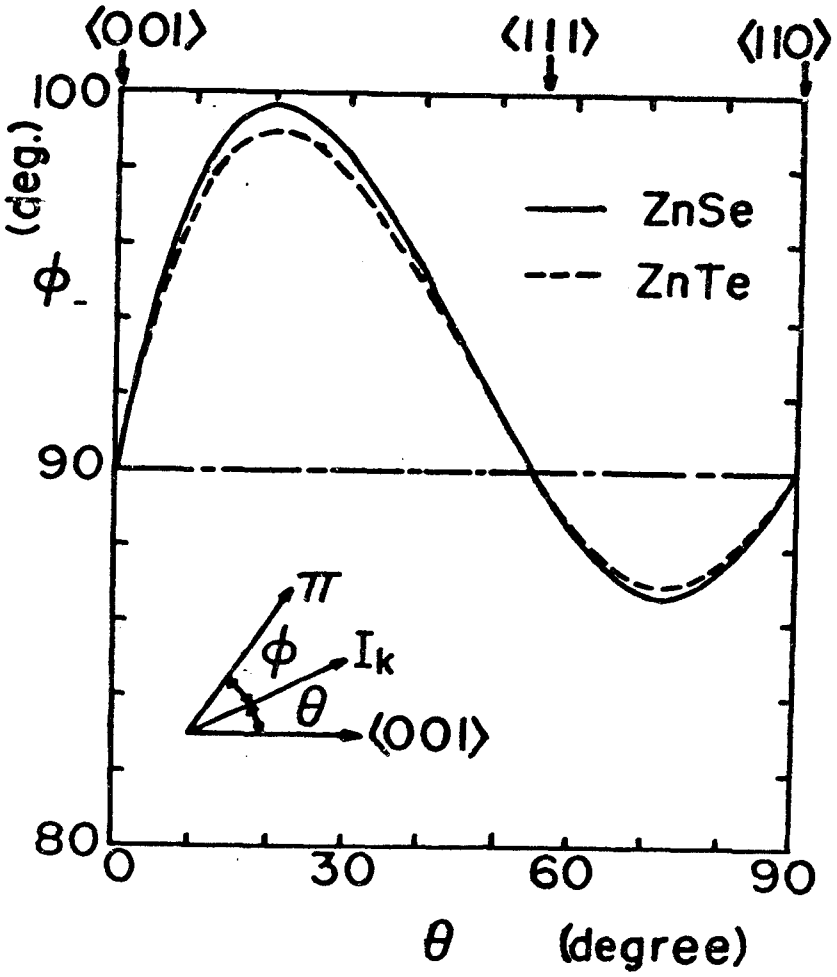

Fig. 7.2. Polarization angle ϕ_- of injected QT phonons into ZnSe and ZnTe as a function of propagation angle θ.

by the ratio of the reflected and transmitted Poynting vectors to the incident one. The calculation is straight forward if we use the particle velocity and stress given in Table 7.I. The reflection coefficient R_p and transmission coefficient T_p for the corresponding acoustic modes are as following:

$$(R_p)_{PT} = \left(\frac{\beta_+ + \gamma\beta_- - \tau}{\beta_+ + \gamma\beta_- + \tau} \right)^2 \qquad (7.2\text{-}18)$$

$$(R_p)_{PL} = \left(\frac{C_{11}}{C_{44}} \right) 1/2 \left\{ \frac{2(1+\gamma)}{\beta_+ + \gamma\beta_- + \tau} \right\}^2 \qquad (7.2\text{-}19)$$

$$(T_p)_{QL} = \left[\frac{\rho' \alpha_+ \{ (1+\beta_+^2)^2 + \beta_+^2 \}}{\rho C_{44}} \right]^{1/2} \left(\frac{2}{\beta_+ + \gamma\beta_- + \tau} \right)^{1/2} \qquad (7.2\text{-}20)$$

and

$$(T_p)_{QT} = \left[\frac{\rho' \alpha_- \{ (1+\beta_-^2)^2 + \beta_-^2 \}}{\rho C_{44}} \right]^{1/2} \left(\frac{2\gamma}{\beta_+ + \gamma\beta_- + \tau} \right)^{1/2} \qquad (7.2\text{-}21)$$

where
$$\gamma = - \frac{(\rho C_{11})^{1/2} + (\rho' \alpha_+)^{1/2}}{(\rho C_{11})^{1/2} + (\rho' \alpha_-)^{1/2}} \qquad (7.2\text{-}22)$$

$$\tau = \frac{(\rho' \alpha_+)^{1/2} \beta_+ + (\rho' \alpha_-)^{1/2} \gamma \beta}{(\rho C_{44})^{1/2}} \qquad (7.2\text{-}23)$$

and ρ' is the mass density of the bonded specimen. The elastic constants C_{11} and C_{44} in eqs.(7.2-18)-(7.2-23) are for CdS. Pure transverse acoustic waves with atomic displacement parallel to the y-direction are not excited in the reflected and transmitted waves due to the fact that the incident waves are pure shear waves with atomic displacement parallel to the z-direction which are generated by acoustoelectric effect.

In Fig. 7.3 we plotted the efficiencies of reflection R_p and transmission T_p for each mode in ZnSe(solid line) and ZnTe(broken-line) which are calculated by using the elastic constants determined from the present work. It is found in Fig.7.3 that the transmission coefficient for the quasi-transverse mode is about 95 % and reaches about 99 % in a typical case($\theta \fallingdotseq 50$). The transmission coefficient for the quasi longitudinal acoustic mode is less than 5 %. These results are evident from the fact the incident wave is polarized parallel to the z-direction and thus the polarization direction of the transmitted wave is strongly polarized in the z-direction . The quasi longitudinal waves are excited weakly because the polarization direction of the QL waves is almost parallel to the x-direction as shown in Fig.7.2. These results are consistent with the experimental observation stated later.

Table 7.I. The particle Displacement velocity[v], the phase velocity V_p, the stress components[T] and the complex acoustic Poynting vector[P_{ac}] of incident, reflected and transmitted acoustic waves.

Incident wave : [PT-mode]

$[v]_I=[z]A_z(PT)$, $V_p=(C_{44}/\rho)^{1/2}$, $[T_5]=-(\rho C_{44})^{1/2}A_z(PT)$

$[P_{ac}]=[x]\frac{1}{2}A_z(PT)^2(\rho C_{44})^{1/2}$

Reflected waves:

PL-mode	PT-mode	PT-mode
$[v]_R=[x]B_x(PL)$	$[v]_R=[y]B_y(PT)$	$[z]_R=[z]B_z(PT)$
$V_p=(C_{11}/\rho)^{1/2}$	$V_p=(C_{66}/\rho)^{1/2}B_y(PT)$	$V_p=(C_{44}/\rho)^{1/2}$
$[T_1]=(\rho C_{11})^{1/2}B_x(PL)$	$[T_6]=(\rho C_{66})^{1/2}B_y(PT)$	$[T_5]=(\rho C_{44})^{1/2}B_z(PT)$
$[P_{ac}]=-[x]\frac{1}{2}B_x(PL)^2(\rho C_{11})^{1/2}$	$[P_{ac}]=-[x]\frac{1}{2}B_y(PT)^2(\rho C_{66})^{1/2}$	$[P_{ac}]=-[x]\frac{1}{2}B_z(PT)^2(\rho C_{44})^{1/2}$

Transmitted waves

PT-mode	QL-mode	QT-mode
$[v]_T=[y]D_y(PT)$	$[v]_T=([x]+[z]\beta_+)D_x(QL)$	$[v]_T=([x]+[z]\beta_-)D_x(QT)$
$V_p=(C''_{66}/\rho')^{1/2}$	$V_p=(\alpha_+/\rho')^{1/2}$	$V_p=(\alpha_-/\rho')^{1/2}$
$[T_6]=-(\rho' C''_{66})^{1/2}D_y(PT)$	$[T_1]=-(\rho'\alpha_+)^{1/2}D_x(QL)$	$[T_1]=-(\rho'\alpha_-)^{1/2}D_x(QT)$
$[P_{ac}]=[x]\frac{1}{2}D_y(PT)^2(\rho' C''_{66})^{1/2}$	$[T_5]=-(\rho'\alpha_+)\beta_+D_x(QL)$	$[T_5]=-(\rho'\alpha_-)^{1/2}\beta_-D_x(QT)$
	$[P_{ac}]=([x](1+\beta_+^2)+[z]\beta_+^2)\frac{1}{2}D_x(QL)^2(\rho'\alpha_+)^{1/2}$	$[P_{ac}]=([x](1+\beta_-^2)+[z]\beta_-^2)\frac{1}{2}D_x(QT)^2(\rho'\alpha_-)^{1/2}$

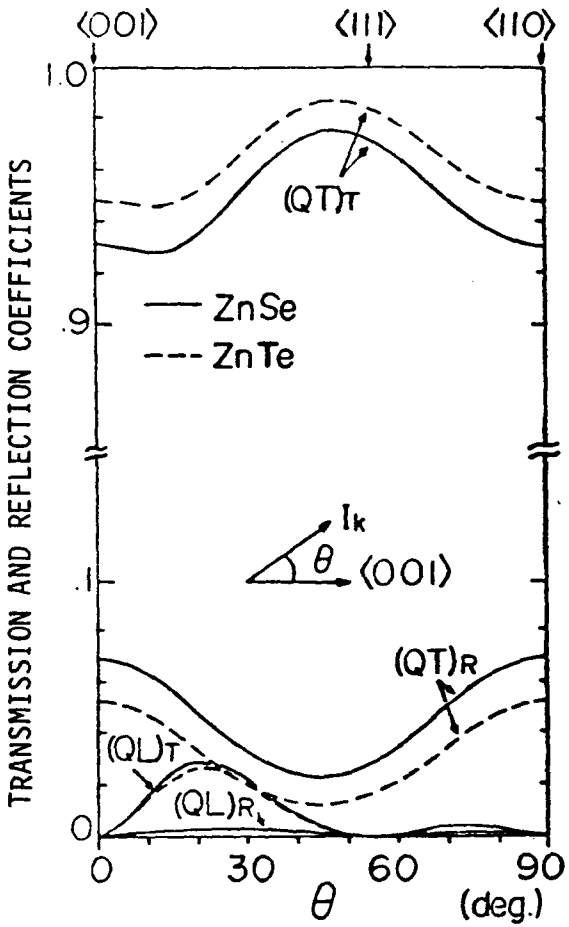

Fig. 7.3. Calculated transmission and reflection coefficients of the complex acoustic Poynting vectors in CdS-ZnSe and CdS-ZnTe bonded systems.

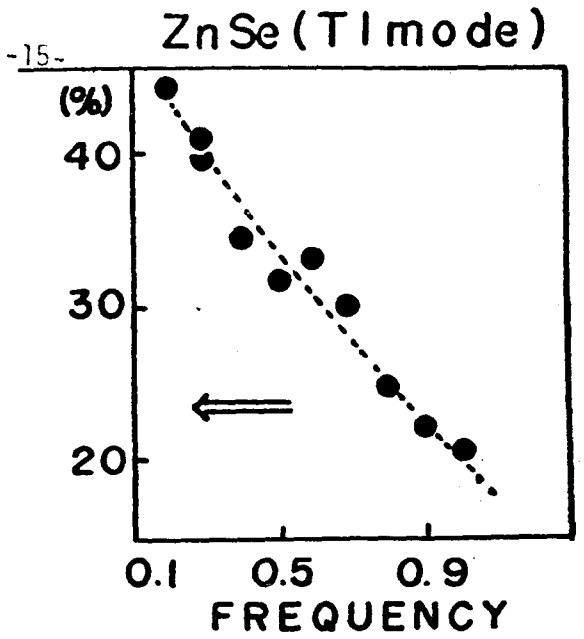

Fig. 7.4. Frequency dependence of transmission coefficients of acoustic Poynting vectors in CdS-ZnSe bonded system.

7.3. Application of Acoustic Injection to an Investigation of Elastic Properties

In the previous section we found that the three kinds of acoustic modes (PT,QT and QL-modes) can be excited in the end bonded specimens by the acoustic injection. The theoretical transmission coefficients of complex acoustic Poynting vectors in the CdS-ZnSe and CdS-ZnTe systems are found to be more than 90% for the arbitrary propagation directions in the $(1\bar{1}0)$ plane. Observed transmission coefficients in the present experiments (Fig.7.4) are smaller than the theoretical values, which seems to be due to the boundary energy loss. We can confirmed experimentally that the considerably strong optical signals (scattering signals) can be detected by using the such injected sound waves. The intensity of injected acoustic power observed in the present measurements depends upon the quality of bonding contact and one can find in Fig.7.4 the maximum transmission coefficient of acoustic Poynting vector is about 50% for the 0.1 GHz acoustic phonons. Experimental transmission coefficient depends on the frequency of the acoustic waves and decreases with increasing the frequency, as shown in Fig.7.4, where the results on the pure transverse (PT) waves propagating in the [110] plane are given for example.

By using various kinds of injected acoustic waves we carried out the following experiments: (1) determination of the three independent elastic stiffness constants (c_{11},c_{12} and c_{44}) in the ZnSe and ZnTe, (2) determination of propagation loss α_L (non-electronic lattice loss) of the transverse acoustic waves in ZnSe and ZnTe in the range of frequencies 0.5∿1.5 GHz. Measurements are performed by using the similar experimental arrangement in Chap.III. but for the light source of He-Ne laser. In order to obtain a good bonded contact we covered the contact with araldite,

which avoided unwanted signals from electro-luminescence near the anode of CdS.

7.3.1 Determination of Elastic Stiffness Constants in ZnSe and ZnTe

We have carried out the measurements of velocities of quasi-transverse sound waves propagating in the several directions in the $(1\bar{1}0)$ plane. Phase velocities of propagating sound waves were estimated from the time delay of scattered light signals as a function of the probing positions. In Fig.7.5 and 7.6 we plot the experimental sound velocities as s function of propagating direction in ZnSe and ZnTe, respectively. The measurements were made by using QT mode waves of 1.0GHz for ZnSe and 0.8GHz for ZnTe. As shown in Table 7.1, the theoretical sound velocity of injected QT mode into ZnSe and ZnTe is given by

$$V_p=\left(\frac{\alpha_-}{\rho'}\right)^{1/2}=\left[\frac{C''_{55}+C''_{11}-((C''_{55}-C''_{11})^2+4C''^2_{15})^{1/2}}{2\rho'}\right]^{1/2} \qquad (7.3\text{-}1)$$

where C''_{11}, C''_{55} and C''_{15} are represented by three independent elastic stiffness constants C_{11}, C_{12} and C_{44} of ZnSe and ZnTe (See eqs.(A.III-7) and (A.III-4). Therefore the phase velocity observed in the present measurements can be calculated as a function of C_{11}, C_{12}, C_{44} and θ. Three independent elastic stiffness constants of ZnSe and ZnTe are obtained as set of three parameters which give a best fitted theoretical curve of phase velocity to that of experimental curve as shown in Figs.7.5 and 7.6. From the least square fit of experimental data points to the theoretical curves(eq.(7.3-1)) we obtained the following three parameters; $C_{11}=8.55$, $C_{12}=4.49$, $C_{44}=4.01\times10^{11}$ (dyn/cm^2) for ZnSe and $C_{11}=7.36$, $C_{12}=5.43$, $C_{44}=3.50$ for ZnTe, which are summarized in Table 7.II together with the results of Lee[88] and Berlincourt.[121]

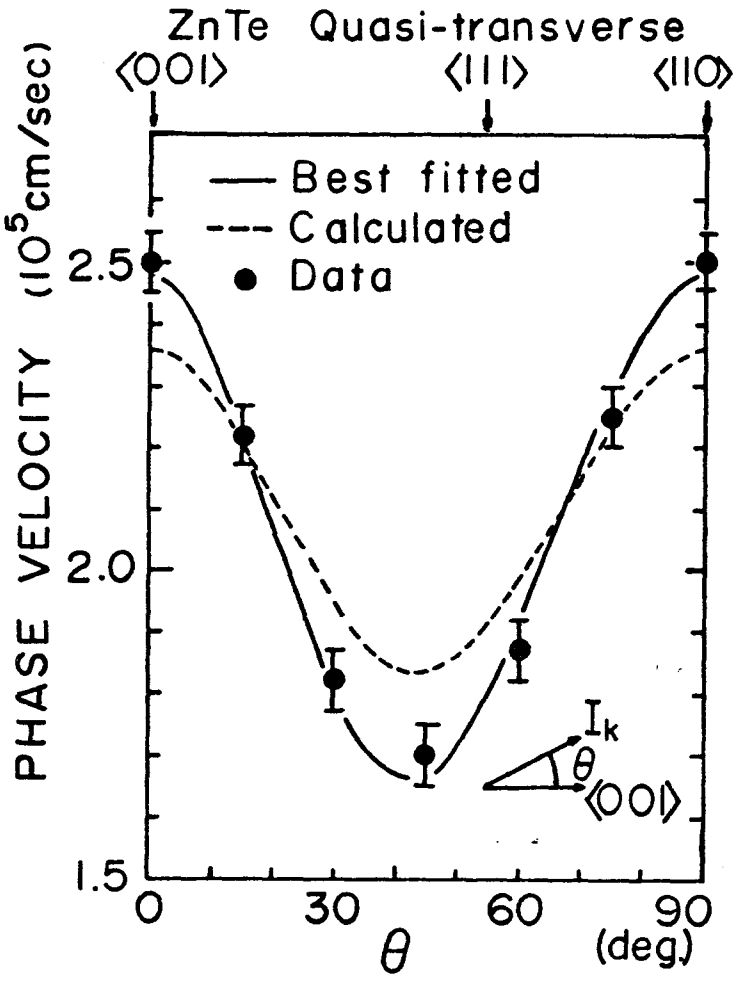

Fig. 7.6. Same as in Fig.7.5 but for the ZnTe.

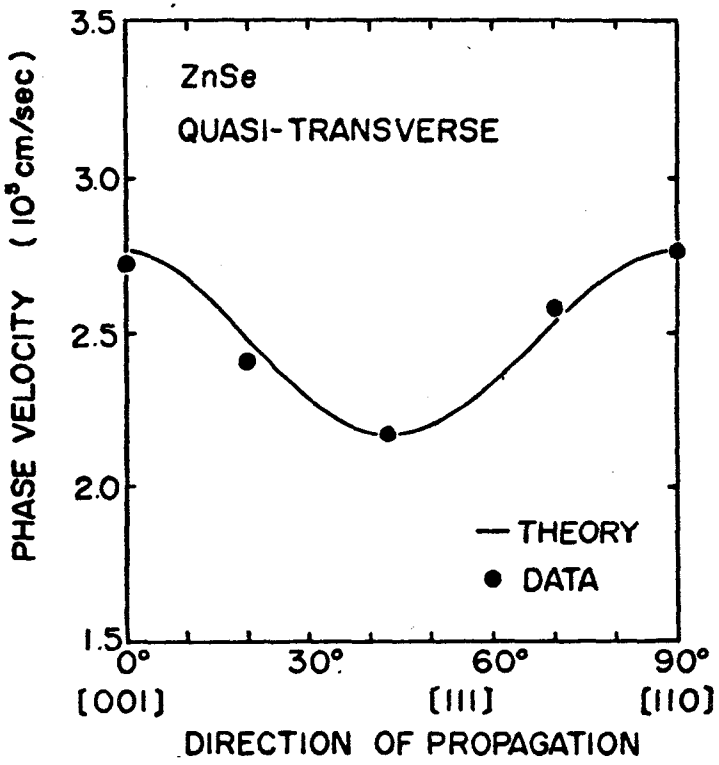

Fig. 7.5. The phase velocity of QT-acoustic waves in ZnSe with frequency 1 GHz as a function of propagation direction in the $(1\bar{1}0)$ plane. The solid line represents the best fitted theoretical variation of velocity using the values of elastic-stiffness constants in Table 7.II.

Table 7.II. Values of the elastic stiffness constants obtained by the best fitting.

	present work			Lee et al.			Berlincourt et al.		
[ZnSe]	C_{11}	C_{12}	C_{44}	C_{11}	C_{12}	C_{44}	C_{11}	C_{12}	C_{44}
	8.55	4.49	4.01	8.59	5.o6	4.06	8.10	4.88	4.41
	(dyn/cm^2)								
[ZnTe]	C_{11}	C_{12}	C_{44}	C_{11}	C_{12}	C_{44}	C_{11}	C_{12}	C_{44}
	7.36	5.43	3.50	7.11	4.07	3.13	7.13	4.07	3.12

7.3.2. Frequency Dependence of Attenuation Coefficients of Injected Sound Waves in ZnSe and ZnTe

The attenuation coefficients of appropriate acoustic frequency can be obtained from the measurement of the intensities of scattered light signals as a funtion of the probing position. In the present study the measurements are carried out by using the T2-mode acoustic waves propagating along the [001]([110])direction with shear polarization parallel to the [110]([001]) direction in ZnSe(ZnTe). The results of ZnSe and ZnTe are shown in Figs.7.7 and 7.8, respectively. The frequency dependence observed in the present work is of the form :$\alpha_L \propto f^{1.45}$ for ZnSe and $\alpha_L \propto f^{1.2}$ for ZnTe, which are inconsistent with the theoretical frequency dependence of Akhieser loss, where α_L is proportional to the square of frequency; $\alpha_L \propto f^2$. Departure from f^2-dependence is also observed in a survey of other materials.[36,37,122] It is not clear why the f-dependence is not quadratic. However, Miller[123] has pointed out that a strong frequency dependence for thermal phonon life time itself gives a deviation from Akhieser type frequency dependence. Tsubouchi and Mikoshiba have proposed that such a non-quadratic frequency dependence reflects non-linear phonon-phonon interaction

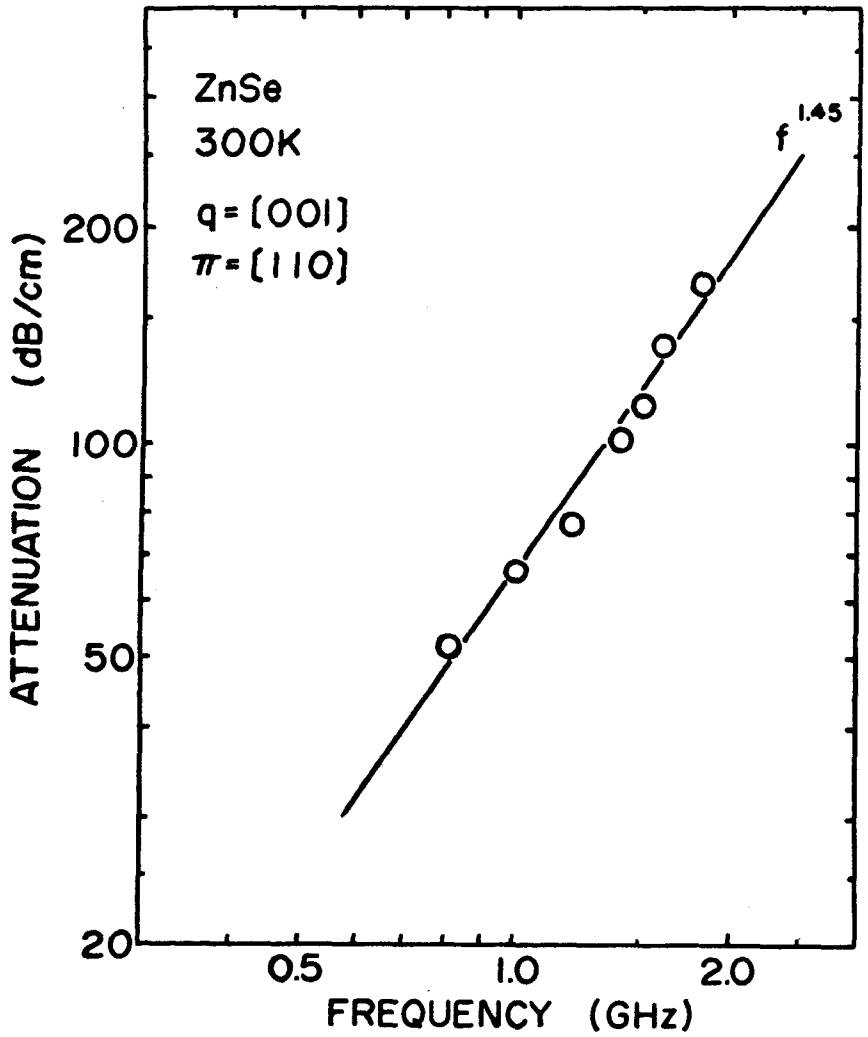

Fig. 7.7. The attenuation coefficients of pure transverse sound waves propagating in the [001] direction with polarization vector parallel to the [110] direction as a function of the frequency in ZnSe.

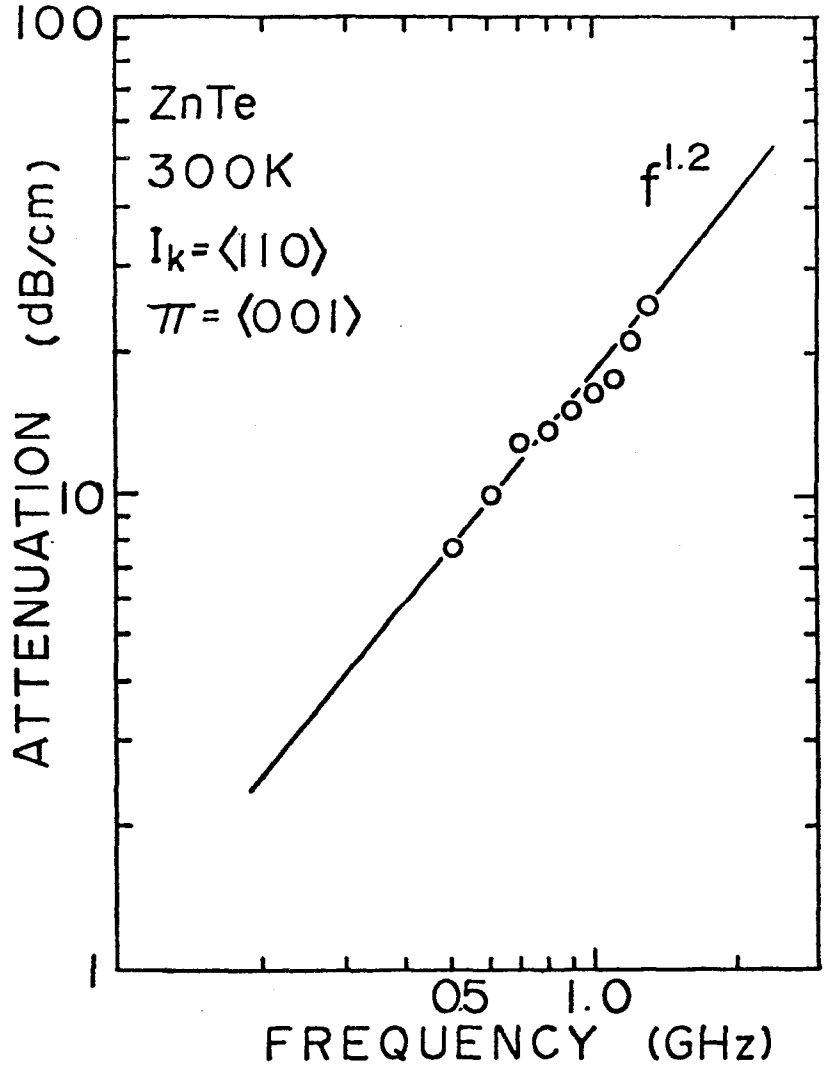

Fig. 7.8. Same as in Fig. 7.7 but for the ZnTe and T2-mode.

in the strong flux limit. In the present method the energy density of amplified acoustic waves in CdS ranges from 10^7 to 10^9 in the frequencies 0.1∿2.0 GHz. From the measurement of scattered light intensity by injected sound waves one can find that the energy of injected acoustic flux is nearly same order of the flux in CdS and thus we cannot neglect the non-linear interaction between the phonons. Such an effect seems to explain the departure from the f^2-dependence.

7.4. Summary

A treatment of acoustic transmission theory is given in order to determine the modes and intensities of injected acoustic waves into ZnSe and ZnTe. It is found that the three acoustic modes (PT-,QT-, and QL-modes) can be excited by the domain injection. From the analyses the transmission coefficients of acoustic Poynting vectors in CdS-ZnSe and CdS-ZnTe systems are found to be higher than 95% in the case of QT-mode acoustic waves. By using such strong injected acoustic packets the measurements of Brillouin scattering are performed and three independent elastic stiffness constants; C_{11},C_{12} and C_{44} are determined in ZnSe and ZnTe. Attenuation coefficient α_L of the transverse acoustic waves are also determined in the frequency range of 0.5 to 1.5 GHZ.

Chapter VIII Conclusions

The results and conclusions obtained in the present work are summarized as follows:

1) The relevant photoelastic constant P_{ijkl} concerning to the resonant Brillouin scattering for different acoustic phonon modes are determined by using the classical light scattering theory.

2) Observed dispersion spectra of Brillouin scattering cross sections by TA phonons show a sharp resonant enhancement near the fundamental edge(M_o-critical point) and also show a resonant cancellation(antiresonance) just below the edge in CdS abd ZnSe.

3) It is found from the microscopic light scattering theory that the electronic virtual excitations of holes(or excitons) associated with the p-like valence bands(Γ_7 and Γ_9) have an important role in the resonance effect in semiconductors.

4) In order to explain the observed dispersion spectra of the resonant Brillouin scattering cross sections 2- and 3-Band models are proposed which take into account of the transition process of the intermediate virtual states associated with the valence bands.

5) Microscopic expression of Brillouin scattering efficiency taking into account of the exciton contributions was found to explain the experimental dispersion spectra of scattering cross sections.

6) The general formulation of resonant Brillouin scattering is derived from the treatment of non-linear susceptibility and from this analysis we find the theoretical resonant dispersions of Brillouin scattering efficiency in the higher photon energy regions(M_1, M_2 and M_3-critical points in addition to M_o-critical

point).

7) Antiresonance-structure in the disperion curves can be explained by the fact that the sign of resonant contribution arising from M_o-critical point is different from that of nonresonant contribution arising from the higher energy M_2-critical point.

8) Dispersion spectra of Brillouin scattering cross sections by mode converted-PL mode phonons are found to show only the resonant enhancement near the intrinsic edge of CdS and never show the structure of resonant cancellation.

9) We find in the analysis of piezo-birefringence theory that the relevant photoelastic constants P_{ijkl} passes through zero while under going a reversal in sign and the features are closely related to the mechanism of resonant cancellation.

10) In the present measurements of optical modulation induced by the propagating acoustic domain we observe a deep and narrow minimum around 5600 Å in CdS.

11) Present dispersion curves of optical modulation are essentially different from those of optical modulation observed in n-GaAs, where the mechanism in the latter case is believed to be associated with Franz-Keldysh effect induced by the piezoelectric field in the domain.

12) The domain induced optical modulation in CdS cannot be explained by the edge-modulation through the Franz-Keldysh effect but the mechanism seems to be associated with the resonant light scattering.

13) The crystal symmetry induced selection rule of Brillouin scattering has broken down in the photon energy region near the fundamental absorption edge in CdS.

14) Observed Brillouin scattering efficiency under the forbidden

polarization conditions shows steep resonant enhancement near the intrinsic band edge of CdS.

15) The electronic virtual excitations of spin orbit splitt off band play a very important role in the resonant-forbidden scattering by piezoelectrically active TA phonons.

16) It is found from the analyses of acoustic transmission theory that three kinds of acoustic phonon modes(PT-, QT, and QL-modes) can be excited in the end bonded ZnSe and ZnTe crystals when we choose proper crystal axis.

17) Injected acoustic waves of quasi-transverse mode are achieved and the attenuation coefficients α_L of the propagating acoustic waves in ZnSe and ZnTe are measured by making use of Brillouin scattering technique.

18) The three independent elastic stiffness constants C_{11}, C_{12} and C_{44} of ZnSe and ZnTe are determined from the measurements of usual Brillouin scattering by making use of acoustic injection technique.

Appendix I. General Formulation of Resonant Brillouin Scattering in Higher Energy Regions

The resonant behavior near the fundamental edge of semiconductors can be explained by Loudon's theory[20] or by the expression of $P_{ijkl}(\omega,M_o)$ of eq.(2.7-19). In this Appendix we discuss the resonant light scattering in a higher photon energy region. The general formulation of $\Delta\varepsilon_2(\omega,\omega_q)$ developed in Chap.II is very useful for the present discussion, which is given by

$$\Delta\varepsilon_2(\omega,\omega_q)=\frac{\pi A_2}{\omega^2}\left[\frac{\delta(\hbar\omega\pm\hbar\omega_q-\varepsilon_{cv'}(\vec{k}))}{\hbar\omega-\varepsilon_{cv}(k)}\cdot dk+\frac{\delta(\hbar\omega-\varepsilon_{cv}(\vec{k}))}{\hbar\omega\pm\hbar\omega_q-\varepsilon_{cv'}(\vec{k})}\cdot dk\right] \quad \text{(AI-1)}$$

where $A_2=2A_1/(2\pi)^3$ and the 2-Band model is adopted for simplicity. After a simple calculation eq.(AI-1) can be written,

$$\Delta\varepsilon_2(\omega,\omega_q)=\pm\frac{\pi A_2}{\hbar\omega_q\omega^2}\left[\delta(\hbar\omega-\varepsilon_{cv}(\vec{k}))d\vec{k}-\delta(\hbar\omega\pm\hbar\omega_q-\varepsilon_{cv'}(\vec{k}))d\vec{k}\right] \quad \text{(AI-2)}$$

As well known the imaginary part of the dielectric constant $\varepsilon_2(\omega)$ is defined as;

$$\varepsilon_2(\omega)=\frac{e^2}{\pi m^2\omega^2}|\hat{\varepsilon}\cdot P_{cv}|^2\,\delta(\hbar\omega-\varepsilon_{cv}(\vec{k}))d\vec{k} \quad \text{(AI-3)}$$

Finally one obtains the expression of the change in the imaginary part of the dielectric constant $\Delta\varepsilon_2(\omega,\omega_q)$ induced by the acoustic phonons by using the general expression of $\varepsilon_2(\omega)$,

$$\Delta\varepsilon_2(\omega)=-\frac{1}{\hbar e}(n_q+\frac{1}{2}\pm\frac{1}{2})S_{kl}\cdot\Xi^{kl}\frac{d\varepsilon_2}{d\omega} \quad \text{(AI-4)}$$

By an analogical treatment one also obtains the expression of ε_1,

$$[\Delta\varepsilon_1(\omega)-1]=-\frac{1}{\hbar e}(n_q+\frac{1}{2}\pm\frac{1}{2})S_{kl}\Xi^{kl}\frac{d\varepsilon_1}{d\omega} \quad \text{(AI-5)}$$

Equations (AI-4) and (AI-5) are simple but important formulation in the estimation of resonant enhancement at higher energy critical points(M_1,M_2, and M_3-critical points).

The dispersions of $\varepsilon_2(\omega)$ for three dimensional M_o, M_1, M_2 and M_3-type critical points are derived by Batz[70] and Matatagui.[71] Acoustic phonon induced change $\Delta\varepsilon_2(\omega)$ can be evaluated from eq.(AI-4) when we know $d\varepsilon_2/d\omega$ given by,[76]

$$[M_0]:\ d\varepsilon_2/d\omega = \begin{cases} 0 & (\omega<\omega_{go}) \\ \frac{C_o}{2}(\omega-\omega_{go})^{-1/2} & (\omega>\omega_{go}) \end{cases} \qquad \text{(AI-6a)}$$

$$[M_1]:\ d\varepsilon_2/d\omega = \begin{cases} \frac{C_1}{2}(\omega_{g1}-\omega)^{-1/2} & (\omega<\omega_{g1}) \\ 0 & (\omega>\omega_{g1}) \end{cases} \qquad \text{(Ai-6b)}$$

$$[M_2]:\ d\varepsilon_2/d\omega = \begin{cases} 0 & (\omega<\omega_{g2}) \\ \frac{C_2}{2}(\omega-\omega_{g2})^{-1/2} & (\omega>\omega_{g2}) \end{cases} \qquad \text{(AI-6c)}$$

$$[M_3]:\ d\varepsilon_2/d\omega = \begin{cases} -\frac{C_3}{2}(\omega_{g3}-\omega)^{-1/2} & (\omega<\omega_{g3}) \\ 0 & (\omega>\omega_{g3}) \end{cases} \qquad \text{(AI-6d)}$$

The change $\Delta\varepsilon_1(\omega)$ which determines the resonant behavior in the light scattering is obtained from the expression of $d\varepsilon_2/d\omega$ by using Kramers-Kronig transformation, which is summarized in the following.

$$[M_o]:\Delta\varepsilon_1(\omega)\propto d\varepsilon_1/d\omega = \begin{cases} C_o'[(\omega+\omega_{go})^{-1/2}+(\omega_{go}-\omega)^{-1/2}] & (\omega<\omega_{go}) \\ 0 & (\omega>\omega_{go}) \end{cases} \qquad \text{(AI-7a)}$$

$$[M_1]:\Delta\varepsilon_1(\omega)\propto d\varepsilon_1/d\omega = \begin{cases} 0 & (\omega<\omega_{g1}) \\ -C_1'[(\omega-\omega_{g1})^{-1/2}]/2 & (\omega>\omega_{g1}) \end{cases} \qquad \text{(AI-7b)}$$

$$[M_2]:\Delta\varepsilon_1(\omega)\propto d\varepsilon_1/d\omega = \begin{cases} -C_2'[(\omega+\omega_{g2})^{-1/2}+(\omega_{g2}-\omega)^{-1/2}]/2 & (\omega<\omega_{g2}) \\ 0 & (\omega>\omega_{g2}) \end{cases} \qquad \text{(AI-7c)}$$

$$[M_3]:\Delta\varepsilon_1(\omega)\propto d\varepsilon_1/d\omega = \begin{cases} 0 & (\omega<\omega_{g3}) \\ C_3'[(\omega-\omega_{g3})]/2 & (\omega>\omega_{g3}) \end{cases} \qquad \text{(AI-7d)}$$

The feature of resonant behavior of the Brillouin tensor(corresponds to the $\Delta\varepsilon_1(\omega)$) for three dimensional M_o,M_1,M_2 and M_3 critical

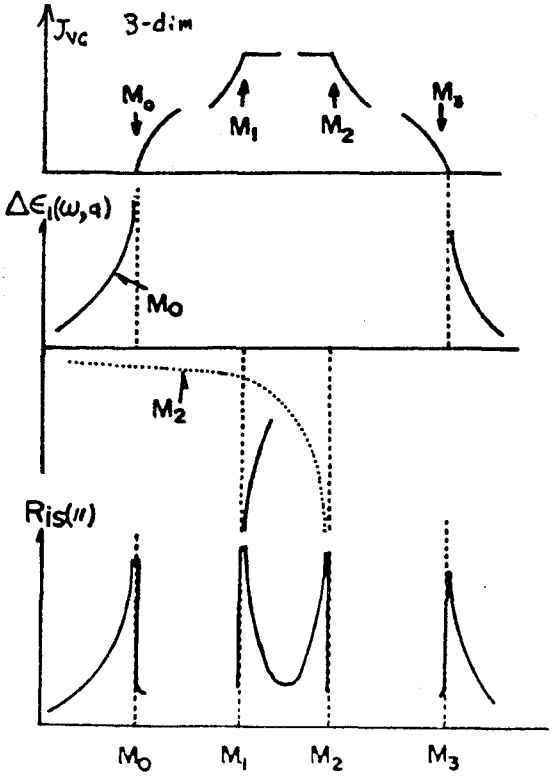

Fig.AI. Joint density of states and real part of modulated dielectric constants and Brillouin efficiencies versus incident photon energy for 3-dimensional critical points.

points are schematically shown in Fig.AI. We find from the figure that the resonant behaviors of M_0- and M_2-critical points are quite similar but for the sign. It is also clear that contribution of M_1- and M_3-type critical points to the total scattering efficiency in the region of fundamental edge is negligibly small because the contributions from those critical points are significant only in the photon energy region $\hbar\omega > \hbar\omega_{g1}(\hbar\omega_{g3})$, where $\hbar\omega_{g1}$ and $\hbar\omega_{g3}$ are the energy gaps of the M_1 and M_3-critical points. Then we suspect that the nonresonant contribution to the total Brillouin scattering cross section in the transparent energy region originate mainly from that of M_2-critical point. This prediction is consistent with the appointment of Cardona, who estimated the nonresonant contribution from Penn-gap.[72]

Appendix II. Correction of Strong Absorption and Depletion of Incident and Scattered Light in Anisotropic Crystals

We present here a derivation of the formula to relate the scattering cross section σ_B with the measured values of I_s and I_o, where we properly take into account the birefringence and the difference in the optical absorption coefficients for the incident and scattered light. The light intensity $I(x')$ propagating in the material is expressed by,

$$I(x') = I_o \exp[-(\alpha_i + \sigma_T)x'] \qquad \text{(AII-1)}$$

where I_o is the incident light intensity, α_i is the absorption coefficient of the incident light, and σ_T is the total Brillouin scattering coefficient. The total scattering coefficient σ_T is defined by the relation $I_t=I_t^o\exp(-\sigma_T b')$, where I_t^o is the transmitted light in the absence of any scattering, I_t is the light transmitted after depletion by scattering, and b' is the optical path length. The quantity σ_T describes how much light is scattered out of the incident beams by phonons of all possible wave vectors that can contribute to the scattering. The differential scattering intensity $dI_s(x')$ during the optical path between x' and x'+dx' in the material is given by,

$$dI_s(x') = I_o\exp[-(\alpha_i+\sigma_T)x']\sigma_B dx' d\Omega_s, \qquad \text{(AII-2)}$$

where $d\Omega_s$ is the solid angle determined by the cone angle of the detector. For the Brillouin scattering in a birefringent material, the angles of incident and scattered light(θ_i and θ_d) with respect to the normal to the sample are different in general. When we define a distance x by $x'\cos\theta_i$, x is the effective optical path length along the direction normal to the surface, and eq.(AII-2) reduce to

$$dI_s(x) = I_o\exp[-(\alpha_i+\sigma_T)x/\cos\theta_i]\sigma_B dx d\Omega_s/\cos\theta_i. \qquad \text{(AII-3)}$$

Light intensity scattered at the point x', is also decreased by absorption and scattering during the path length x"(=b'-x'), where $x'\cos\theta_d=b-x$, and b is the width of the sample in the scattering plane. Therefore the actual Brillouin scattered light intensity is given by,

$$\begin{aligned} dI_s(x,b) &= dI_s(x)\exp[-(\alpha_d+\sigma_T)x''] \\ &= I_o\exp\Big[-(\alpha_i-\alpha_d\cos\theta_i/\cos\theta_d)+\sigma_T\Big(1-\frac{\cos\theta_i}{\cos\theta_d}\Big)\frac{x}{\cos\theta_i} \\ &\quad -\frac{(\alpha_d+\sigma_T)b}{\cos\theta_d}\Big]\times\sigma_B dx d\Omega_s/\cos\theta_i, \end{aligned} \qquad \text{(AII-4)}$$

where α_d is the absorption coefficient of the scattered light. Integrating eq.(AII-4) over the sample width, we obtain

$$\frac{I_s}{I_o} = \frac{\sigma_B d\Omega_s}{(\alpha_i-\alpha_d n_d/n_i)+\sigma_T(1-n_d/n_i)} \exp\left[-\frac{(\alpha_d+\sigma_T)b}{\cos\theta_i}\right]$$

$$\times\left(1-\exp\left[-\{(\alpha_i-\alpha_d n_d/n_i)+\sigma_T(1-n_d/n_i)\ \frac{b}{\cos_i}\right]\right) \qquad \text{(AII-5)}$$

where n_i and n_d are the refractive indices for the incident and scattered light, respectively, and we used a relation $n_i\cos\theta_i = n_d\cos\theta_d$. Noting that $|n_d/n_i-1|\ll 1$ and $(\alpha_i-\alpha_d n_d/n_i)\gg\sigma_T(1-n_d/n_i)$ near the absorption edge($\alpha_d\gg\sigma_T$) we find from eq.(AII-5)

$$\frac{I_s}{I_o} = \frac{\sigma_B d\Omega_s}{(\alpha_i-\alpha_d n_d/n_i)} \exp[-\alpha_d b/\cos\theta_d]$$

$$\times\left(1-\exp[-(\alpha_i-\alpha_d n_d/n_i)b/\cos\theta_i]\right) \qquad \text{(AII-6)}$$

In the region far from the edge($(\alpha_i-\alpha_d n_d/n_i)b/\cos\theta_i \ll 1$) we obtain

$$\frac{I_s}{I_o} = \sigma_B d\Omega_s b\exp[-(\alpha_d+\sigma_T)b/\cos\theta_d]/\cos\theta_i, \qquad \text{(AII-7)}$$

or

$$\frac{I_s}{I_t^d} = \sigma_B d\Omega_s b/\cos\theta_i \qquad \text{(AII-8)}$$

where I_t^d is the transmitted beam for the light polarization in the same direction as the scattered light.

Appendix III. Representation of Elastic Constsnt Tensor for Arbitrary Coordinate System in Cubic Crystals.

The following analysis can be applied to all crystals with cubic system. As we mentioned in Chap.VII, a ZnSe(ZnTe)crstals is bonded to a CdS specimen and the long axis of the ZnSe makes an arbitrary angle θ with respect to the [001] crystal axis in the $(1\bar{1}0)$ plane. Therefore the analysis can be very simplified when the

elastic constant matrix is expressed in the new coordinate system where x axis is taken to be the long axis of the specimen. For this purpose we apply the following procedure. First, the ZnSe(ZnTe) crystal is rotated around the [001] axis by 45° to locate the $(1\bar{1}0)$ plane parallel to the x axis, and we obtain the elastic constants C'_{ijkl} in this system. Second the [001] axis of the crystal is rotated by an angle θ in the $(1\bar{1}0)$plane and we obtain the elastic constants C''_{ijkl} in the coordinate system. When a rotation is applied to coordinate system r_j, we obtain the new coordinate system r'_i as $r'_i=a_{ij}r_j$, when $[a_{ij}]$ ia unitary transformation matrix element. The elastic constant C_{pqrs} is transformed by the rotation to C'_{ijkl}:

$$C'_{ijkl} = a_{ip}a_{jq}a_{kr}a_{ls}C_{pqrs} \qquad \text{(AIII-1)}$$

The transformation matrix $[a_{ij}]$ is given by

$$[a_{ij}]=\begin{bmatrix} 1/\sqrt{2} & 1/\sqrt{2} & 0 \\ -1/\sqrt{2} & 1/\sqrt{2} & 0 \\ 0 & 0 & 0 \end{bmatrix} \qquad \text{(AIII-2)}$$

for the 45° rotation around the [001] axis. Therefore we obtain the following expression for the elastic stiffness tensor,

$$\begin{bmatrix} C'_{11} & C'_{12} & C'_{13} & 0 & 0 & 0 \\ C'_{12} & C'_{11} & C'_{13} & 0 & 0 & 0 \\ C'_{13} & C''_{13} & C'_{33} & 0 & 0 & 0 \\ 0 & 0 & 0 & C'_{44} & 0 & 0 \\ 0 & 0 & 0 & 0 & C'_{44} & 0 \\ 0 & 0 & 0 & 0 & 0 & C'_{66} \end{bmatrix} \qquad \text{(AIII-3)}$$

with $C'_{11}=(C_{11}+C_{12})/2+C_{44}$, $C'_{12}=(C_{11}+C_{12})/2-C_{44}$, $C'_{13}=C_{12}$

$C'_{33}=C_{11}$, $C'_{44}=C_{44}$, and $C'_{66}=(C_{11}-C_{12})/2$ (AIII-4)

where contracted notation is used. The second step of the transformation is rotation of an angle around the new axis $y'(=r'_2)$ and the corresponding transformation matrix is given by,

$$[a_{ij}] = \begin{bmatrix} \cos\theta & 0 & -\sin\theta \\ 0 & 1 & 1 \\ \sin\theta & 0 & \cos\theta \end{bmatrix} \qquad \text{(AIII-5)}$$

Using this matrix and the relation of eq.(AIII-1) we can obtain the elastic stiffness tensor matrix $[C''_{ijkl}]$ for the system in Fig.7.1 ;

$$\begin{bmatrix} C''_{11} & C''_{12} & C''_{13} & 0 & C''_{15} & 0 \\ C''_{12} & C''_{22} & C''_{23} & 0 & C''_{25} & 0 \\ C''_{13} & C''_{23} & C''_{33} & 0 & C''_{35} & 0 \\ 0 & 0 & 0 & C''_{44} & 0 & C''_{46} \\ C''_{15} & C''_{25} & C''_{35} & 0 & C''_{55} & 0 \\ 0 & 0 & 0 & C''_{46} & 0 & C''_{66} \end{bmatrix} \qquad \text{(AIII-6)}$$

where

$$C''_{11}=C'_{11}\cos^4\theta+2C'_{13}\sin^2\theta\cos^2\theta+C'_{33}\sin^4\theta+C'_{44}\sin^2 2\theta,$$

$$C'_{12}=C'_{12}\cos^2\theta+C'_{13}\sin^2\theta \ ,$$

$$C''_{13}=C'_{11}\sin^2\theta\cos^2\theta+C'_{13}(\cos^4\theta+\sin^4\theta)+C'_{33}\sin^2\theta\cos^2\theta-C'_{44}\sin^2 2\theta,$$

$$C''_{22}=C'_{11},$$

$$C''_{23}=C'_{12}\sin^2\theta+C'_{13}\cos^2\theta \ ,$$

$$C''_{25}=(C'_{12}-C'_{13})\sin 2\theta/2$$

$$C''_{33}=C'_{11}\sin^4\theta+2C'_{13}\sin^2\theta\cos^2\theta+C'_{33}\cos^4\theta+C'_{44}\sin^2\theta \ ,$$

$$C''_{35}=\{(C'_{11}-C'_{13})\sin^2\theta+(C'_{13}-C'_{33})\cos^2\theta+2C'_{44}\cos 2\theta\}\sin 2\theta/2 \ ,$$

$$C''_{44}=C'_{44}\cos^2\theta+C'_{66}\sin^2\theta \ ,$$

$$C''_{46}=(C'_{66}-C'_{44})\sin 2\theta/2 \ ,$$

$$C''_{55}=(C'_{11}-2C'_{13}+C'_{33})\sin^2 2\theta/4+C'_{44}\cos^2 2\theta \ ,$$

$$C''_{66}=C'_{44}\sin^2\theta+C'_{66}\cos^2\theta \ . \qquad \text{(AIII-7)}$$

References

1) L. Brillouin, Ann. Phys.(Paris) 17 (1922)88.

2) A. Smekal, Naturwiss. 11 (1923) 873.

3) C. V. Raman, Ind. J. Phys. 2 (1928) 387.

4) M. Cardona, Surface, Sci., 37 (1973) 100.

5) R. C. C. Leite, and S. P. S. Porto, Phys. Rev. Lett. 31(1966)10.

6) J.M.Ralston, R.L.Wadsak and R.K.Chang, Phys. Rev. Lett.25 (1970)814. ; See also, Proceeding of the Second International Conference on Light Scattering in Solid, edited by M.Balkanski, (Flammarion, Paris, 1971)

7) J.F.Scott, T.C.Damen, R.C.C.Leite and W.T.Silfvast, Solid State Comunn. 7(1969)953.

8) M.I.Bell, R.N.Tyte and M.Cardona, Solid State Commun.13(1973) 1833.

9) F.Cerdeira, W.Drebrodt and M.Cardona: Proc.11 th Intern. Conf. Physics of Semiconductors(Polish Scientific. Publ. Warso 1972) pp1142.

10) J.L.Lewis,R.L.Wadsack and R.K.Chang : In Light Scattering in Solid, ed by M.Balkanski(Flammarion Sciences, Paris,1971)pp41.

11) T.C.Damen and J.F.Scott, Solid State Commun.9(1971)383.

12) W.Drebrodt, W.Richter, F.Cerdiera and M. Cardona, Phys. Stat. Solid,(b) 60(1973)1755.

13) R.W.Rubloff, E.Anastassakis, and F.H.Pollak, Solid State Commun. 13(1973)1755.

14) A.S.Pine, Phys. Rev. B5(1972)3003.

15) D.K.Garrod and R.Bray, Phys. Rev. B6(1972)1696.

16) M.Yamada, K.Ando, C.Hamaguchi and J.Nakai, J. Phys.Soc. Japan, 34(1972)1314.

17) U.Gelbart and A.Many, Phys. Lett. A43(1973)389.

18) K.Ando and C.Hamaguchi, Phys. Rev. B11(1975)3876.

19) K.Ando and C.Hamaguchi, Prog. Theor. Phys. Suppl. No 57(1975) 105.

20) R.Loudon, Proc. R. Soc. Lond. A275(1963)218 ; J. Phys.(paris) 26(1965)677.

21) A.K.Gangly and J.L.Birman, Phys. Rev. 162(1967)806.

22) R.Berkowicz and D.H.R.Price, Solid State Commun. 14(1974)195.

23) R.Berkowicz and K.Skettrup, Phys. Rev. B11(1975)2316.

24) K.Yamamoto, K.Misawa, H.Shimizu and K.Abe, J. Phys, Chem. Solid. 37(1976)181.

25) K.Ando, M.Yamada and C.Hamaguchi, Japan J. appl. Phys. 13 (1973)1467.

26) K.Tsubouchi and N.Mikoshiba. Japan J. appl. Phys. 14(1975)309.

27) C.Hamaguchi, K.Ando, M.Sanya and M.Yamada, Proc. Symposium on Microwave Acoustics, Lancaster(1974)203.

28) K.Ando and C.Hamaguchi, Solid State Commun. 16(1975)57.

29) K.Ando, K.Yamabe, S.Hamada and C.Hamaguchi, J. Phys. Soc. Japan 41(1976)1593.

30) C.Hamaguchi and K.ANdo, Solid State Phys. 11(1976)377.

31) G.B.Benedek and K.Fritsch, Phys. Rev. 149(1969)647.

32) A.R.Hutson and D.L.White, Phys. Rev. Lett. 7(1961)237.

33) J.Zucker and S.Zemon, Appl. Phys. Lett. 9(1966)398. ; Phys. Rev. 10(1967)212.

34) A.Ishida and Y.Inuishi, Phys. Lett. 27A(1968)123.

35) D.L.Spears, Phys. Rev. B2(1970)1931.

36) E.D.Pallik and R.Bray, Phys. Rev. B3(1971)3302.

37) M.Yamada, C.Hamaguchi,K.Matsumoto and J.Nakai, Phys. Rev. B7 (1973)2682 ; references there in.

38) L.L.Hope, Phys. Rev. 166(1968)883.

39) D.F.Nelson, P.D.Lazay and M.Lax, Phys. Rev. B6(1972)3109.

40) C.Hamaguchi, J. Phys. Soc. Japan 35(1973)832.

41) K.P.Jain and G.Choudhury, Phys. Rev. B8(1973)676.

42) B.A.Weinstein and M.Cardona, Phys. Rev. B1(1973)2795.

43) B.Bendow and J.L.Birman, Optics Commun. 1(1970)267.

44) R.L.Schmidt, B.D.McCombe and M.Cardona, Phys. Rev. B11(1975) 746.

45) R.M.Martin, Phys. Rev. B10(1974)2620.

46) C.H.Wu and J.L.Birman, Solid State Commun. 14(1974)465.

47) R.M.Martin, Phys. Rev. 134(1971)4.

48) A.Pinczuk and E.Burstein, Surface Science 36(1973)153.

49) P.Y.Yu and Y.R.Shen, Phys. Rev. Lett. 32(1974)373.

50) J.F.Nye, Physical Properties of Crystatsls(Clarendon Press, Oxford 1957)

51) R.Loudon,:The Quantum Theory of Light(Oxford University Press, Ely House, London W.I.)

52) Yamada and C.Hamaguchi, Solid State Commun. 17(1975)879.

53) G.L.Bir and G.E.Pikus, Soviet Phys. Solid State. 2(1961)2039.

54) G.D.Whitefield, Phys. Rev. 121(1961)720.

55) G.H.Wannier, Phys. Rev. 52(1937)191.

56) Optical Properties of Solid, (edited by F.Abeles Laboratire d' optique, Paris France, 1972)pp323.

57) G.E.Pikus, Fiz. Tverd, Telas, 6(1964)324 ; Soviet Phys. Solid State 6(1964)261.

58) P.Y.Yu and M.Cardona, J. Phys. Chem. Solids, 34(1973)29.

59) D.W.Langer, R.N.Euwema, K.Era and T.Koda, Pys. Rev. B2(1970) 4005.

60) J.J.Hopfield, J. Phys. Chem. Solid 15(1960)97.

61) M.Cardona and G.Harbeke, Phys. Rev. 137(1965)A1467.

62) M.Cardona, K.L.Shaklee and F.H.Pollak, Phys. Rev. 154(1967)696.

63) J.E.Rowe, M.Cardona and F.H.Pollak, in II-VI Semiconducting Compounds, edited by D.G.Thomas(Benjamin,New York,1968)

64) D.J.Thomas and J.J.Hopfield, Phys. Rev. 116(1959)573.

65) D.E.Aspness, Phys Rev. B5(1972)4022.

66) W.Franz, Z. Naturforsch. 139(1958)484.

67) L.V.Keldysh, Zh. Eksperim. iTeor. Fiz., 34(1958)1138.

68) J.Armstrong, N.Bloembergen, J.Ducing and P.S.Pershan, Phys. Rev. 127(1962)1918, and references therein.

69) See, for instance, A.Messiah, Quantum Mechnics(Interscience, New York, 1962)pp.724.

70) M.Batz, Solid State Commun. 5(1967)985.

71) E.Matatagui and M.Cardona, Phys. Rev. 176(1968)950.

72) D.Penn, Phys. Rev. 128(1962)2093.

73) M.Tanaka, M.Yamada and C.Hamaguchi, J. Phys. Soc. Japan, 38 (1975)1708.

74) M.Yamada : Private Communications.

75) M.San'ya and C.Hamaguchi : Private Communications.

76) M.Yokogawa : Private communications

77) D.L.Spears and R.Bray, Phys. Lett. 29A(1969)542.

78) K.Yamabe, K.Ando and C.Hamaguchi, to be published in Japan J. appl. Phys.

79) K.yamabe, K.Ando and C.Hamaguchi, Bull.Phys. Soc. Japan, Annual. Meeting(Kyoto)pp172.

80) Y.Yamada, in Ph. D. thesis(1973)

81) K.Ando and C.Hamaguchi, Phys. Lett. 58A(1976)41.

82) C.W.Higginbotham, M.Cardona and F.H.Pollak, Phys. Rev. 184 (1969)184

83) D.Dutton, Phys. Rev. 112(1958)785.

84) J.M.Bieniewski and S.J.Czyzak, J. Opt. Soc. Am. 53(1963)496.

85) D.F.Nelson and M.Lax, Phys. Rev. B3(1971)2778.

86) D.E.Blossey, Phys. Rev. B3(1971)1382.

87) B.A.Auld: Acoustic Fields and Waves in Solid. John Wiley and Sons (1973).

88) B.H.Lee, J. Appl. Phys. 41(1970)2984.

89) F.H.Pollak and M.Cardona, Phys. Rev.172(816)1968.

90) E.Matatagui, A.G.Thomas and M.Cardona, Phys. Rev. 176(1968)950.

91) M.San'ya and C.Hamaguchi, J. Phys. Soc. Japan, 38(1975)786.

92) C.S.Kumarm P.O.Sliva and R.Bray, Phys. Rev. 169(1968)680.

93) D.L.Spears and R.Bray, Appl. Phys. Lett. 12(1968)118.

94) J.D.Dow and M.Bowen, R.Bray and D.L.Spears, Phys Rev. B10 (1974) 303.

95) D.L.Spears ; in his Ph.D. Thesis(June ,1969)

96) C.S.Kumar and W.G.Hutchinson, J. Appl. Phys. 40(1969)4687.

97) K.yamamoto, M.Yamada and K.Abe J. Phys. Soc. Japan. 29 (1970) 1521.

98) E.Kohn and M.Lampert, Phys. Rev. B4(1971)4479.

99) D.Dow and D.Redified, Phys. Rev. B1(1970)3358.

100) T.Hata, M.Ishigaki and T.Hada, Appl. Phys. Lett. 26(1975)549.

101) K.Ando and C.Hamaguchi: Bull. Phys. Soc. Japan, Annual Meeting (Fuhuoka), 1973, ppl72.

102) T.Hata, M.Ishigaki, K.Hada,: Bull. Phys. Soc. Japan, Annual Meeting(Kanazawa), 1974, pp373.

103) R.Berkowicz and B.P.Kietis, Phys. Stat. Solid, 28(1975)425.

104) W.Frantz, Z. Naturf. 13a(1958)484.

105) L.V.Keldysh, Zh. eksper. Teor. Fiz. 34(1958)1138.

106) M.Gal and J. Schanda, Phys. State. Solids. 33(1969)163.

107) R. Williams, Phys. Rev. 117(1959)1487.

108) H.Kuzmany and W.Lederen, Z.Phys. 243(1971)266.

109) R.Berkowicz : Ph.D. Thesis.(1976).

110) P.J.Colwell, M.V.Klein, Solid State Commun. 8(1970)2095.

111) P.F.Williams, S.P.S.Porto, in Light Scattering in Solids.

,edited by Balkanski(Flammarion Science, Paris, 1971)pp70.

112) R.M.Martin, T.C.Damen Phys. Rev. Lett. 26(1971)86.

113) R.H.Callender, S.S.Sussman, M.Selders and R.K.Chang, phs. Rev. B7(1973)3788.

114) W.Dreybrodt, W.Richter and M.Cardona, Solid State Commun. 11(1972)1127.

115) W.Dreybrodt, W.Richter, F.Cerdeira and M.Cardona, Phys Stat. Solid. (b)60(1974)145.

116) R.W.Rubloff, E.Anastasskis and F.H.Pollak, Solid State Commun. 13(1973) 1755.

117) D.C.Hamiltonian, Phys. Rev. 188(1969)1221.

118) Y. Toyozawa, Prog. Theor. Phys. 20(1958)53.

119) A.Compaan, and H.Cummins, Phys. REv. Lett. 31(1973)41.

120) M.V.Keins and S.S.S.Porto, Phys. Rev. Lett. 22(1969)782.

121) D.Berlincourt, H.Jaffe and L.R. Shiozawa, Phys. Rev. 129(1963) 1009.

122) N.I.Meyer and M.H.Jϕorgenson, Festkorper Probleme X ed. o. Madelung(Vieweg, Braunschweig, Germany, 1970)pp21.

123) P.B.Miller, Phys. Rev. 137A1937.